2-1-2015

Aluminum-carbon nanotube nanocomposite for silicon solar cell back metallization

Kareem El-Rafei

THE AMERICAN UNIVERSITY IN CAIRO
الجامعة الأمريكية بالقاهرة

SCHOOL OF SCIENCES AND ENGINEERING

Aluminum-Carbon Nanotube Nanocomposite for Silicon Solar Cell Back Metallization

A thesis submitted to

Mechanical Engineering Department

in partial fulfillment of the requirements for the degree of

Master of Science of Mechanical Engineering

By

Kareem Sherif El-Rafei

Under the supervision of

Dr. Amal M.K. Esawi

Professor, Department of Mechanical Engineering

The American University in Cairo

Dr. Osama Tobail

Senior Research Scientist, Egypt Nanotechnology Center (EGNC)

Cairo University, Sheikh Zayed Campus

Fall 2015

The American University in Cairo

Aluminum-Carbon Nanotube Nanocomposite for Silicon Solar Cell Back Metallization

A Thesis Submitted by

Kareem Sherif El-Rafei

B.Sc. Mechanical Engineering, 2011

To the Department of Mechanical Engineering

January / 2016

In partial fulfillment of the requirements for

The degree of Master of Science in Mechanical Engineering

Has been approved by

Dr. Amal M. K. Esawi

Thesis Committee Chair / Adviser _____

Professor, Department of Mechanical Engineering, The American University in Cairo

Dr. Mohamed El-Morsi

Thesis Committee Reader / examiner _____

Associate Professor, Department of Mechanical engineering, The American University in Cairo

Dr. Iman El-Mahallawi

Thesis Committee Reader / examiner _____

Cairo University, Metallurgy Department, Faculty of Engineering

Acknowledgements

I would like to thank all those who have supported me throughout this project. First, I want to express my deepest gratitude and thanks towards my advisor, Dr. Amal Esawi. She had always helped me with resources, excellent scientific knowledge, expertise and guidance during the last two years and in fact, without her continuous support, patience and encouragement, this project would have never been a reality today.

Second, I would like to thank Dr. Osama Tobail for his support and excellent feedback and ideas which have been extremely beneficial and whom I have learned a lot from. I consider myself very fortunate indeed to have worked with Dr. Amal and Dr. Osama. They have always provided me with support and guidance whenever required, round the clock.

Third, I would like to thank Dr. Anke Klingner for helping us obtain the CTE readings. She had dedicated a lot of time and effort for this task. Her help and professional support was truly priceless; and for that I am extremely grateful.

Fourth, I would like to express my deepest gratitude to Dr. Mustafa Arafa for giving me full access to the Vibrations lab. Without his support and guidance, a crucial part of this report would not never been achieved.

Fifth, I would like to thank Eng. Ehab Salama who has guided me throughout the practical phase of this project and was extremely patient with me. I learned a lot from him, and I owe him a lot indeed. Also I would like to thank Eng. Moataz for his patience and personal encouragement to persist on.

Sixth, I would like to thank Eng. Ahmed Nour, Eng. Ahmed El-Beltagy, Eng. Ahmed El-Ghazaly, and the lab engineers at YJ-STRC. Also Eng. Zakaria, Technician Hussein and the technicians of the MENG labs in general. They have provided a lot of support and help, selflessly aiding me in my practical work to achieve not just good but the best results.

Finally, I would like to thank the American University in Cairo for awarding me the Research Grant, especially Dr. Adham Ramadan for extending the grant duration several times, without which it would have been impossible to go on.

Abstract

With the global push towards having thinner silicon solar cells, the bowing problem arising from the thermal mismatch between the Aluminum electrode and the Silicon wafer in the cell becomes more critical. The thinner the cells the more the bowing and the higher the probability of cracking and hence yield losses and lower cell efficiency. The main objective of this work was to explore the effect of introducing CNT into the composition of the Al paste in order to reduce the Coefficient of Thermal Expansion (CTE) of the resulting composite and hence reduce the bowing problem. Two types of samples were produced: Cylindrical and Wafer samples. The first consisted of 26 compacted and sintered at 500^{o}C powders of the following consistencies: Un-Milled Al, Milled Al, 2%, 5% and 10% CNT-Al. CTE was measured by a Dilatometer DIL 801, TA instruments device. Electrical Performance was measured for the same samples via varying the voltage and measuring the current, then calculated the resistance taking the latter as an indicator for the Resistivity. In both tests, it was found that the 10% CNT-Al samples gave the highest results: in terms of CTE, it resulted in around 20% reduction, and in case of electrical performance, it increased the resistivity by around 3.8%. For the wafer samples, Un-Milled Al, Milled Al and 10% CNT-Al powder-based pastes were prepared using a patented recipe that was modified for the current work, and then the pastes were printed using Spin Coating technique on 9 wafers which were heated at 160^{o}C for around 3 hours. A Contactless Wafer Geometry Gauge device was used to measure the bow and warp. Bow results were inconclusive, however the warping revealed promising results as it was clearly shown that the 10% CNT-Al paste caused the lowest warp per unit thickness of paste printed, average warp to Al paste layer thickness ratios for all 3 pastes were 0.59, 0.35 and 0.24 for the Un-Milled Al, Milled Al and 10% CNT-Al pastes respectively. SEM images of the Top & cross-sectional views of the wafer showed that while the Un-Milled Al and 10% CNT-Al wafers provided an almost uniform layer, the thickness of the layer of the Milled Al paste was relatively irregular due to employing irregular techniques of printing and un-even powder particle size.

Table of Contents

List of Figures

List of Tables

Chapter 1

Introduction

1.1. General Setting

Nowadays, there is a global trend towards switching from depending on fossil fuels as a source of energy to renewable energy sources like solar and wind energy. Naturally, this resulted in a need to make the renewable energy economical (the goal is to reach a cost of $1/Watt) (Hilali et al, 2007), and in the case of solar energy, this was translated more specifically into reducing the thickness of silicon wafers used in manufacturing solar cells. This was based on two fundamental reasons:

1. The silicon wafer constitutes a major part of the cost function of producing a solar panel, estimated to be more than 50% of the total manufacturing cost of the solar cell (Soon-gil et al, 2010), (Kim et al, 2005).
2. Reducing the wafer thickness will reflect positively on the electrical efficiency of the solar panel (T. Koval et al, 1996).

Currently, the solar wafers have a thickness ranging from 270-200 µm, and the goal is to go down to 150 µm cell (Soon-gil et al, 2010). At 100 µm, it is assumed that the max theoretical efficiency for a given Silicon solar cell will be attained, which is around 30% (Bowden et al, 2000).

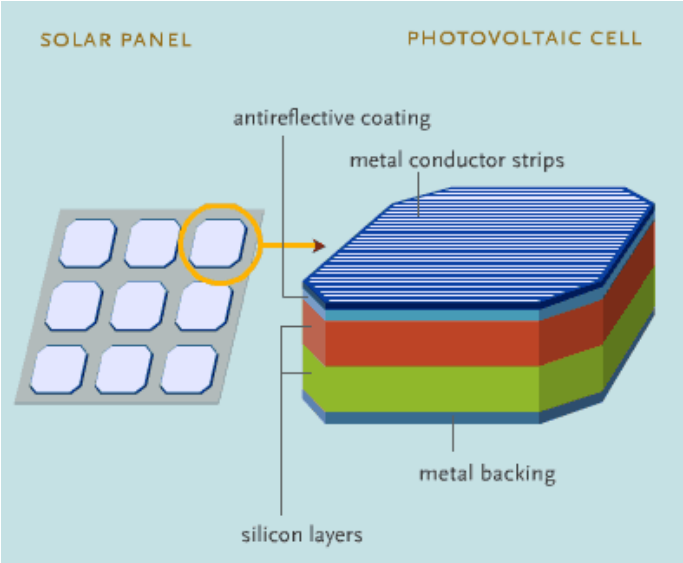

Figure 1 Main Layers of the Silicon Solar Cell, figure adopted from http://www.pbs.org/wgbh/nova/solar/insi-nf.html

It is important to note that a typical solar cell has the following five main layers in this order from top to bottom, see Figure 1 and Figure 2**:**

1. Encapsulate: a glass or a transparent layer that protects the cell
2. Front Contact (Conductor Strips)

   Found on top of the silicon wafer (Front Side), and is mainly made up of silver paste. It acts as the negative electrode of the cell.
3. Anti-reflective Coating
4. Silicon wafer
5. Rear/Back Electrode (Metal Backing)

   Found on the lower side of the wafer (Back Side), and is mainly made up of Aluminum paste. It acts as the positive electrode of the cell.

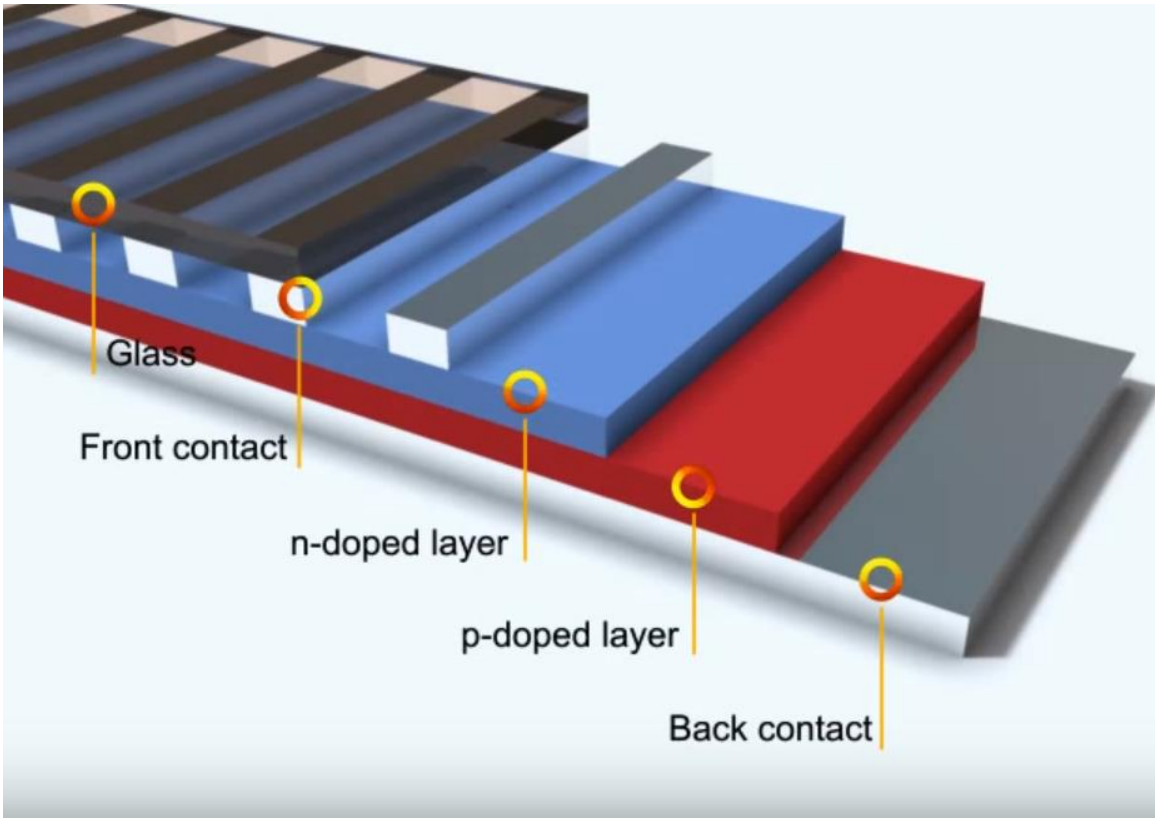

Figure 2 Layered view of the Silicon Solar Cell. Figure adopted from Schwenke, Thomas; "Solar energy / Solar photovoltaics / Photovoltaic effect (3D animation)", 2011, https://www.youtube.com/watch?v=1gta2ICarDw&feature=related

1.2. Manufacturing a Solar Cell

Metal pastes are screen-printed above and below the Silicon wafer. After printing the pastes, there comes another step where the silicon wafer plus the Aluminum (Al) and Silver (Ag) pastes are co-fired together in a belt furnace (usually an infrared furnace is used for the firing step) according to a certain firing profile, see Figure 3, where the wafer moves from one zone to another (each zone has its own predefined temperature) at a relatively high speed which can be as high as 500 cm per min (Soon-gil et Al., 2010). This step is crucial to fix the Aluminum and Silver metals to the silicon wafer, hence constituting the positive and negative electrodes respectively of the solar cell. In a typical firing profile, the wafer is to be subjected to a high temperature of around 700°C to 900°C, way beyond the Aluminum melting point of 660°C, but the extent of that exposure is limited to a time frame of a few seconds to some minutes (Rose et al, 2007), the total firing process taking typically around from 1 to 5 minutes (Brenner et Al., 2013). After the accelerated heating to 900°C, there follows a rapid cooling down to room temperature. As depicted in Figure 3, the Targray company, which is famous for manufacturing Al pastes, has a typical firing profile depicted on their website indicating that the duration of the co-firing step does not exceed 2 min, with the actual firing taking around 0.5 - 1 min, and the rest is just cooling.

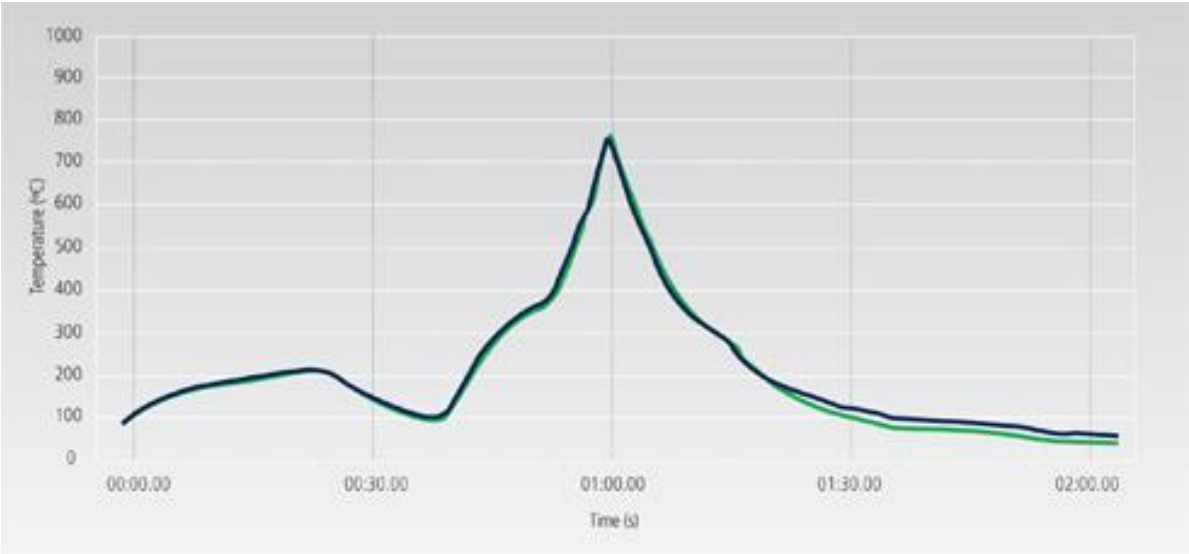

Figure 3 "A typical firing profile". Figure adopted from Targray Co. site, http://www.targray.com/solar/crystalline-cell-materials/aluminum-paste

During the co-firing stage, the Al paste melts. A fraction of this melted Al that is next to the Si wafer dissolves some of the Silicon wafer forms forming a liquid eutectic layer, see Figure 4 and Figure 5. Of course the thickness of such a layer depends on the variables of the firing stage, such as the total duration of heating or the temperatures of the heating zones. As the temperature of the firing stage decreases and the resulting eutectic mixture starts to cool down, a layer that is rich in Aluminum dopant starts to grow out of the Silicon (van Amstel et al, 2009). This layer is referred to as the "Back Surface Field (BSF)" layer, which increases the solar cell efficiency in converting energy (Brenner et Al., 2013) as it reduces the "effective minority carrier recombination velocity", which in turn increases the solar cell operational efficiency (Soon-gil et Al., 2010). It is worth noting that it is believed that at least a 20 µm thick layer of Aluminum is required to create an operational BSF layer (Soon-gil et Al., 2010). Due to the fact that this is a direct reaction between Al and Si (solid-solid), it occurs much quicker than a dopant diffusion process, hence having a BSF layer is much favored (Soon-gil et Al., 2010).

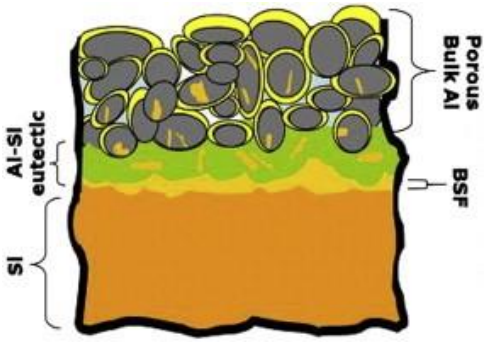

Figure 4 Model of cross-sectional view of the solar cell showing different layers of the rear side of the wafer. Figure adopted from Amstel et al (2011)

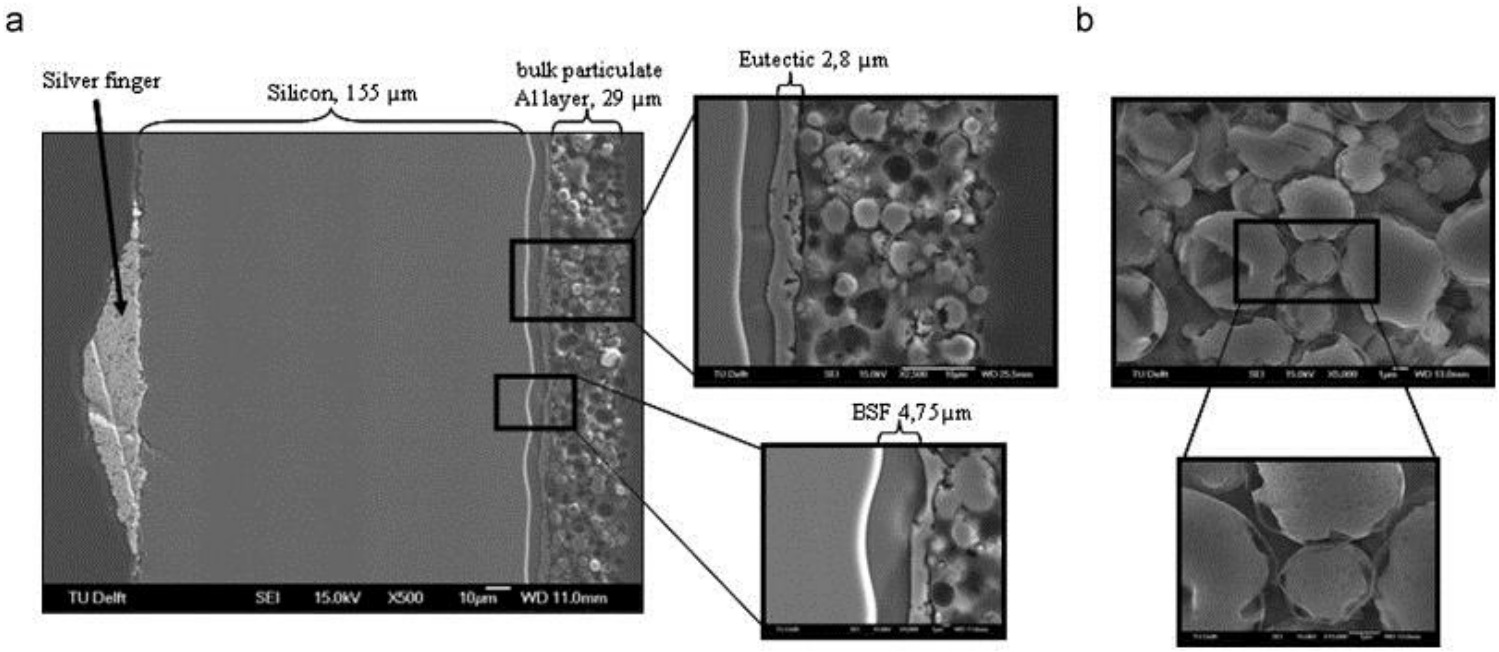

Figure 5 SEM Cross-sectional View of a 200µm thick Solar Cell showing the 5 different cell layers, front side to the left (Silver Finger) and rear side at the right (Al Bulk Layer). Figure adopted from Amstel et al (2011)

1.3. Identifying the Problem: Solar Cell Bowing

As part of the main process of cell assembly, the co-firing is followed by later soldering of the solar panel. Since both processes include heat application hence both are contributing mainly to the bowing of the solar cell, see Figure 6, which can be described as such:

The bowing problem occurs due to the thermal mismatch between the Silicon (Si) and Aluminum (Al). The coefficient of thermal expansion (CTE) can be defined as "as the fractional increase in length per unit rise in temperature" (ASM International, 2002). The CTE of the Silicon (Si) is 4 x 10^{-6} $^{o}C^{-1}$ and for the Al it is 23x10^{-6} $^{o}C^{-1}$ (Soon-gil et Al, 2010), meaning that for a given increase of 1^{o}C in temperature, Al of the back side electrode will expand roughly around 6 times more than the Silicon wafer to which it is attached. This will lead to the overcoming of the bending stress of the wafer and bowing thus occurs (Schneider et al, 2001).

Thus, in a nutshell, the solar cell will suffer from bowing deformation as the back Al side will tend to stretch more than the silicon wafer, as depicted in Figure 6 and Figure 7, resulting in a concave-warped wafer.

Figure 6 A 160 µm bowed thick solar cell. Figure adopted from Bunkenburg et Al, "Enabling thin wafers for today's high efficiency silicon solar cells"

"Bowing (cell Warpage) is defined as the maximum deflection height of the center of the fired cell at room temperature when measured upon a flat surface" (Brenner et al, 2013). In Figure 7, the bow is described as concave, as the direction of deflection is inward towards the center of the wafer, i.e. the wafer is caving in, hence the deflection is described as "concave".

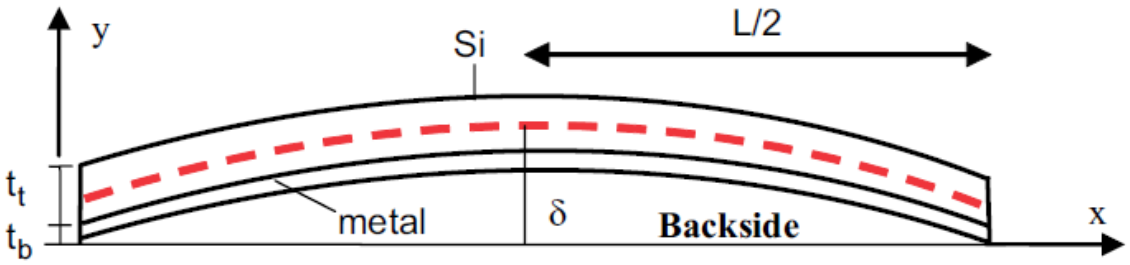

Figure 7 Schematic diagram depicting the behavior of a Si wafer with a metallic contact on its lower/backside. Figure adopted from Hilali et Al., 2007, "Bow in screen-printed back-contact industrial silicon solar cells"

This information combined with the growing trend towards having thinner and larger silicon wafer means that the bowing problem will only become more pronounced, for instance, it was found that standard wafers of thickness around 300 µm and area of 125 x 125 mm develop a bow of less than 0.5 mm, but that bow can increase more than 10 times for wafers of 200 µm thickness. The bow for a wafer of 98 cm^2 area is shown in Figure 8 (Schneider et al, 2001).

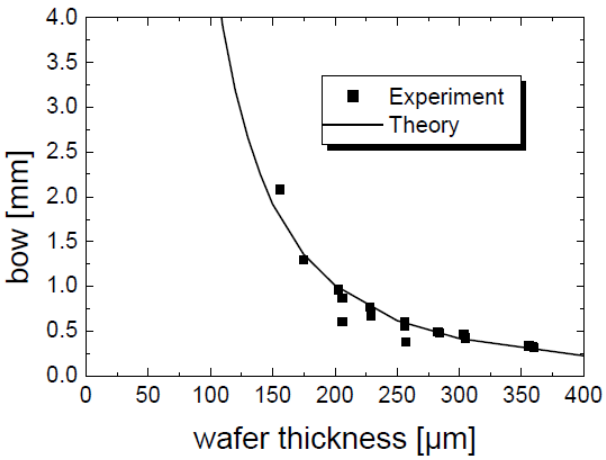

Figure 8 The resulting bow for a given wafer thickness, comparing theoretical and experimental results. Wafers used had a surface area of 98 cm^2 (Schneidere et al, 2001)

1.4. Why is Bowing a Problem?

First of all, the bowing deformation is permanent, meaning that the wafer does not return to its original straight shape after some time (certain proposed de-bowing techniques will be discussed later in the literature review section). If extra relatively-expensive flattening techniques are applied, this would affect the final cost of producing the cell.

Second, this bow jeopardizes the structural integrity of the wafer, as it results in the formation of residual stresses in the solar panel which makes it susceptible to fracture (Amstel et al, 2009).

Furthermore, the bow makes it difficult to handle solar cells during the lamination step in the assembly of the panel, and might cause breakage of the cell as well. Cracks and fractures in the solar cells result in decreasing the level of efficiency of the solar panels throughout its operational lifetime.

Since there is a global push towards reducing the thickness of silicon wafers which shall result in the amplification of the negative consequences of the bowing problem, hence with such an urgent need to go thinner, the bowing problem represents an obstacle that would impede such efforts, hence the urgent need to attend to it as soon as possible.

1.5. Carbon Nanotubes (CNT)

CNTs are basically layers of Graphene "rolled" into cylinders, where each Carbon atom is joined to another 3 ones via Covalent bonds (Esawi, 2014). These cylinders have a very small diameter, that can be as low as a few nm, while their length can be several 100 million times longer, i.e. in the cm scale. CNT, Figure 9, combine properties from both Diamond and graphite (Esawi, 2014), such as high thermal conductivity (Deng et al, 2007), high Electrical conductivity (comparable to copper), large current-carrying density (Kaushik et al, 2015), a very low Coefficient of Thermal Expansion (Yosida, 2000), and high tensile strength. See table 1 for detailed information about CNT properties.

Figure 9 Physical Appearance of Carbon nanotubes, figure adopted from Microphase Ltd., http://www.microphase.jp/e/e_product0201.html

There are 3 main classifications of CNT, in terms of structure (Figure 10):

i. Single-Walled CNTs (SWNT)
ii. Double-Walled CNTs (DWNT)
iii. Multi-Walled CNTs (MWNT)

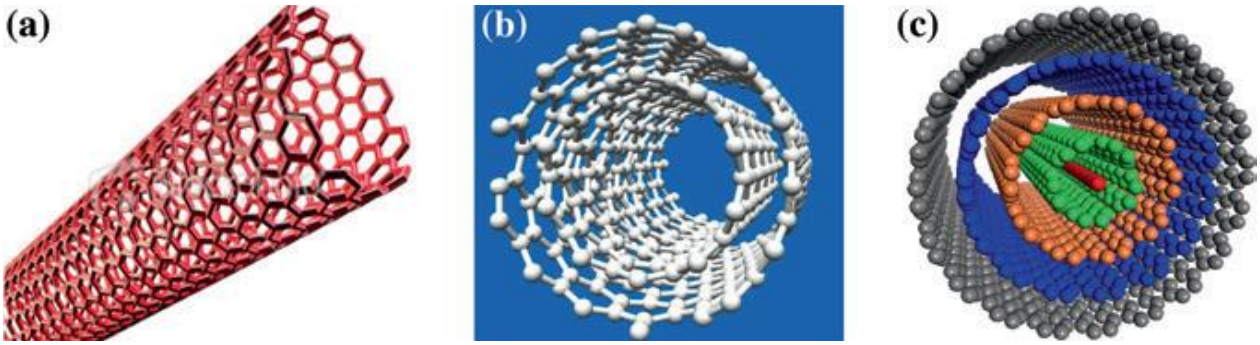

Figure 10 Types of CNT Structures: a. SWNT, b. DWNT, c. MWNT. Figure adopted from (Kaushik et al, 2015)

As can be seen in Figure 10, the main difference between the various structures of the CNT is the number of concentric tubes; SWNT has only 1 tube, DWNT has 2 and so forth. SWNT has a diameter of around 1-2 nm, and a length of around 0.2-5 µm, the radial distance between one concentric tube to the next is around 0.36 nm and in the case of the MWNT, the concentric tubes are united together by Van der Waals forces (Esawi, 2014)

Table 1 Basic Properties of CNTs

Property	Magnitude
Coefficient of Thermal Expansion (CTE)	0 (Yosida, 2000),
Current-Carrying density	+ 10^3MA/cm^2 (Kaushik et al, 2015)
Tensile Strength	30-100 GPa (Liu et al, 2012)
Young's Modulus (SWNT)	+1000 GPA (Kaushik et al, 2015)
Young's Modulus (MWNT)	270-950 GPa (Coleman et al, 2006)

The properties of the CNT are several times better than the most-commonly used materials strength-wise, thermally and electrically, as explained before, and hence the range of possibilities of combining CNT with other materials to form composites with improved properties is infinite.

Note: There are two methods to produce MWNT: Arc and Chemical Vapor Deposition. The first technique produces CNT of higher quality than the second. Thus based on Coleman et al (2006), MWNT produced by arc method had a Young's modulus of around 270-950 GPA while MWNT produced by Chemical Vapor Deposition technique had a lower range (estimated to be around 300 GPa) due to the presence of more defects.

Chapter 2

Literature Review

There have been many approaches towards addressing the bowing problem, these can be summarized as such:

2.1 Adding Antimony Oxide

Kim et al (2012) developed an Al paste to be used in the Solar Cell production. This paste had an active ingredient added, the Antimony Oxide, to reduce the resulting bow in solar panels and improve its electrical performance. In the patent, the inventors sought to compare between different paste compositions. First, 5 pastes were prepared containing Antimony Oxide, the differences lay in varying the amounts of its main constituents which were:

1. Al Powders (≈74% of total weight)
2. Organic Vehicle (≈23-24.25%)
3. Dispersant (≈ 0.5%)
4. Glass Frits, Leaded and Lead-Free (≈1-2%)
5. Antimony Oxide (≈0.25-0.75%)

A second set of 8 pastes were prepared where in the first 6 Antimony Oxide was replaced by either the Organic Vehicle, Glass frits or a combination of both. In the remaining 2 pastes, the organic vehicle was reduced to be replaced by glass frits and Antimony Oxide.

The sintering of the solar panels stage occurred over 6 Zones of different temperatures: 500°C, 550°C, 650°C, 730°C, 820°C and 910°C, with the wafers moved from one zone to the next at a belt speed of 220 rpm.

In addition to checking the bow generated and the Electrical performance of the paste in terms of "Photoelectric conversion efficiency", Bead generation was observed and a Hot Water test – dipping the panel before the sintering stage in a hot water bath of 70°C- was done to check for any bubble generation which would indicate that the electrode was not stable or has high affinity to react with humidity in the air. Based on these four tests, the 13 pastes (set 1 + set 2) were compared

together. It was found that the pastes containing Antimony Oxide in the following amounts: 0.25-0.75% of total paste weight had the least bow (1.5 mm and less versus 4-6.5 mm for the other pastes) and the best electrical properties, no bead generation and successfully passed the hot water test. However, in the case of the pastes containing above the 0.75% level (2 pastes were developed containing 1 and 1.5% of the total weight Antimony Oxide), they did not pass the hot water test, and hence the reliability of the electrode was jeopardized.

2.2 Adding Fly Ash to Al

Rohatgi et al (2006) considered adding fly ash to the Al to reduce the resulting composite's CTE, given that the CTE of the fly ash is around $6.1 \times 10^{-6}\ C^{-1}$. CTE samples of a diameter of 6 mm and a length of 50 mm were prepared. The percentage volume of the fly ash cenospheres of the total composite volume was estimated to be around 64%, with a particle size in the range of 100-150 μm (a sieve was used). Infiltration pressure technique was applied to make the composite, 2 variables were changed: time and pressure. Infiltration time had 2 levels of variation: 3 and 7 min, and the Infiltration Pressure variable had 2 levels: 35 and 62 kPa. To remove the stresses, after the infiltration, the CTE samples were annealed at a temperature of 340°C for 2 hours. Then using a Dilatometer device, the linear thermal expansion was measured for a temperature range from 30 to 400°C. Once at 400°C, the samples were held at that temperature for 10 min and then the device shutdown and the samples were left to cool in the device on their own. The CTE test was done twice to investigate the effect of the thermal cycling on the composite. The average recorded CTE value of the samples was around $12 \times 10^{-6}\ C^{-1}$. Furthermore, it was found that the samples with longer infiltration time and pressure had a lower CTE. This is due to the fact that the less the voids present between the particles, the lower the CTE of the developed composite. The higher the pressure applied and the longer the duration of this applied pressure, the lower the presence of voids and hence the lower the CTE of the composite, 16% less than that with longer time and higher pressure, according to the study. Finally, it was also noted that the second thermal cycle had slightly increased the recorded CTE, which was attributed to the yielding effect due to thermal mismatch between the fly ash (cenosphere) and the Al.

2.3 Adding Silicon Di-Oxide

Rose et al (2007) presented a patent describing how to make a low-bow Al paste, introducing Silicon Di-Oxide (SiO_2) as the active ingredient that would reduce the overall bending of the wafer. The paste generally consisted of the Organic Vehicle (around 24-25% of total paste weight), the Al powders (around 75%), the active agent and glass frits.

In this study, 2 main sets of samples were prepared:

Set 1 had 8 different Al pastes, with 2 active ingredients: Crystalline and Amorphous SiO_2, 4 samples each. No glass frits were contained in these pastes. The wafers used were 5 inch square, 270 µm thick. The pastes were printed and fired in a furnace with 4 firing zones with the following different temperatures: 450°C, 520°C, 575°C and 950°C. the speed of the moving belt was set at 2150 mm/min. It was found that compared to the control, both the Amorphous and the Crystalline forms of SiO_2 reduced the bowing, however, the bow was most significant in the case of Amorphous SiO_2. The critical level of SiO_2 is 0.3% of the total paste weight. It was found that above this level, the electrical performance deteriorated for the Amorphous form, and below it, there was no much significant change in the electrical performance for both the amorphous and crystalline forms. Furthermore, when comparing all the results, it was found that adding less than the critical level of SiO_2 in the amorphous form to the paste resulted in a much reduced bow compared to the crystalline paste, and the electrical efficiency was not much affected.

Thus the second set of wafer samples was prepared. The wafers used this time were 6 inch square 180 µm thick wafers, with the same firing profile as before. 8 samples were prepared, the paste had glass frit this time. The composition of the glass frits was: SiO_2, ZrO_2, $B2O_3$, ZnO, MgO, TiO_2, Na_2O, Li_2O and Bi_2O_3. By varying the percentage weight of the glass and SiO_2, the electrical performance and the resulting bow could be improved. It was found that glass frits did increase the electrical efficiency: compared to a control, by having 0.5% of the weight to be glass, and no SiO_2, the electrical efficiency was increased by 1%, and in another sample adding both the frits and SiO_2, by around 0.15 – 0.25%, had a significant effect on the bow.

2.4 Comparing commercially-available Al-Pastes

Bähr et al (2005) studied different commercially available pastes, some labeled as low-bow pastes, comparing them with regards to the bowing and electrical performance, and thus the one that caused the least bow was selected. The pastes used either contained lead or were water soluble. Standard multi-crystalline silicon wafers were used, the wafers had the following size specifications:

Square side length 100, 125, 150 and 156 mm, Thicknesses: 90, 100, 150, 200, and 310 µm. As for the results, by varying the Al paste used, a min bow ranging from 0.7 to 1.5 mm was achieved for solar cells of thickness 150 µm, with average electrical efficiency of 14%. Below such thickness, losses in Voltage and Current densities were observed. For a 100 µm thin solar cell, a 2mm bow was observed, and the highest noted electrical efficiency was 13.9%, i.e. the electrical efficiency had not drastically differed from the that of the 150 µm thick cells.

2.5 Altering Design Parameters

Amstel et al. (2011) studied the Al on the rear side in terms of its microstructure and mechanical properties. Nano-indentation was used to estimate the Young's modulus of the Al-Si particles, and the measurements of the bow were used to determine the overall Young's modulus, taking into account the effect of the paste on the development of the bow. Such knowledge thus helps in defining the mechanical limits of the solar panel, and hence designs could be improved accordingly. Youngs' modulus of Al-Si particles and that of the rear side were found to be 72 and 43 GPa respectively.

2.6 Using Pb and Cd free Al Pastes

Caroll et al. (20th European PV Conference, 2005) presented another indirect attempt: The study aimed at developing Pb & Cd-free Al paste via reducing the amount of lead frit in it. One of the lead-free pastes developed showed promising results with respects to the bowing effect. Using 5 inch solar wafers with a 180 µm thickness, 4 pastes were compared: 1 paste had lead, and the others were lead-free. For a given firing range from 850 to 950^{o}C, the bowing effect of one of the lead-free pastes (given the name G4) decreased as the firing temperature was increased, and it became less pronounced than the bow of the conventional lead-containing paste (G1), at one point

went as low as 0.750 mm versus 2.114 mm at a temperature of 925°C. The efficiency of G4 was noted for the same firing temperature range, and it was found to be very close to that of G1, which was around 14%. Note: The same experiment was repeated with larger wafers: 6 inch 210 µm thick wafers, however, the bowing of G4 this time did not decrease, but it remained hovering in the range from 0.402 to 0.473 mm, which the author had pinned for further investigating.

Kim et al (2005) had a similar approach, worked on producing a lead-free low bow Al paste via varying its constituents, such as the size of the metal powder particles, chemistry of the glass, the organic vehicle, morphology and the additives used. The prepared pastes were screen printed on the wafers with a 200 mesh screen, varying the quantity of paste printed from 0.055 to 0.035 grams per square inch. The wafers were then co-fired with the silver paste on the front side and the Al paste on the backside. The wafers were passed through 3 firing zones: 780°C, 830°C and 930°C, each had a length of 7.5, 15 and 7.5 inches respectively, wafers were moved at a belt speed of 2 inches per second. Bowing test was performed with a drop dial gauge after the wafers had Al paste printed on them and were fired as described before. For testing the electrical performance, IV curve was used to determine the resistance from the slope. Wafers used had the following dimensions: 5" x 5" x thickness, the latter was 235 and 180 µm (2 sets of wafers with different thicknesses). There was no information provided on the formulation of the paste but only that three main ones were prepared: A, B and C. A had lead while the others did not. Incidentally, Paste A caused the most bow compared to Pastes B and C, each developed an 0.8, 0.6 and 0.4 mm bow respectively in a 235 µm - thick wafer.

2.7 De-bowing

Bunkenburg et al (Despatch Industries) presented a simple "thermal de-bowing" step which was added after the co-firing process to release the stresses and hence reduce the bow created. Standard 156 x 156 mm wafers were used, the thickness varying as such: 140, 160 and 180 µm. Commercial Al paste was used with no specific optimizations. Just after the firing process was finished in the "Despatch" furnace, the cell bow was measured via putting it on a glass panel and averaging the measurements of different points of the wafer (corners and center of sides). The thermal de-bowing process came next, the cells were put in a Despatch IL-RTS where they were cooled down rapidly to -55°C and then heated back again to 20°C, the process took around 50 seconds with the wafers

being moved at a belt speed of 3700 mm/min. This was repeated for all 3 wafer categories with the different thicknesses described above, keeping in mind that the firing and the de-bowing thermal processes were kept constant all along. Again, the bow was measured immediately after this step and it was found to be as follows: For the 140 µm wafers, the de-stressing method removed up to 65.7% of the bow. For the 160 µm wafers, 71.3% of the bow was removed, and finally for the 180 µm wafers 75.4% of the bow was removed. A device called "Pasan I-V tester" was used to measure the electrical performance of the solar cells after the firing step and once again after the de-bowing step. It was found that there was no overall change in the electrical efficiency of the cell due to the de-bowing process. On the downside, however, it was found that there was a re-bowing effect due to heating again at a step designed to simulate a worst-case scenario of the soldering step which normally follows the firing process when manufacturing the solar cells. In this worst-case scenario test, the wafers were heated to a temperature of 250^{o}C for 5 seconds (the wafers reached a peak temperature of 266^{o}C). The grow reformed by 77.5% 96.0% and 111.6% for the 140, 160 and 180µm thick wafers respectively. Also, the bow was measured at certain intervals of time: after 15,20 and 30 days of the original de-bowing treatment. It was found that the bow reformed and continued to grow again till the 15th day at which it leveled off for the 140 and 160 µm wafers, and leveled off on the 20th day for the 180 µm wafer. On the 20th day the bow had increased by 17.2%, 17.3% and 129.1% for the 140, 160 and 180µm thick wafers respectively.

Other aspect of the study was to observe the effect of varying the thickness of the Al paste layer. It was found that they were positively related: as the paste amount deposited (and hence thickness per wafer) was increased from 1.59 to 1.79 grams (12.58% increase), the average bow was found to have increased from 6.53 to 8.51 mm respectively, an increase of 28.82% in measured bow length. The study also observed the effect of using commercial "low-bow" pastes to reduce the bow, and it was found that a noticeable reduction was observed for the 3 wafer thicknesses, recording a min of 57% bow reduction for the 160µm wafers and a max of 70% for the 180 µm wafers.

Zhang et al (2009) followed a similar strategy by cooling down the wafer after the firing process in a refrigerator to -60^{o}C then back to room temp. A set of strain gauges was used to measure the

strain during and after the cooling process. This process of sub-cooling was used to remove the elastic strain developed and hence "de-bow" the wafer.

2.8 Lowering CTE via developing CNT-Al composites

There have been a lot of studies focusing on studying the mechanical behavior of CNT composites, however, very few did study the thermal behavior.

The following three consecutive studies -Tang et al 2004, Deng et al 2006, Liu et al 2012- focused on adding CNT to Al in order to reduce the CTE of the resulting composite. The three studies focused mainly on the following applications: packaging materials (for electronic devices) and aerospace structures, with each study building on the one before as presented below in a chronological order. The analysis behind this is that the CNT have a very low coefficient of expansion, almost equal to zero (Tang et al, 2004), and hence when combined with Al it would act as a hindering agent for expansion. **It is worth noting that all 3 studies concentrated mainly on measuring the CTE reduction, and their work was directed towards fulfilling the demand for other applications other than that of the bowing problem of the solar cells described before, hence their work neither included measuring solar cell bow nor measuring the electrical performance of resulting CNT-Al composite; the relevance of each shall be explained later in the following section.**

Tang et al. (2004) mixed Nano Al particles with single walled Nano tubes (SWNT), which were purified first. The percentage of the SWNT in the mixture was varied from 0 to 20 % of the total volume. TEM was used to ensure that the SWNT were homogenously dispersed in the mixture by soaking both the Al powder with the CNT in alcohol, then subjected the mixture to a 30-min ultrasonic rotation session. Later, the resulting mixture was dried and compacted under a pressure of 1.5 GPa into discs of the following dimensions: Diameter 8 mm, height 1 mm. With the initial compaction taking place at room temp, later consolidation occurred at 380 C, and at slightly less pressure of 1 GPa, the consolidation phase took 30 min. A dilatometer was used to take the CTE measurements at an interval of 50^{o}C, with the heating rate being 5^{o}C/min for a total temperature range of 20 to 250^{o}C. This range was chosen as it is the same as the working temperature range for the electronic packaging material, which was the main application this study was focusing on. The results of the CNT-Al samples were contrasted against Al (coarse-grained) and Silicon (single

crystal). The deduction was that as the CNT content in the mixture was increased, the CTE value decreased; the CTE of the 15% CNT-Al sample had a value which was around 25% of the CTE of course-grained Al, and as a general conclusion it was found that adding CNT up to 15% of the volume of the mixture can lead to around 65% reduction in the CTE. It is worth noting that the 20% CNT-Al sample led to a reverse effect: instead of having an even more-reduced CTE value, the CTE actually increased, which was attributed to agglomeration of the CNT, i.e. the tendency of the CNT to stick together, and not become evenly dispersed within the mixture.

Deng et al. (2006) worked on multi-walled carbon nanotubes (MWNTs). 1% of the total weight of the composite fabricated in this study was MWNTs which was added to 2024 Al matrix. Nitric acid was used to purify and disperse the MWNT. All samples in the study were fabricated by cold pressing then hot extrusion, the final samples having cylindrical shape of the following dimensions: 6mm (diameter) and 25mm (height). CNT dispersion was checked using field emission scanning electron microscope (FESEM) via examining the pull-out length of the CNT and relating these observations with the interfacial strength between the CNTs and the Al matrix surrounding it, which were found to be well in the case of the 1% MWNT composite. CTE measurements were taken at a range between 25 to 400^{o}C using a Thermomechanical Analyzer device (TMA). These measurements were contrasted against the measurements of 2 control samples: Pure Al and 2024 Al matrix. It was found that the 1% MWNT-Al composite resulted in the lowering of the CTE by 12% as compared to the Pure Al sample, and 11% against the 2024 Al matrix, these CTE results were reported at a temperature of 50^{o}C.

Liu et al. (2012) investigated the effect of having 1.5% and 4.5% of the total volume of the sample to be CNT on the tensile properties and the CTE. The samples were fabricated as follows: the CNT were mixed with 2009Al powder, the latter acting as the matrix for the composite, in a "bi-axis rotary mixer", the rotation speed was 50 rpm, and it lasted for 8 hours. The CNT content was of course changed according to the sample being fabricated, in one case it was 1.5% of the total volume, and in another it was 4.5%. As for the control sample, it was a 2009Al one with no CNT content in it. The powders were then cold compacted, followed by a degassing stage, then came the hot compression into cylindrical billets which had the following dimensions: a diameter of 55 mm and a length of 50 mm. A new mixing technique was adopted in this study: The Friction stir processing (FSP), where a tool is rotated and moved over a specific region resulting in much

deformation which ensures thorough mixing is achieved. Following the hot pressing step mentioned before, the powders were hot forged at a temperature of 450°C into 10 mm-long disc plates, which were later subjected to FSP, the tool rotational speed being 1200 rpm, and the translation speed being 100 mm/min. the output is then further T4-treated, and SEM and TEM was used to check the CNT distribution within the composite. Finally, the thermal samples were prepared by machining the FSP output into cylinders of the following dimensions: 5 mm diameter, 20 mm length. The device used for measuring the CTE was Dil 402 PC, the heating rate was 5°C/min, and the thermal range for taking the measurements was from 20 to 200°C. It was found out that the CNT were properly dispersed within the matrix following the FSP step, and that the SEM and TEM showed no CNT cluster formations, however, non-severe CNT damage was reported. As for the CTE, the 1.5 % volume CNT-2009Al sample resulted in a reduction of 9.3% in the CTE, and the 4.5 % volume CNT sample reduced the CTE by 29%. These experimental results were compared to those obtained by 2 mathematical models: Rule of mixtures (ROM) and Schapery's model, the latter was found to be more spot-on with regards to agreement with the experimental results obtained, while ROM was found to be a bit overestimating. Schapery's model attributes the reduction in CTE to be due mainly to the large interface area between the CNT and the Al matrix, hence the CNT were able to constrain the thermal strain and thus lower the overall composite CTE.

Chapter 3

Objectives

3.1 Need for investigation

In all the literature reviewed, so far the introduction of CNT-Al into the solar cell structure has not been investigated at all. True, the effect of lowering the CTE of the Al by introducing CNTs has been investigated, as shown in (Tang 2004, Deng 2006, Liu 2012), however, none of these studies were directed at the solar cell application, which extend beyond the lowering of the CTE of the Al in the cell to include the examination of the Electrical performance and bow development of the solar cell as well.

3.2 Purpose and scope of the study

The general objective of this study was to reduce the bowing problem of the Silicon solar cell via replacing the Al powders used in the paste printed on the back electrode of the solar cell with Al-CNT composite. Such a composite shall be tested, as shall be mentioned later on, to check that it could fully act as a substitute for the original Al metal paste. The scope will be limited to testing the:

i. **Thermal** performance in terms of quantifying CTE reduction resulting from the introduction of CNTs.
ii. **Electrical** performance in terms of the effect of introducing CNTs on the resistivity.
iii. **Bow/Warp** development due to the introduction of CNT to the Al paste composition

3.3 Justification/value

Creating a composite paste product that could reduce the bowing problem of the solar panels means increasing the efficiency of solar panels and aiding the attempts towards reducing solar panel thickness, hence sustaining the world's quest towards developing a true efficient and a developed solar energy industry, as well as economically providing solar energy to the masses. Furthermore, such a boom in solar energy industry will decrease the Carbon emissions released into the air which means reducing the contribution to the global warming problem, a good step on the road to easing the transition towards having a green industry and ultimately a green-oriented global society.

Chapter 4

Materials & Experimental Procedure

4.1 Roadmap

Before each major part of this chapter, a basic brief explanation and a representation of the main subsections shall be discussed. This was done in order to make it easier for the reader to follow the experimental steps, many as they may be, and get an understanding of the overall procedure as a whole. The general layout was depicted in Figure 11, and a more detailed representation was provided for Parts 1 and 2 as shall be presented later on.

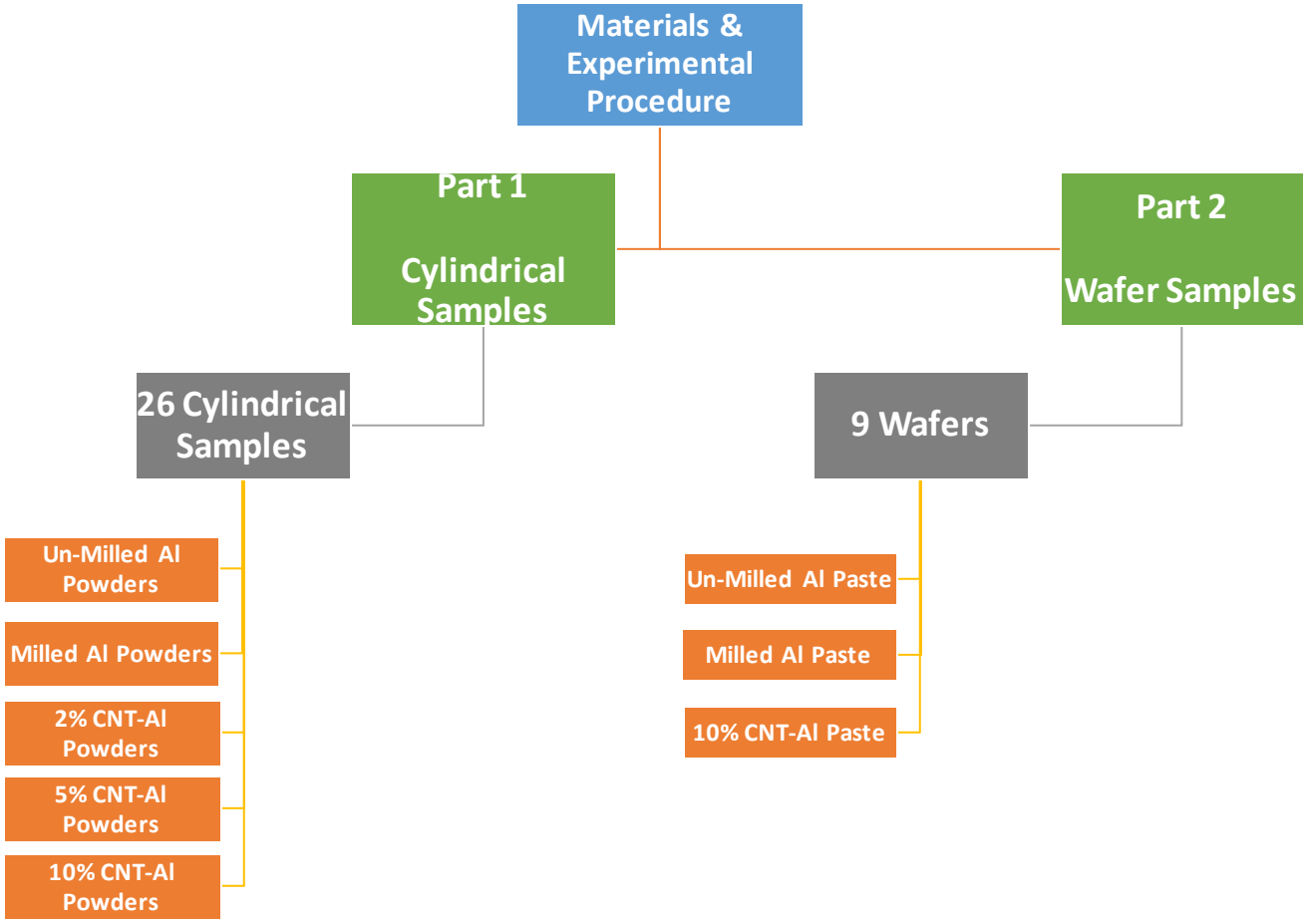

Figure 11 Roadmap of Methodology Section

4.2 Part 1: Cylindrical Samples

Check Figure 12 to view a graphical representation of the main sections of part 1.

I. Cylindrical Samples - Fabrication

A set of 26 samples of compacted Al powders and CNT were fabricated.

Powders used were:

i. Un-Milled Al powder (5 Samples)

ii. Milled Al powder (6 Samples)

iii. 2% CNT- Al powder (6 Samples)

iv. 5% CNT- Al powder (5 Samples)

v. 10% CNT- Al powder (4 Samples)

II. Testing

1. Measured the CTE of the compacted cylindrical samples using a Dilatometer.
2. Measured the Electrical performance of the samples in terms of Resistivity. A DC generator device was used, and the Resistivity was determined accordingly.

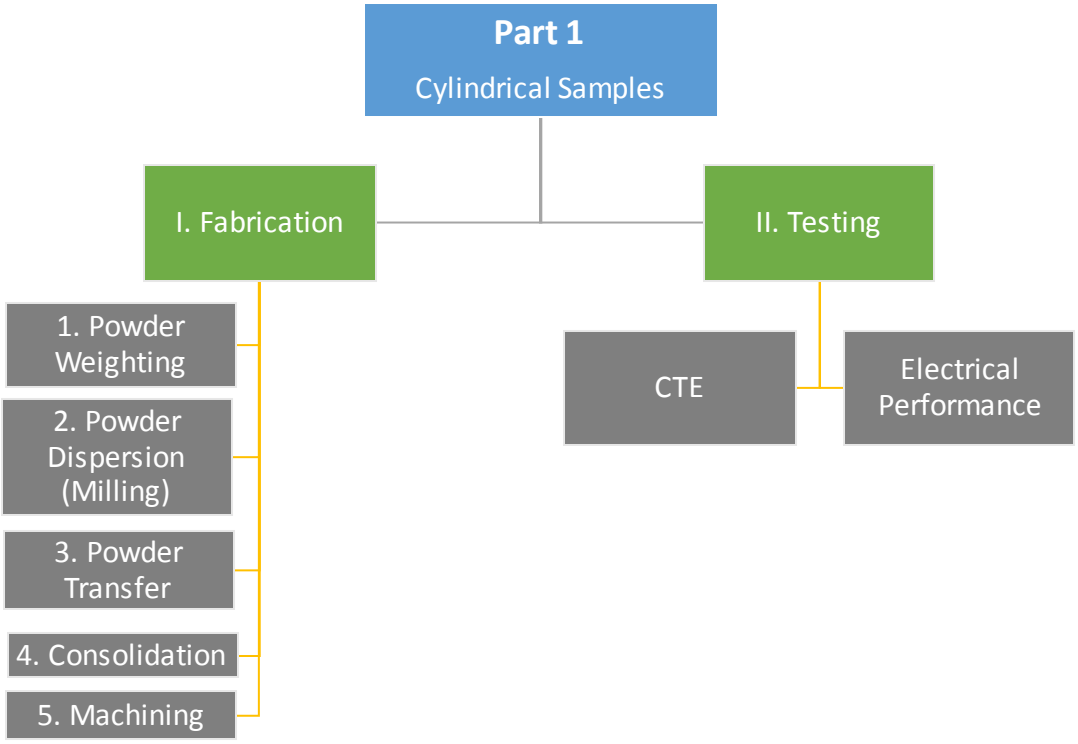

Figure 12 Roadmap of Part 1 of Methodology section – Cylindrical Samples

4.2.1. Cylindrical Samples - Fabrication

Step 1: Powder Weighing

The Aluminum and CNT powders were accurately weighed in the glove box, see Figure 13 and Figure 14, which was filled with Argon, an inert gas that provides a clean (dust-free) safe working environment; Argon prevents Al powders from quickly reacting with the air and forming an oxide layer, as well as it prevents the powders from bursting into flames when they were removed after milling, the latter being a high energy process that shall be described later on in more detail. Al powders were supplied by Al-Poco, APS- 45 μm, and the CNTs were supplied by Thomas Swan in the UK. They were MWNT, with an average diameter of 12-20 nm and a length of tens of μm.

Figure 13 Glovebox: Exterior View

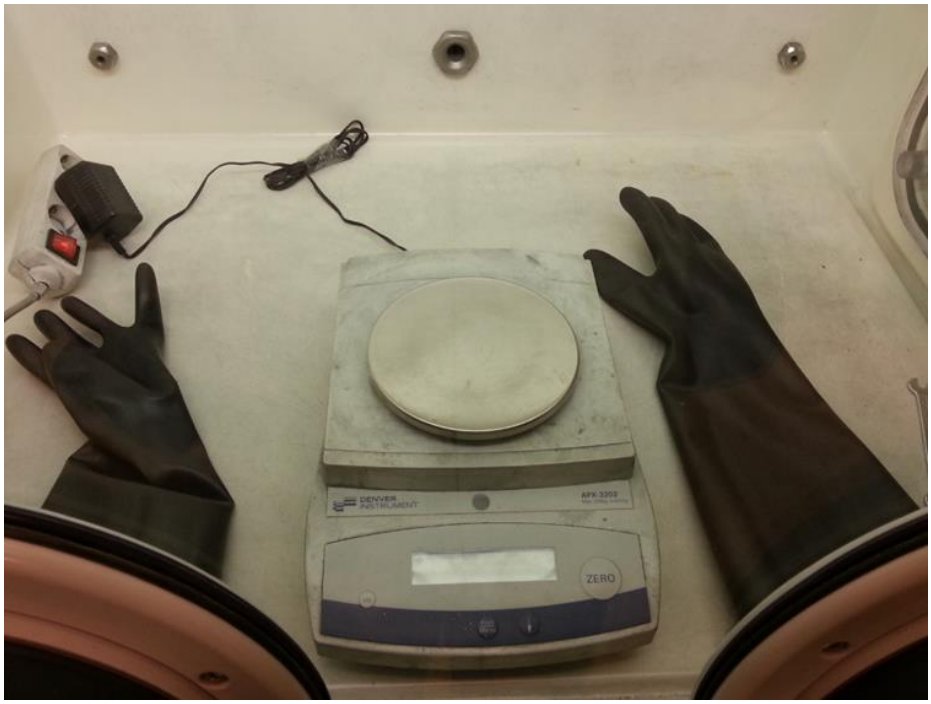

Figure 14 Glovebox: Interior View, electric balance and gloves.

The powders were added according to required final composition as follows:

Table 2 Sample Preparation: Powder Weights - Al and CNT Per One Stainless Steel / Milling Container

Sample	CNT powder weight per container (grams)	Al powder weight per container (grams)	Process Control Agent (µL/milling Container)
Un-Milled Al	-	29.54 ± 0.05	-
Milled Al	-	29.54 ± 0.05	265
2 % CNT-Al	0.59	28.95 ± 0.05	165
5 % CNT-Al	1.48	28.06 ± 0.05	50
10 % CNT-Al	2.95	26.59 ± 0.05	30

Using the electronic balance available inside the glovebox, see Figure 14, the Al and the equivalent amount of required CNTs powders were weighed for each sample, as shown in Table 2. As shall be explained in the following section, a stainless steel container was used to contain the powders, usually 2 containers were prepared per one sample (more shall be explained about the containers in the following section). It is worth noting that the numbers in Table 2 were used to prepare the powders for one container only. The Un-Milled Al powders indicate that the Al powders were used as given, without any further processing or milling applied to them

Note: the main function of the Process Control Agent (PCA is Ethanol of high purity grade.) was to maintain the balance between cold welding and re-fractioning processes that occur during high energy ball milling, hence helps in maintaining the particle size distribution so that it prevents coarsening.

Step 2: Powder Dispersion - Milling

High Energy Ball Milling can be described as a process that involves powder processing in its solid state. Basically, a stainless steel container, Figure 15, was used to contain the powders. Inside, there were 42 stainless steel balls that have a diameter of 10 mm, and an overall mass of 147.69 grams. The machine has a main sun gear, Figure 16, that rotates in one direction, while the containers - the planets - rotate with the sun gear in the opposite direction along their own axes, i.e. the sun rotates anti-clockwise, and the planets rotate clockwise, see Figure 17. To maintain machine balance as it rotates at a high speed, it is worth noting that a pair of identical stainless steel clamps and containers containing the exact amount of powders must be placed at opposite ends of the main rotating sun gear.

Figure 15 Stainless Steel Ball Milling Container and Clamp

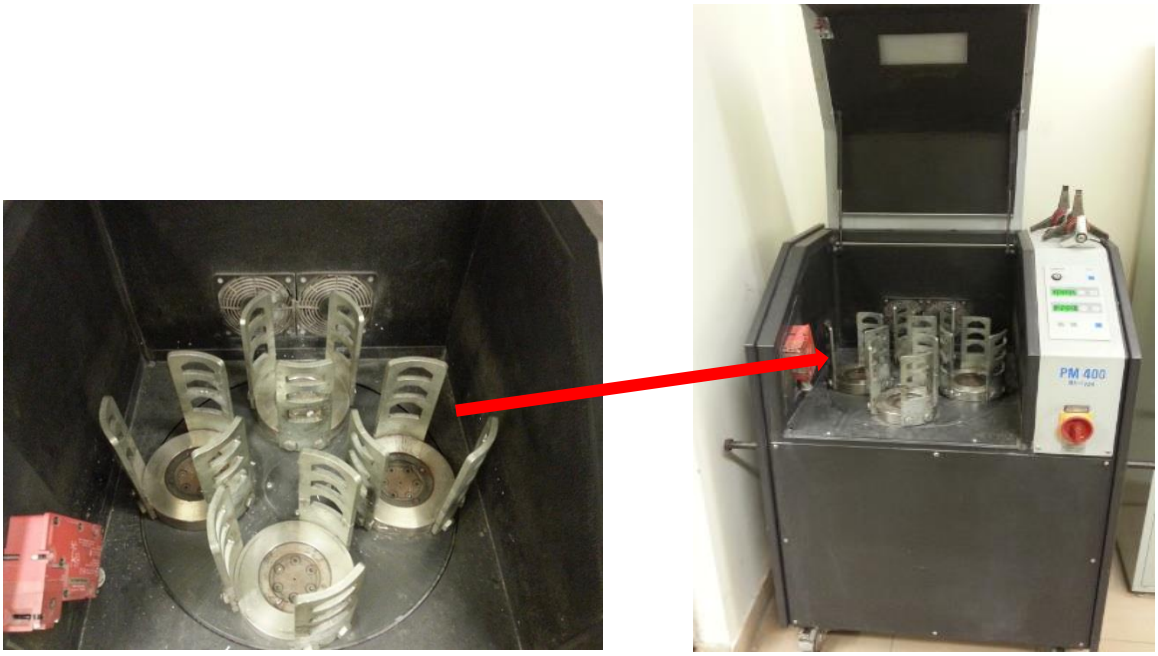

Figure 16 Stainless Steel container holders (Left) in Planetary Ball Milling Machine (Right)

The reason why one resorted to ball milling to mix the powders instead of simple mixing, for example using a Turbula mixer, was that the CNTs have a very small size and thus they tend to cluster together and agglomerate. Ball milling helps disperse the CNTs homogeneously together as the Al and CNT powders were put together in the stainless steel containers with the 42 stainless steel balls which start moving around at a high speed hitting the powders and breaking any clusters, Figure 17.

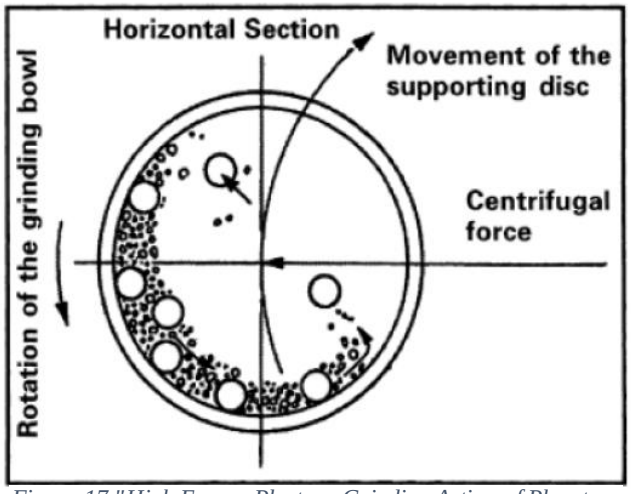

Figure 17 "High Energy Plaetary Grinding Action of Planetary Mills", figure adopted from Esawi, "MENG 530: Nanostructured Materials", 2014

Since the ball milling is a high energy process, thus to prevent heat build-up inside the containers the machine was set on an automatic program that would have it working for 10 min, then to remain inactive for twice the period, i.e. 20 min, and so forth. So, for a total hour of actual milling, the machine worked 3 hours; 1-hour milling and 2 hours resting.

Milling Parameters

The speed of rotation of the containers	400 RPM
The relative ball weight to powder ratio	5:1 respectively
Total Milling Time	3 hours
Actual Milling Time	1 hour

Step 3: Powder Transfer

After ball milling, the stainless steel containers were taken back to the glove box, where the tightly sealed milling containers were opened and the powders transferred to tightly-sealed glass jars as shown in Figure 18. It was important to take this step inside the glove box's inert gas environment as it will:

1. Prevent the powders from bursting into flames given that the ball milling process is a high energy one that adds considerable energy to the powders due to the rapid severe collisions that takes place inside the milling containers
2. Prevents the oxidization of the Al powders which would affect their properties.

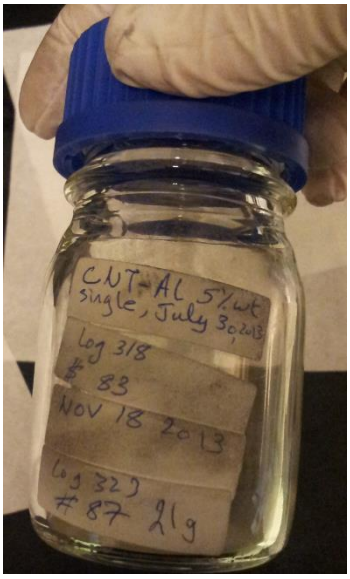

Figure 18 Glass Jar used in powder transfer to compaction machine

Step 4: Consolidation Process

i. <u>Compaction</u>

Powders were then transferred into a die, which has a cylindrical cavity. Uniaxial loading was then applied according to the following specifications: 35 bars for 1 hour at room temperature. Such pressure was achieved via employing a Hydraulic press machine, as shown in Figure 19. The output of this step is called a "Green Compact", which is simply the powders compacted into a cylindrical shape. Note: Before moving on to the next step, the Sintering, the extrusion tool/adaptor was attached to the die (this shall be explained later in the Extrusion step in more detail)

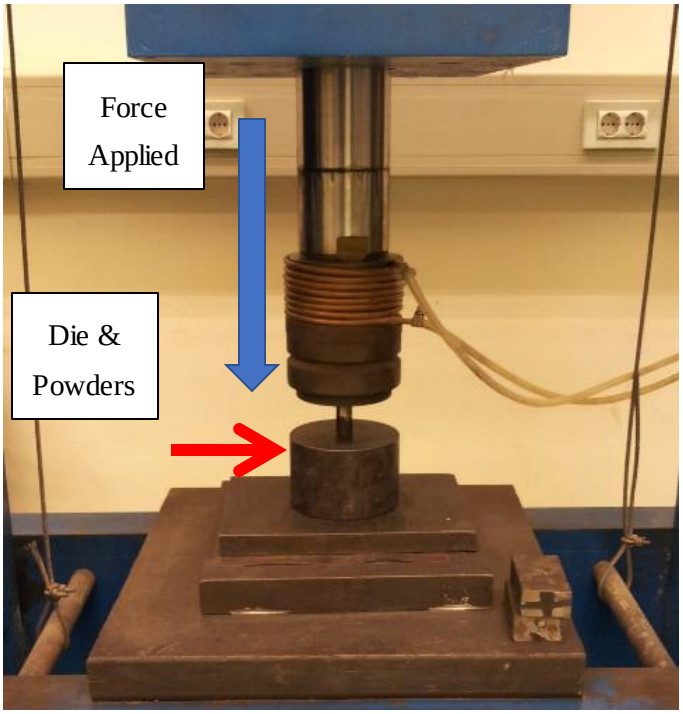

Figure 19 Hydraulic Press Machine

ii. Sintering

The die with the powders compacted inside it were then transferred to be put inside the loops of an electric heating coil, Figure 20, and then the coil and die were covered in a white heat insulator, Figure 21. The powders were left to heat at a high temperature for around an hour; The electric heating coil automatically adjusted the temperature to be on average 500 ± 10°C. A thermocouple was used to provide feedback of the sample temperature to the controller. Note: The electric heater device was properly calibrated before being used.

Figure 20 Electric Heating Coil - Sintering Step

Figure 21 Sintering Step: Left: the electric coil with the die inside and covered by white insulator. Right: Electric Heater Controller

iii. Extrusion

As mentioned before, prior to the sintering step, an extrusion adaptor/tool, Figure 22, was attached to the die using screws, so that right after the sintering step was done, the sintered powders were extruded at a ratio of 4:1, and the extrudate, Figure 23, had a final diameter of around 10 mm. This was achieved by putting the die plus the attached extrusion adapter on the Hydraulic press, and using a cylindrical ram, the compressed and now-sintered powders were pushed out of the die through the extrusion tool/adaptor.

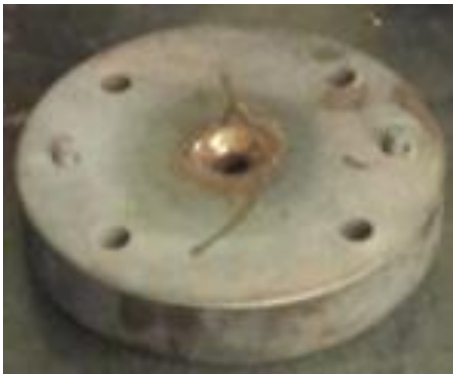

Figure 22 Extrusion tool to be attached

iv. Cooling

The extruded sample was left protruding out of the extrusion tool to slowly cool at room temperature till the following morning, a duration of roughly around 15-20 hours. Such slow cooling was advised in order to avoid any extra hardening of the sample that may turn it perhaps too brittle to the extent that it could break easily upon attempting to get it out of the die. Figure 23 depicts the extrudate after its removal from the die next day. Final extrudate diameter was 10 mm and length was roughly around 80-90 mm.

Figure 23 Extrudate sample after being removed from the die.

Step 5: Machining

The extrudate was then machined using the lathe machine, into 2 or 3 smaller cylinders, see Figure 24. The final diameter was specified based on the indicated Dilatometer device sample parameters that will be used in the next stage. Thus, the samples were machined into the following dimensions:

Figure 24 Cylindrical Samples: Extrudate machined into these small cylinders

Diameter: 4.5 mm **Length**: 15 mm

Around 2 extrudates of each powder category were produced, i.e. the five steps mentioned above were repeated at least 10 times (Twice per powder composition). **A total of 26 small cylindrical samples were produced** (some extrudates were irregular and yielded only 2 cylindrical samples, such as in the case of the 10% CNT-Al sample, which was always brittle and broke upon extraction from the die in step 4)

i.	Un-Milled Al	5 Samples
ii.	Milled Al	6 Samples
iii.	2% CNT- Al	6 Samples
iv.	5% CNT- Al	5 Samples
v.	10% CNT- Al	4 Samples

4.2.2. Cylindrical Samples - Testing

The Dilatometer

The device used to measure the CTE of different samples was the dilatometer: DIL 801, TA instruments, Figure 25. The system has the device plus a data capturing and a software analysis package. The device can be used to measure expansion of solid materials in air, inert gas or vacuum. It can cover a temperature range of -160°C to over 2000°C and CTE accuracy of 0.03 x 10^{-6} K^{-1} ("TA Instruments-Dilatometry" manual)

Figure 25 DIL 801, "TA Instruments – Dilatometry" manual

Test 1: Measured CTE

1. The length and the diameter of the cylindrical sample was measured once again using a Vernier caliper and was recorded into the PC software controlling the device
2. Each sample was put inside the sample tray of the dilatometer, see Figure 26.

Figure 26 Dilatometer Sample Tray, adopted from "TA Instruments – Dilatometry" manual

3. The device heater was turned on. The heating rate was set to be 5°C /min. Heating range was set to be from ambient temperature to around 490°C.

The heating rate was adopted from the literature (Tang et al, 2004), and the heating limit of around 490°C was set to avoid reaching a critical stage where Al will start to melt and damage the device. The resolution of the data recording process was set to be very high, meaning that the data were recorded at every small change in temperature (around 0.1-0.2°C), however, for the sake of convenience, the CTE readings were shown here at steps of 10°C.

Test 2: Measured Electrical Resistance

The same samples used in CTE measurements were used in the electrical resistivity measurements. The device used was a simple HP DC generator, Figure 27. The setup is shown in Figure 28, where the cylindrical sample was connected to the generator via crocodile wires. Electrical resistivity is defined as:

Figure 27 DC Generator used in Electrical Resistivity Measurement

$$\textbf{Resistivity} = \frac{\textbf{Resistance X Area}}{\textbf{Length}}$$

Since the area and the length of the samples were almost identical, therefore via measuring the resistance, one could get a good indicator of the electrical performance of the samples in terms of their resistivity. Resistance was indirectly measured via varying the voltage and measuring the corresponding current (I) reading, as shall be explained.

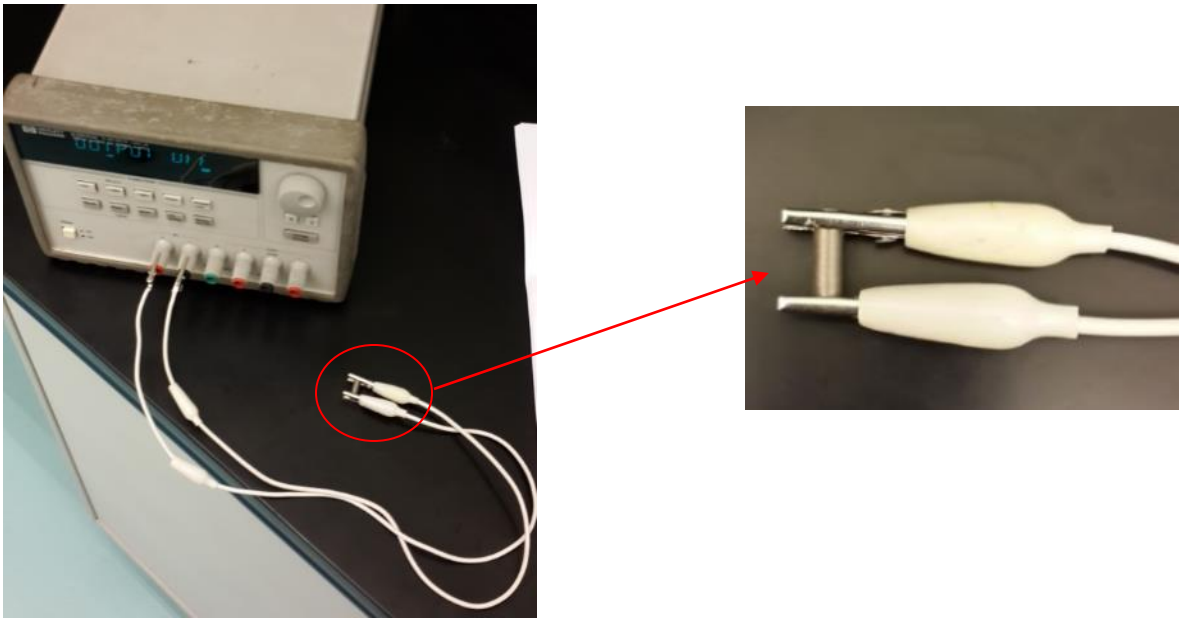

Figure 28 Electrical Resistivity measurement device setup (Left), A Sample connected at its ends by crocodile wires (Right)

The steps for determining the resistivity of the 26 cylindrical samples are:

1. Connected the two ends of a cylindrical sample via 2 crocodile wires to the positive and negative terminals of the DC generator, Figure 28.
2. Varied the voltage from 100 to 1600 mV, at increments of 100 mV and recorded the corresponding value of the current. The reason behind choosing the 1600 mV as the upper limit for the range of testing was because it was noted that beyond it, the crocodile wires heat up and the resistance values changed considerably afterwards; they started to decrease quickly and became very unstable.
3. After the range was covered, the generator was switched off, the wires were left to cool and then the sample was replaced with the next one. It is worth noting that, like in the case of taking the CTE readings, the recorded current readings were randomly taken, meaning that no specific pattern was adopted.
4. Voltage - Current curves for each of the 26 samples were plotted and the resistance of each sample was obtained from the slope of its corresponding trend line.
5. The resistances of each powder category was compared to the other in order to get an idea about the effect of adding CNT on the electrical resistivity. For further details, kindly check the Results section later on.

4.3 Part 2: Wafer Samples

See Figure 29 to view a graphical representation of the main sections of part 2

1. Prepared Al powder-based pastes using the following powders:
   i. Un-Milled Al Powder: (named: Paste 1)
   ii. Milled Al Powder (named: Paste 2)
   iii. 10% CNT-Al Powder (named: Paste 3)
2. Printed Al paste on the backside of a set of 9 Silicon wafer samples:
   i. Un-Milled Al Paste (Printed on 3 Silicon wafers)
   ii. Milled Al Paste (Printed on 3 Silicon wafers)
   iii. 10% CNT-Al Paste (Printed on 3 Silicon wafers)
3. Measured the bow and warp of the silicon wafers before and after heat application. A "Contactless Wafer Geometry Gauge" device was used

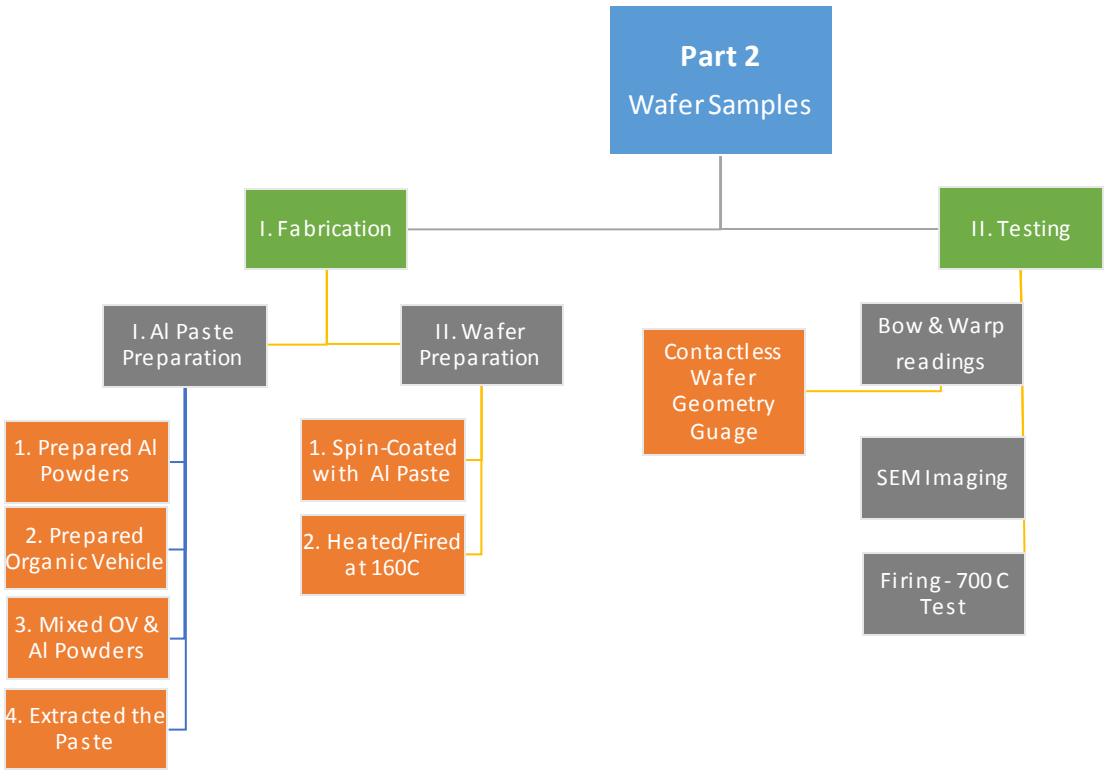

Figure 29 Roadmap of Part 2 of Methodology section – Wafer Samples

4.3.1 Al Paste Preparation

Original Al Paste recipe

The recipe for the Al paste preparation was adopted from a patent by Kim et Al. (2012). The main recipe outlined in the work goes as follows:

1. **Al powder**

   Constitutes 74% of the total weight of the paste, particle size can be in the range of Nano or a Micro meter scale.

2. **Antimony Oxide**

   Considered to be the proposed active agent that will act on reducing the overall CTE of the Al composite

3. **Organic Vehicle**

   Constitutes around 24% of the total weight of the paste, and is used to allow the mixing and the printing of the paste. It is usually made up of:

   i. Binder resin: Ethyl Cellulose

   ii. Solvents: Terpineol and
   Butyl Carbitol Acetate or BCA (diethylene glycol monobutyl ether acetate).

   The ratio of Ethyl Cellulose: Terpineol: BCA is 1:4.5:4.5 in terms of their respective weights.

4. **Glass Frit**

   Can be lead-based or lead-free. The one used in the main recipe was Lead-based glass frit with a ratio of 1% of the total weight of the paste. Its use is optional.

5. **Dispersant**

   Can be either of the following acids - stearic, palmitic, myristic, oleic acid, or Lauric acid. The weight could be around 0.5% of the total weight of the paste

For the purpose of the current research, the original recipe was modified by limiting the constituents to include only:

1. Al Powders 2. Organic Vehicle: Binder and solvent

Experiments made using the original recipe resulted in mixtures that were found to be extremely viscous, and thus the printing of the paste on the wafer was unsuccessful, resulting only in a dry smudge on the wafer (given the available printing resources that shall be described later in the following section).

Thus it was important to experiment in order to come up with a less viscous mixture that could still hold the Al powders and be easily printed afterwards. Hence, after many trials during which the ratios of the constituents of the organic vehicle as well as the ratio of the organic vehicle to the Al powders used were changed, the modified version of the original patented recipe for the Al paste was adopted.

Modified Al Paste recipe

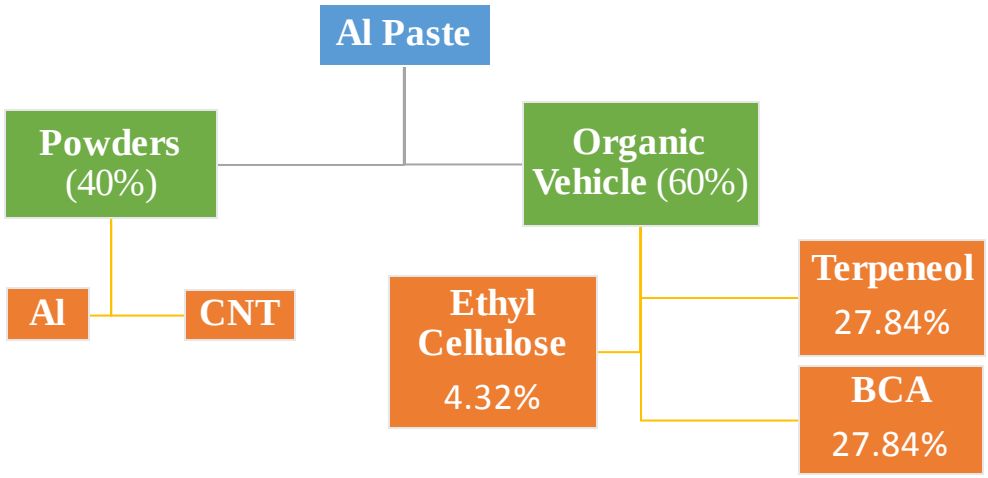

Figure 30 Modified Al Paste Recipe

Figure 30 shows a graphical representation of the constituents of the modified Al-paste recipe.

1. **Al powder**

   Constitutes around 40% (instead of 74%) of the total weight of the paste, particle size can be in the range of Nano or a Micro meter scale.

2. **CNT**

   CNT replaced Antimony Oxide as the active agent in such a way that of the 40% constituting the Al powders mentioned above, 10% were to be replaced with CNT, if a CNT-Al paste was to be prepared. However, if the user wishes to have a pure Al paste, without CNT, then the 40% of the total paste weight allocated to the powders will be only Al powders.

3. **Organic Vehicle (OV)**

   Constitutes around 60% (instead of 24%) of the total weight of the paste as follows:

   i. Binder resin: Ethyl Cellulose

   ii. Solvents: Terpineol and BCA

   The relative weight ratios of the Ethyl Cellulose to the Terpeneol & BCA are: 3.1:20:20 respectively. These together form 60% of the total paste weight.

It was found that preparing 85g of the paste was enough to cover 3 wafers, as shall be later shown, i.e. 51g of OV and 34g of powders were mixed together to give the amount of paste needed to prepare 3 wafers, see Table 3

Table 3 For 85g of paste produced, these were the weight amounts of the OV and the Powders according to the modified recipe

Organic Vehicle Constituents (g)			Paste Constituents (g)		(g)
Ethyl Cellulose	Terpineol	BCA	OV (Sum)	Powders	Total
3.67	23.67	23.67	51	34	85

Note

In reality, the 51 g of the OV was made 52g to account for the milling process that may cause evaporation of the OV, as shall be shown later.

Step 1: Preparing the Powders

The following powders were prepared:

1. Un-Milled Al 34g see Figure 31
2. Milled Al 34g see Figure 32
3. 10% CNT-Al 34g see Figure 33

The procedure for preparing the powders was the same as the one mentioned earlier for preparing the cylindrical samples, except in the case of the 10% CNT-Al powders, the PCA was not used this time. According to the recipe, a total of 34g of each of these powders were required, hence 2 milling containers were used, each yielding around 27-29g of powders per stainless steel container. In the case of the 10% CNT-Al powders, which tended to stick to the milling container from inside (which can be attributed to not using the PCA) forming a very strong layer, this led to a decrease in the yield of the milling container to become around 17-18g of powders.

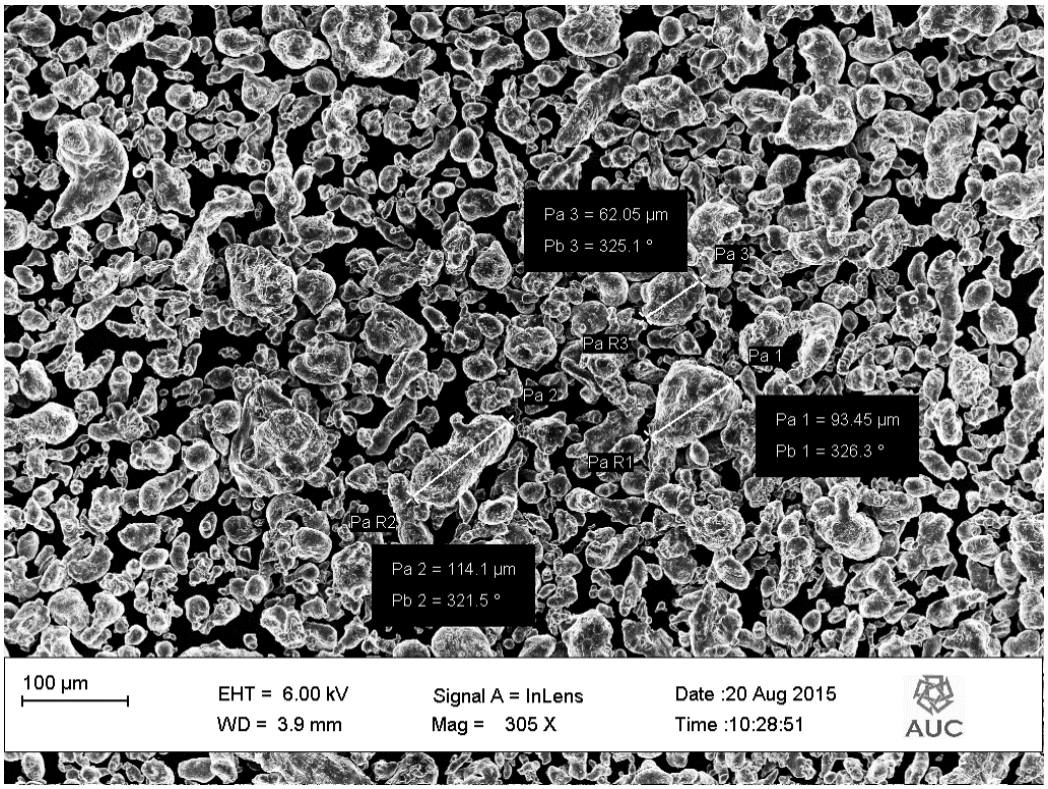

Figure 31 SEM image of the Un-Milled Al Powders

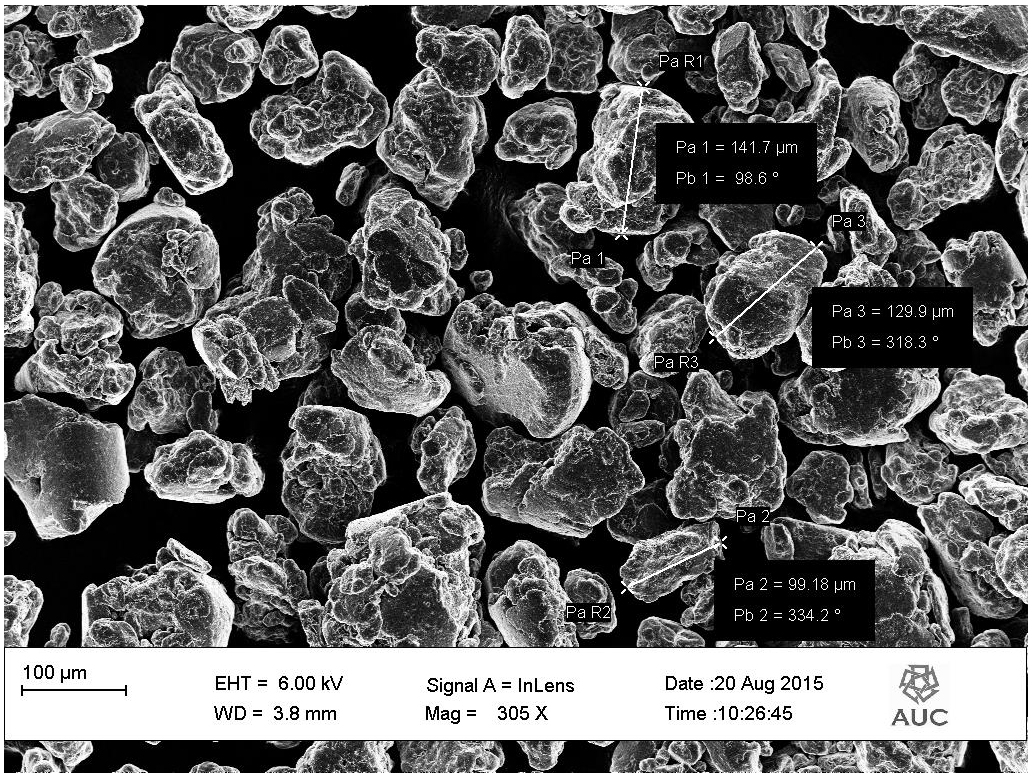

Figure 32 SEM image of the Milled Al Powders

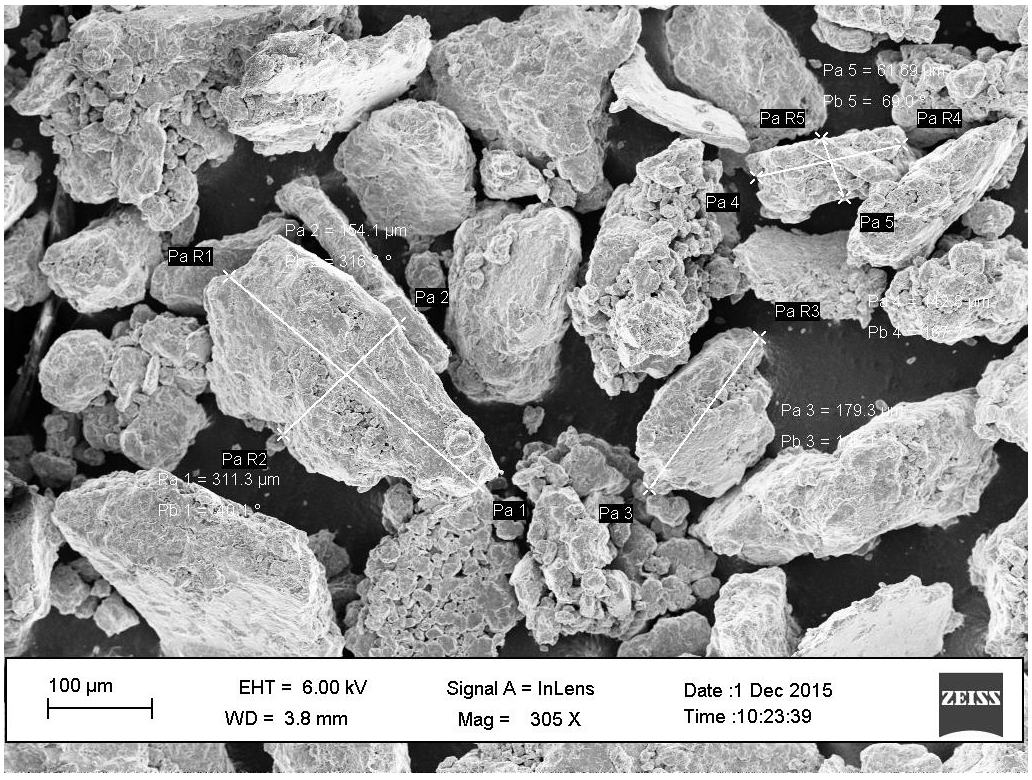

Figure 33 SEM image of the 10% CNT- Al Powders

Observations

It is worth noting that the average particle size for the Un-Milled Al powders (estimated to be around 60 µm), Figure 31, was lower than that of the Milled Al (around +120 µm), as shown from the dimensions on the SEM image in Figure 32. The 10% CNT-Al powders, Figure 33, however were showing particles of relatively large and small sizes (150-300 µm and around 20 µm respectively). This was attributed to the partial disintegration of the particles during milling due to time limitations. It is worth noting that the smaller the particle size, the easier the mixing of the paste later on.

Step 2: Preparing the Organic Vehicle

To ensure consistency throughout the experimental process, a large amount of the OV was prepared in advance. From this OV stock all subsequent Al paste formulations (Un-Milled Al, Milled Al and 10% CNT-Al pastes) were prepared. The OV recipe followed is outlined in Table 4 OV Recipe for bulk OV production below. These were the same ratios as those in Table 3 for the Ethyl Cellulose, BCA and Terpineol, however, the bulk amount prepared now was 431g and not just 51g as before.

Table 4 OV Recipe for bulk OV production

OV Constituents	Ethyl Cellulose	Terpineol	BCA
Weight Ratio (g)	31	200±0.05	200±0.05

A powerful kitchen blender (800 Watt) with sharp blades, was used to ensure the quick and thorough dissolving of the Ethyl Cellulose in the Terpineol + BCA mixture. This method of mixing was resorted to after many hours of fruitless high energy milling, as the Ethyl Cellulose is a very sticky material that tends to stick to the balls of the milling container rather than break and dissolve.

The OV was prepared as follows:

1. In a glass beaker, 31g of Ethyl Cellulose were measured
2. The jug of the blender was put on a highly sensitive digital balance (hundredth of a gram) and the reading was zeroed.
3. Using a medical syringe, the respective weights of Terpineol and the BCA, see Table 4, were added directly into the jug.
4. The jug was attached to the blender motor and the mixing was started.
5. While mixing the Terpineol and the BCA, small amounts of Ethyl Cellulose were added gradually to ensure complete dissolving of the latter.
6. The blending process did not stop till all the Ethyl Cellulose completely dissolved and the OV mixture became clear.
7. The OV was then stored in a tightly sealed glass container.
8. For extra precaution, the mixture was left overnight (around 12-15 hours) to further ensure that all the Ethyl Cellulose has properly dissolved before any of it was used.

Step 3: Mixing the OV & Al Powders

Following the preparation of the 2 main constituents of the Al Paste: the OV and the Al Powders were combined in a stainless steel milling container, Figure 34, and then milled together to properly dissolve the powders in the OV prepared. Note: Anytime the OV was used, the whole stock was transferred from the glass container to the blender to be thoroughly mixed for a few minutes. After taking the required amount, the OV was returned back to the glass container to be stored again.

The following were the amounts added per stainless steel milling container (see Table 5):

Table 5 Mixing ratios of the paste constituents per milling container

Al-Paste Constituents	OV	Al-Powders
Weight Ratio (g)	52±0.1	34±0.05

The milling process parameters are:

i. Duration: 30 min
ii. Rotational Speed: 250 rpm
iii. 42 Stainless steel balls / container

Note: According to the modified recipe, the ratio of the OV and the powders to the total weight of the paste should be 60 to 40 to 100 respectively, i.e. the weight of the OV in the paste should be 1.5 times the weight of the powders, so one would have to add to the 34 g of the Al powders a 1.5 x 34 = 51g of OV, however, an additional gram of OV was added to account for any evaporations of the OV due to the high temperature that results from the milling process.

Figure 34 The Organic Vehicle (OV) inside the milling container

The milling speed was set to be 250 rpm instead of 400 rpm as it was noticed from the experimentation phase that high milling speeds and durations created a lot of heat inside the milling container which caused the OV to evaporate and hence reduced the viscosity of the extracted paste. So, after several trials, it was found that the above-mentioned parameters produced a well-mixed paste with an acceptable level of viscosity.

Step 4: Extracting the Paste

Following the milling step, the paste was transferred into a tightly sealed glass jar, the same as that used earlier to store the Al powders. This extraction process was done using a funnel and a sieve, Figure 35, to avoid any spills while transferring the paste, and to extract as much paste as possible. The paste extracted from one milling container had a total volume of much more than 30 mL of paste, more than enough to cover 3 wafers.

Figure 35 Transferring the paste from the milling container to the glass jar

It is extremely important to note that the paste should be used within hours of processing, for it tends to split into phases after being left overnight, meaning that part of the OV becomes separated from the thicker denser phase of wet powders (Al powders + some OV). This splitting can be reversed by thorough mixing again, however, due to the fact that milling is a high energy process, extra milling might lead to evaporating the OV which may increase its viscosity and hence make the spreading of the paste over the silicon wafer later on harder to achieve. Also, since the amounts of Al paste prepared were not large, and - as just mentioned - that the paste tends to stick to surfaces, thus the process of transfer from the jar to the milling container and back again to re-mix the paste will lead to further losses in the paste amount. The splitting could perhaps be attributed to the fact that the OV in the modified recipe developed specifically for this study was present in

much more quantity than the recommended amount in the original recipe, hence the excess would simply separate from the rest of the OV that had already mixed with the powders.

The output of this step was three glass sealed glass jars containing 3 types of Al pastes:

1. Un-Milled Al powder-based paste (Paste 1)
2. Milled Al powder-based paste (Paste 2) Figure 36
3. 10% CNT - Al powder-based paste (Paste 3) Figure 37

Figure 36 Milled Al powder-based paste

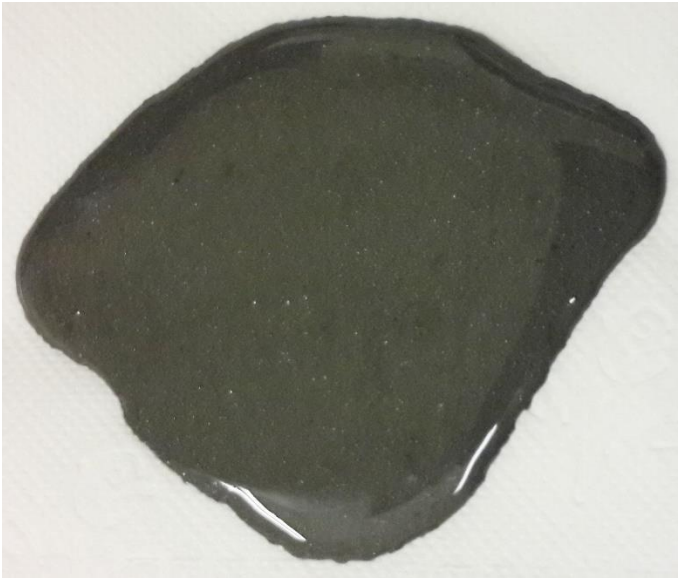

Figure 37 10% CNT-Al powder-based paste

Note there is a color difference between each paste: the milled Al paste, Figure 36, had a silver shiny appearance, while due to the presence of CNT, the 10% CNT-Al paste had a black shade, Figure 37.

4.3.2 Silicon Wafer Sample Preparation

The wafers were obtained from Addison Engineering Inc., with the following basic specifications:

Resistivity: 4-6 Ohm-cm

Grade: Prime

Diameter: 6 inches

Thickness: 625 ± 25 μm

Step 1: Spin Coating – Al Paste

Following the preparation of the three main Al pastes mentioned in the previous section, the next step was to spread the paste over a silicon wafer. The technique followed to do that was the "Spin Coating technique". Basically, the spinner device, see Figure 38, has a circular platform which can rotate according to a predefined program.

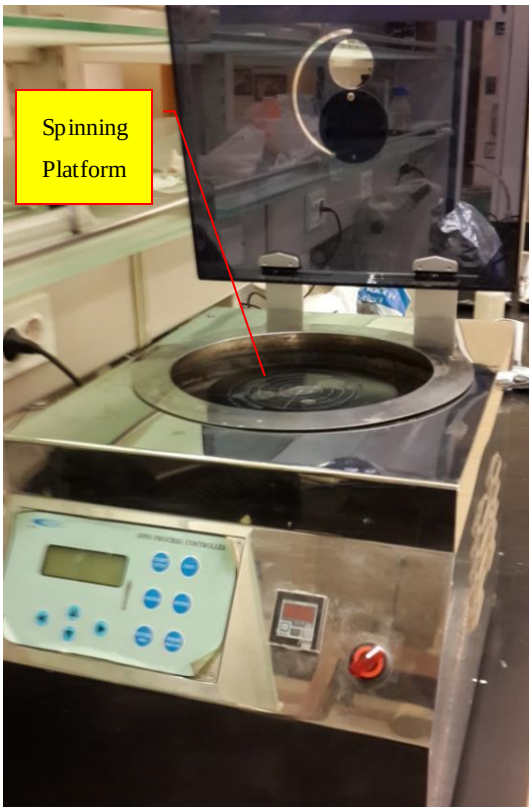

Figure 38 Spin Coater Device

The spin coating step went as follows:

1. A silicon wafer was mounted on the device which uses a vacuum pump to fix the silicon wafer in a contactless fashion. The wafer was put in the center of the mounting platform via following the guidelines drawn on it. The polished side was set to point downwards, so that the paste would be printed on the backside of the wafer; the unpolished side.
2. Using a medical syringe, 10 ml of the paste prepared earlier was measured and then added at the center of the silicon wafer. Each jar of the 3 pastes developed in the previous step provided enough paste to cover up to 3 wafers.
3. Before spinning, the paste drop was left to settle on the center of the wafer for a brief period (30 to 90 seconds). This was done to avoid the paste spluttering when rotated at a high speed.
4. The spinning program was initiated; its parameters were:
   i. Accelerate from 0 to 650 rpm in 10 seconds
   ii. Total duration of spinning was 10 seconds i.e. the wafer will accelerate from 0 to 650 rpm in 10 seconds then stop once the 650 rpm was achieved.
5. Process was repeated 9 times; 3 times per each of the 3 Al Paste jars produced before, resulting in 9 coated silicon wafers.

Notes regarding the Spin Coating Step

The parameters of the spinning program were set based on experimentations with the paste compositions and the spreading quality. It was found that at very high speeds (+1000 rpm), the paste did not cover all the wafer which may be attributed to perhaps problems in the spinning mechanism not being 100% horizontal or that the paste itself splits and its wet contents fly off the wafer.

In the case of the first 3 prepared samples using paste 1, the spinning program was not strictly adopted, it was rather based on short bursts of the program combined with visual feedback to determine if the paste has completely covered the wafer. For the remaining 6 samples developed from pastes 2 and 3, the spinning program was identical and was strictly applied. This rather affected the thickness of the layer spread, as shall be shown in later results, of the first 3 wafers but otherwise, in all cases, the paste was spread all over the wafer, see Figure 39.

Figure 39 Spin Coating Al Paste: Early Trial. Coated Wafer on Spinning Stage/Platform

Step 2: Firing the Wafer Samples (160°C)

This step is the equivalent of the co-firing stage in the real industrial process of manufacturing solar panels. Basically, the 9 samples were transferred into a furnace, where a heating program was initiated. The program parameters were defined as follows:

1. Gradual heating from room temperature to 160°C, in around 1 hour.
2. Stay at 160°C for 3 hours and 15 min. Visual inspection showed that after around 2 hours of heating at 160°C, the samples seemed dry, however, the heating phase was extended by further 75 min to ensure complete dryness.
3. Total recorded heating time was 4 hours, 15 min.

As mentioned earlier, it is worth reminding once again that the co-firing process can go up to 900°C for a period of 1 to 5 min. The reasons why a similar firing profile was not adopted here are:

1. In the real co-firing process, the wafer moves from one firing zone to another at a high belt speed, a process which requires special belt furnaces not available at AUC.
2. The wafers naturally required relatively more time to dry than the average wafer developed in the industry because:
    i. The layer of the Al paste coated on the wafer was much thicker than that of the industry, the former being around 120 µm versus the latter being 40-20 µm. This was because the methods adopted for printing the Al paste were unconventional; unlike those used in the industry due to a limitation in available resources.
    ii. The modified paste used here had more OV, a liquid, than the Al powders.
3. A sample was tried with heating at 900°C, however, it failed. The Aluminum melted and collected in small visible spherical beads on the wafer surface. This was because in the industry, the wafers stay at the 900°C for a very brief period as it moves from one zone to another.

The spin coater device used did cover the wafer with paste, however it was noted that not all the paste was homogeneously distributed, as shall be shown later in the Results section. This led to the fact that some parts of the wafer dried faster than the others. Before settling on the above-

mentioned heating parameters, some samples were independently heated at 100°C, 150°C and 200°C. It was noted that samples heated more than 200°C, even for a small period of time, showed some powdering on the surface, indicating that the Al powders were not properly sticking to the wafer surface. Hence, to ensure the complete evaporation of the OV at a suitable heat gradient, it was recommended that, based on the experimental testing performed, the heating profile described above to be adopted, that the temperature of the heating should not go beyond 200°C.

Figure 40 shows that the Un-Milled Al Samples (first row) had a dull silver color, while the Milled Al Samples (second row) had a rather shining silver color, and the 10% CNT-Al samples had an almost black-grey color (third row). The color differences may not be fully apparent due to the printing quality, in reality there was a noticeable difference though between all 3 categories.

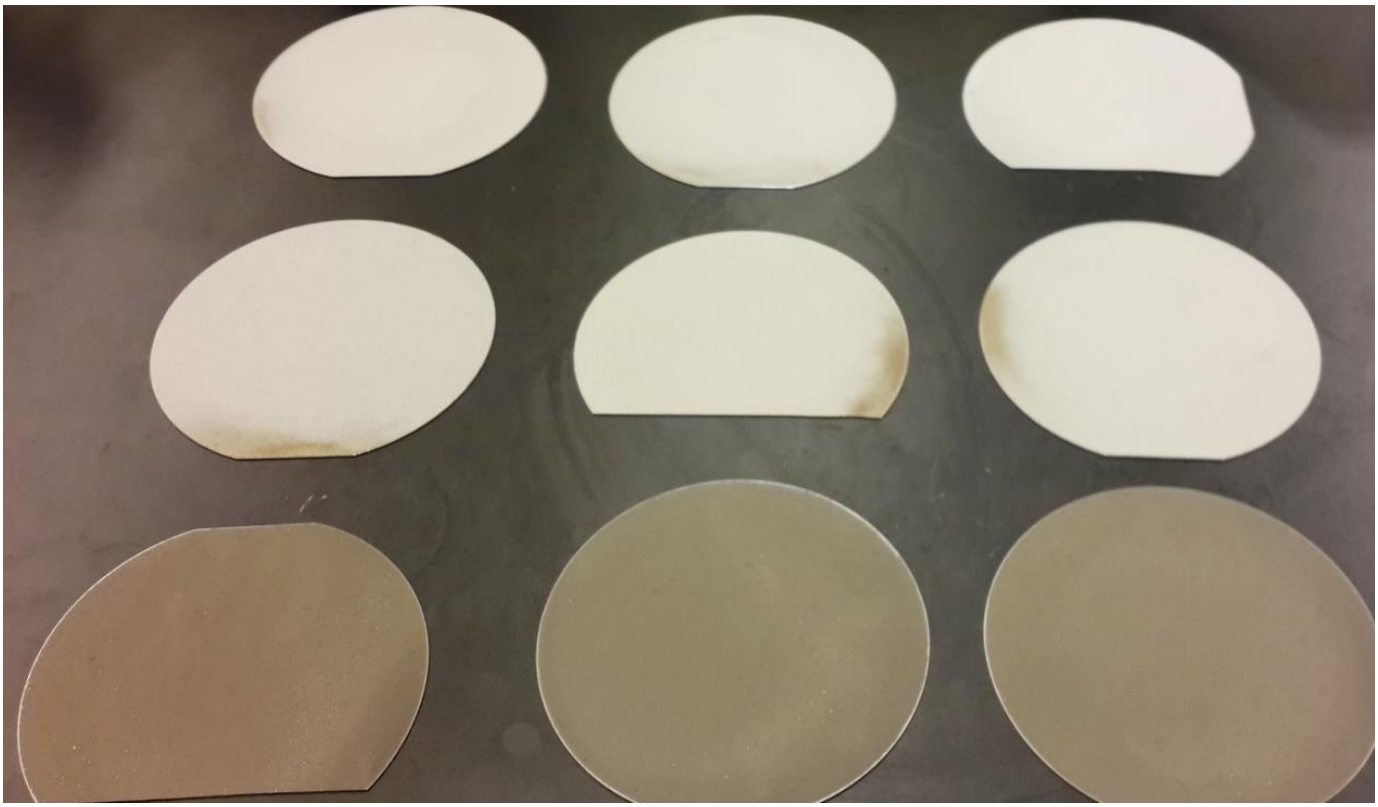

Figure 40 The 9 wafers after the heating and SEM sample cutting step

4.3.3 Silicon Wafer Sample Testing

The device used to measure the bows and the warps generated in the silicon wafers due to heating is called "Contactless Wafer Geometry Gauge", Model "MX 203-8-37", see Figure 41. It has a resolution of up to 0.1 µm, and can handle 150 mm and 200 mm wafers with 21 and 37 measuring points respectively, Figure 42.

Figure 41 "Contactless Wafer Geometry Gauge", Model MX 203-8-37. Figure adopted from Eichhorn Hausmann "MX 203-8-37 Contactless Wafer Geometry Gauge"

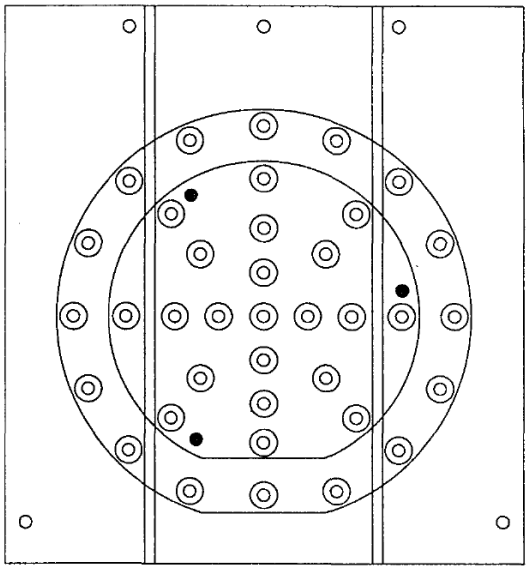

Figure 42 Plot of the measuring sensor points for the 150 mm and 200 mm wafer sizes. Figure adopted from Eichhorn Hausmann "MX 203-8-37 Contactless Wafer Geometry Gauge"

Step 1: Preparing Wafer Samples

During the spin coating step, some minimal amounts of the paste got on the other side of the wafer while it was being removed from the spin coater device. After heating, it was noticed that these smudges dried on the opposite side of the wafer and hence required cleaning. Acetone was used to remove these dried smudges, so that in the end the polished (front) side of the wafer was clean, and the un-polished (back) side or the lower side of the wafer was covered with a dried layer of Al paste as intended.

Step 2: Measured Thickness, Bow and Warp – Before and After Wafer Firing

The silicon wafer samples were measured for bow, warp and thickness using the Contactless Wafer Geometry Gauge device twice: once before printing the Al paste, and another time afterwards, so that the difference would represent the effect of the co-firing of the wafer with the paste coated on it.

The wafer was inserted into the device drawer with the polished side facing upwards, and the backside with the paste on it was downwards. The device has 2 plates each having a set of contactless capacitive sensors that basically measure the distance to the surface of the wafer which was inserted in between the plates. The device took less than a few seconds to provide a reading, then the wafer was replaced by the next one and so forth. This process was repeated for all 9 wafers.

<u>The following geometrical characteristics were measured:</u>

1. The average thickness
2. The bow in X and Y dimensions
3. The total warp of the wafer

Each of these characteristics was explained in more detail in the following pages, in order to get a better understanding of the readings presented in the results section.

1. The Average thickness

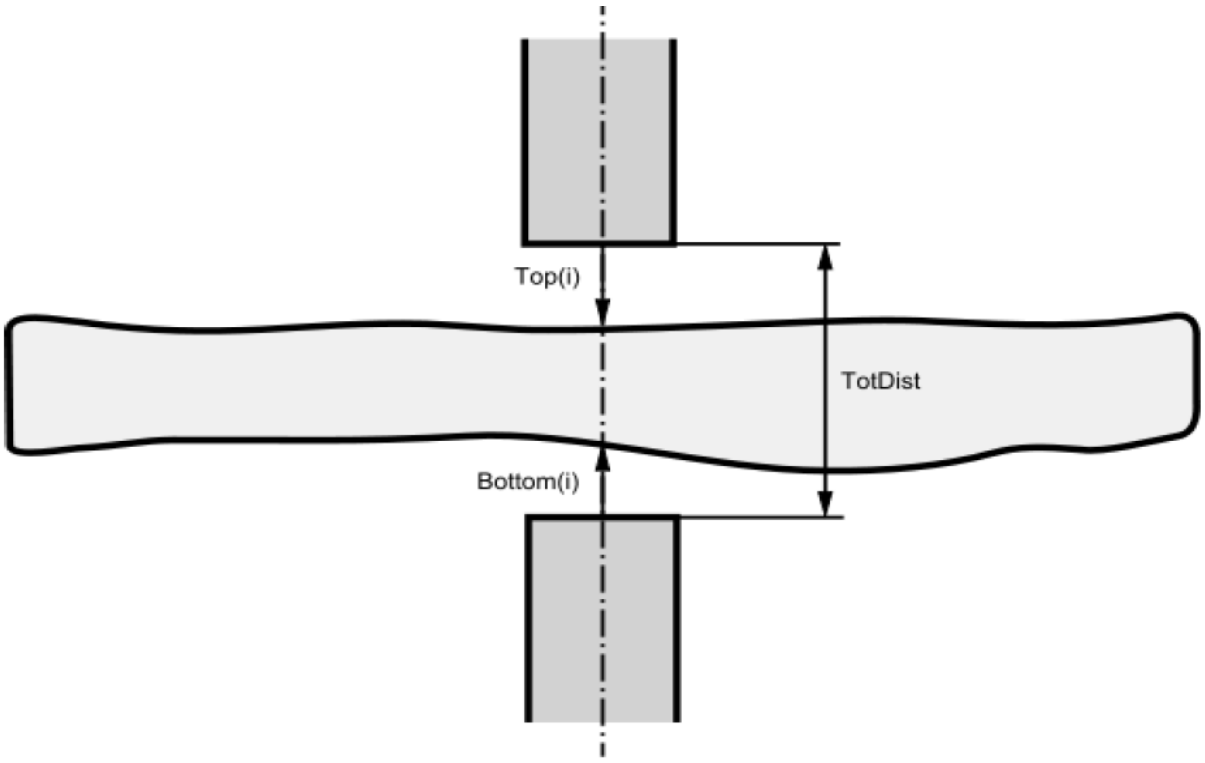

Figure 43 How the local thickness of a wafer is measured: Contactless Wafer Geometry Gauge device. Figure adopted from Contactless Wafer Geometry Gauge Manual, Eichhorn Hausmann, 2004.

Figure 43 shows how the variables outlined below were measured. Note that there is a set of sensors above and below the wafer.

Top(i): is the distance from the top sensor to the wafer surface, see figure 39

Bottom(i): is the distance from the bottom sensor to the wafer surface

TotDist: is the total distance between both sensors

LThk Local Thickness: Thk(i) = TotDist – [Top(i) + Bottom(i)]

AvgThk Average Thickness $= \frac{\sum Thk(i)}{n}$

i.e. summation of all the local thickness readings over their number.

StdThk Standard Thickness: Standard Deviation of the mean thickness

2. The Bow in X and Y dimensions

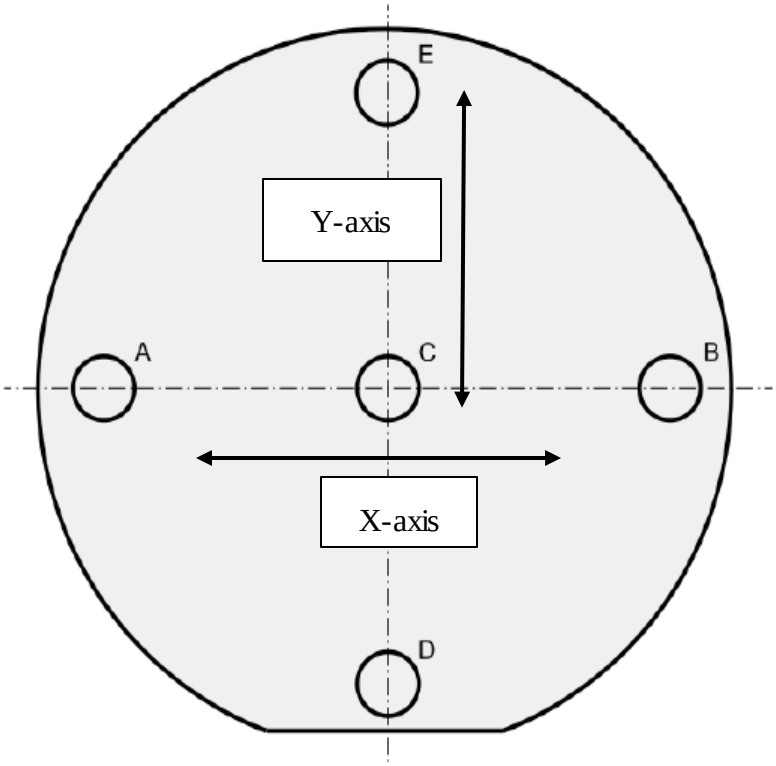

Figure 44 Top View: Main points on the wafer for Bow-X and Bow-Y measurements. Figure adopted from Contactless Wafer Geometry Gauge Manual, Eichhorn Hausmann, 2004

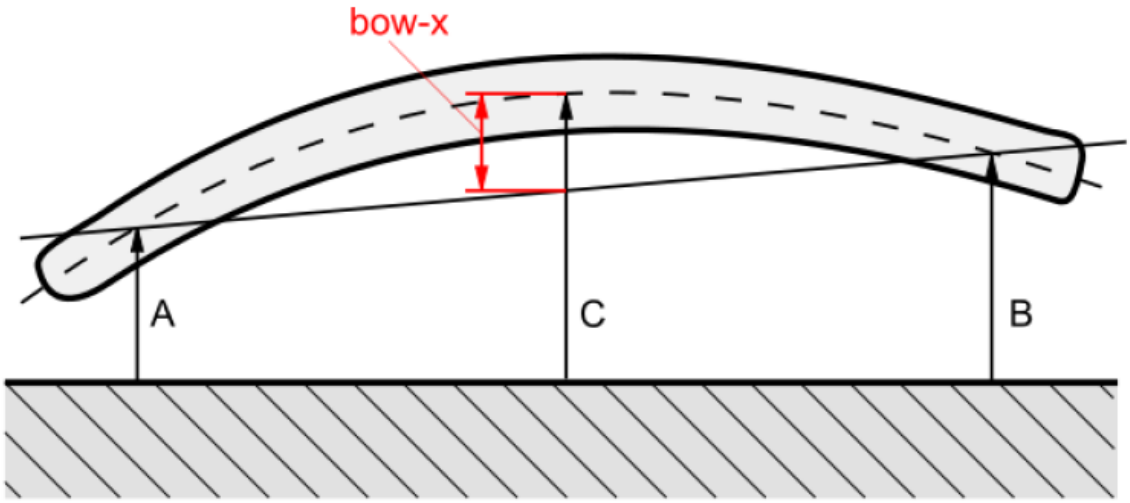

Figure 45 Cross-sectional View: How Bow-X is measured, Contactless Wafer Geometry Gauge device. Figure adopted from Contactless Wafer Geometry Gauge Manual, Eichhorn Hausmann, 2004

According to the device manual, see Figure 44 and Figure 45:

$$\text{Bow(X)} = C - \frac{A+B}{2} \qquad \text{Bow(Y)} = C - \frac{D+E}{2}$$

3. The Total Warp of the Wafer

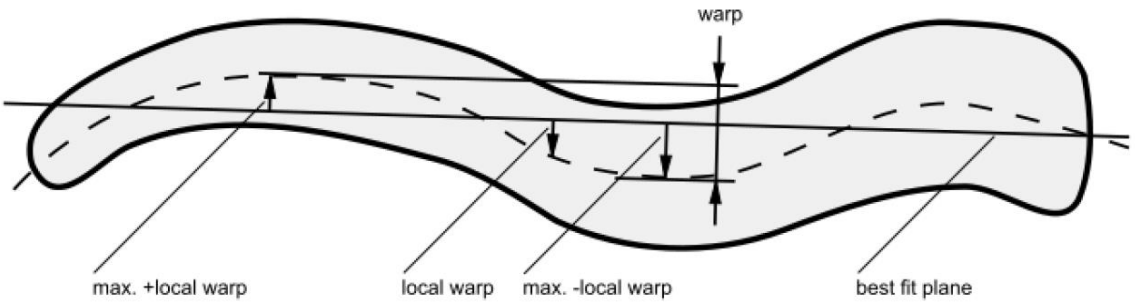

Figure 46 How the local and total warps of a wafer were measured: Contactless Wafer Geometry Gauge device. Figure adopted from Contactless Wafer Geometry Gauge Manual, Eichhorn Hausmann, 2004

A best fit plane is computed using the "least squares fit algorithm", Figure 46, and the deviations of the surface of the wafer with respect to this plane were the local warp values. There were deviations above and below the line, the max ones above and below the plane were called "max + local warp" and "max - local warp" respectively. The total warp is defined as the "sum of the absolute values of those 2 extrema" ("Contactless Wafer Geometry Gauge" manual, Eichhorn Hausmann GmbH, 2004)

Step 3: SEM Sample Preparation

To get a better understanding of the behavior of the paste, it was necessary to get SEM images of the top and cross-sectional views of the wafers. Since the SEM cannot contain large wafers in its compartment, hence it was required that part of the wafer should be cut to get an "SEM sample". So, of the 9 wafers prepared, 1 was chosen from each category; thus 3 wafers were cut using a simple diamond pen cutter to get 3 small rectangular pieces (around 1 cm x 1 cm).

Chapter 5

Results & Discussion

5.1 Roadmap

The chapter was divided into two main parts:

Part 1: Cylindrical Samples (see Figure 47)

I. CTE
II. Electrical Resistance

Part 2: Wafer Samples (see Figure 64)

I. Bow & Warp
II. SEM Images
III. Firing Test (700^{o}C)

In section 5.1, the CTE and the electricity measurements (volt and current) for all 5 sample categories (The Un-Milled Al, Milled Al, 2% CNT-Al, 5% CNT-Al, and 10% CNT-Al) were represented in graphs.

Another subsection was added to the CTE and electrical resistance sections; the normalization subsection. This is basically a section that offers a summarized view of all the representative sample readings, the latter were normalized, so that it would be easier to get a picture about the situation in one glimpse.

Note

For full CTE and Electrical measurements, check Appendix A and B, respectively. For the sake of reporting the results in a simple compact form, the readings were approximated to the nearest unit, i.e. for example: the last CTE value reported in the 20s temperature range (e.g. 29.99) was taken to be the CTE value at a temperature of 30^{o}C, and so forth.

5.2 Part 1: Cylindrical Samples

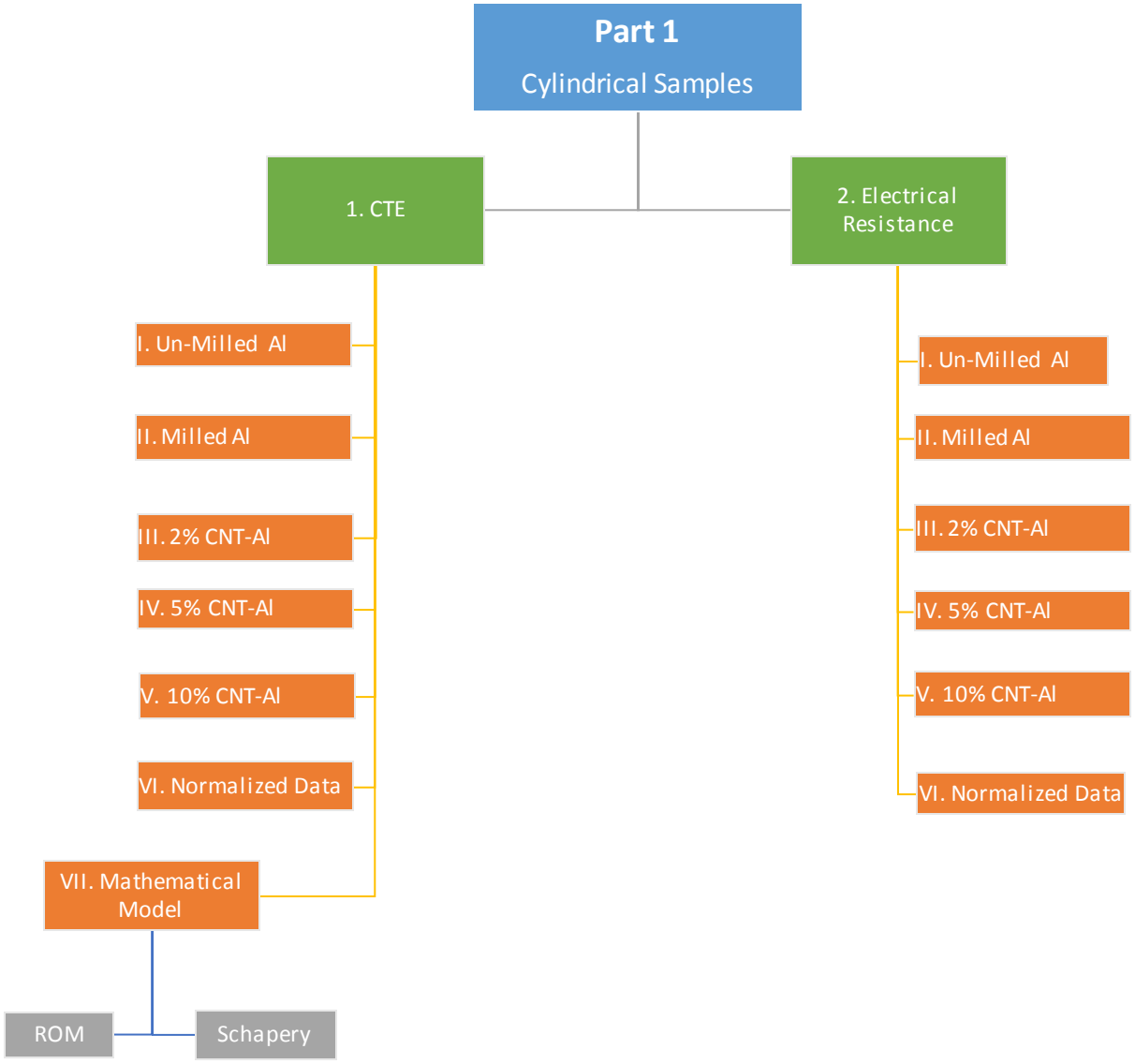

Figure 47 Outline of different sections of Part 1 of the Results & Discussion Chapter: Cylindrical Samples Part

Figure 47 is an outline of the first part of the results and discussion chapter, showing the different subsections so it would be easier for the reader to have an overview of the whole chapter.

5.2.1 Cylindrical Samples: CTE

I. Un-Milled Al Samples

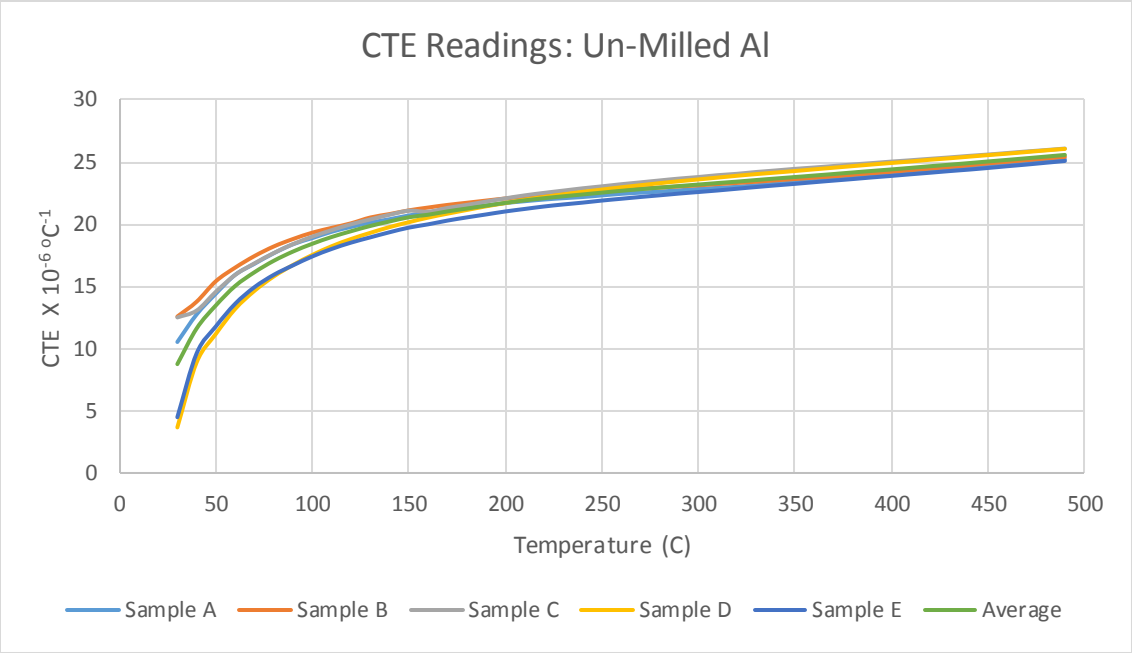

Figure 48 Un-Milled Al Cylindrical Samples: CTE Readings

II. Milled Al Samples

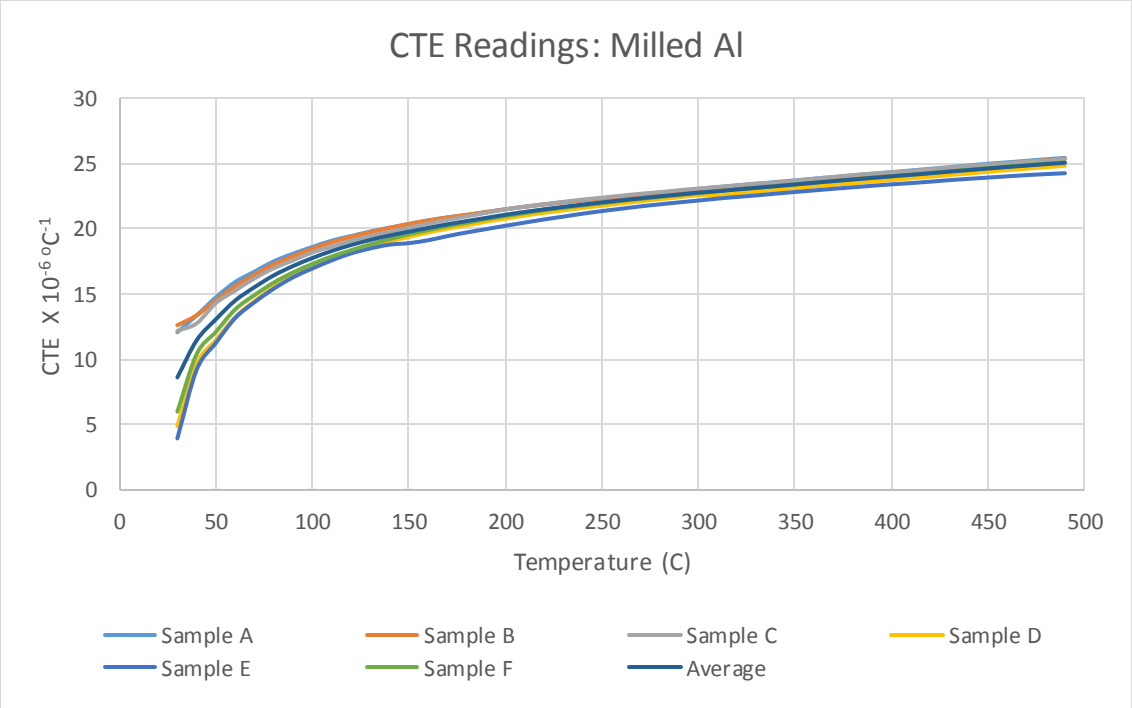

Figure 49 Milled Al Cylindrical Samples: CTE Readings

III. 2% CNT-Al Samples

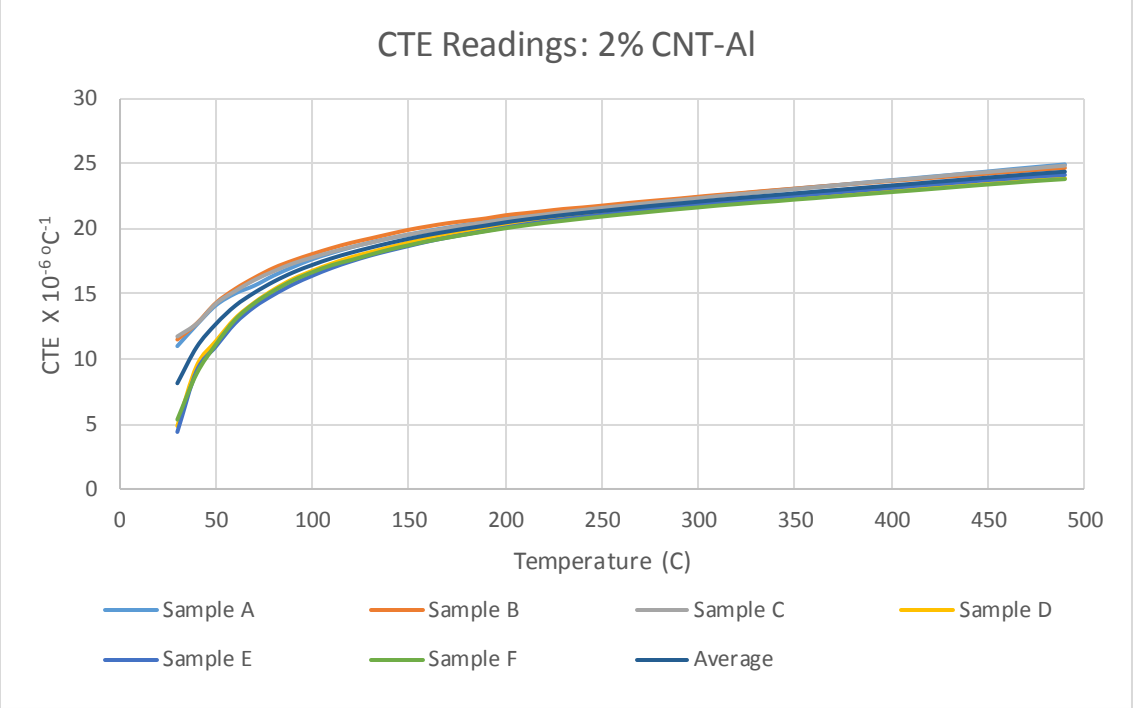

Figure 50 2% CNT- Al Cylindrical Samples: CTE Readings

IV. 5% CNT-Al Samples

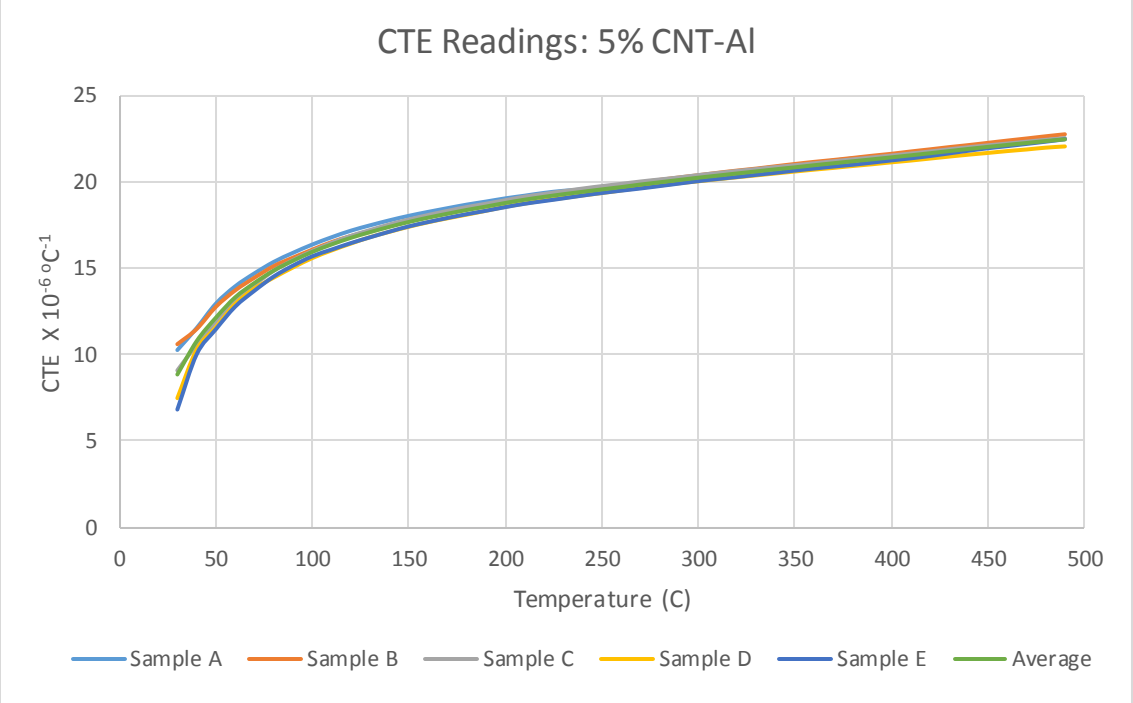

Figure 51 5% CNT-Al Cylindrical Samples: CTE Readings

V. 10% CNT-Al Samples

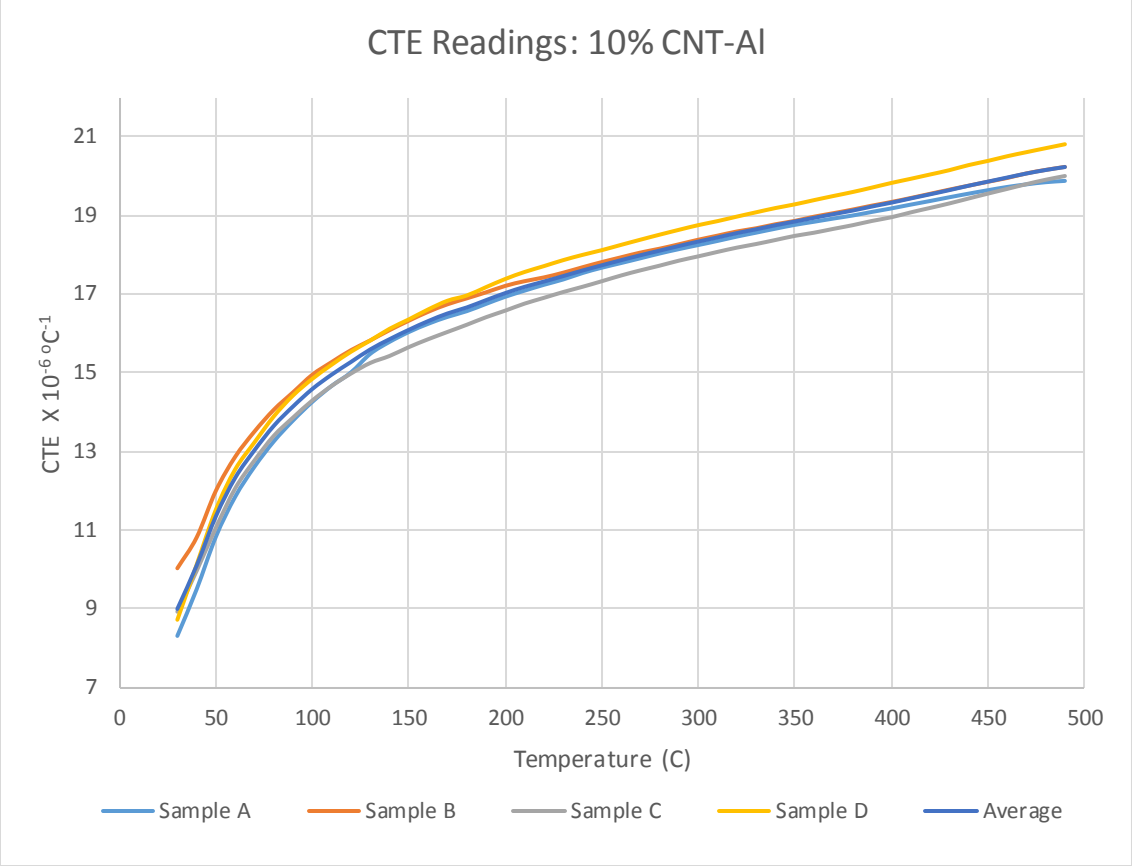

Figure 52 10% CNT-Al Cylindrical Samples: CTE Readings

Observations

Figure 48 to and including Figure 52 represent the CTE readings for individual samples of each powder category. Looking at any of these curves, starting from 100°C it is noticeable that the readings were all more or less clustered in a tight band, with little or no anomalies or outlier curves or exceptions. Taking into consideration that all CTE readings of the 26 cylindrical samples were randomly taken, this reflects positively on the precision of the results.

Also, comparing the graphs together, it seems that as the CNT content of the sample was increased from 0 to 10%, the CTE was reduced, as shall be shown in the next sections.

VI. Normalized Data

Figure 53 shows the CTE values for some of the selected samples for the temperature range from 100-490°C. This was done prior to normalization of the data.

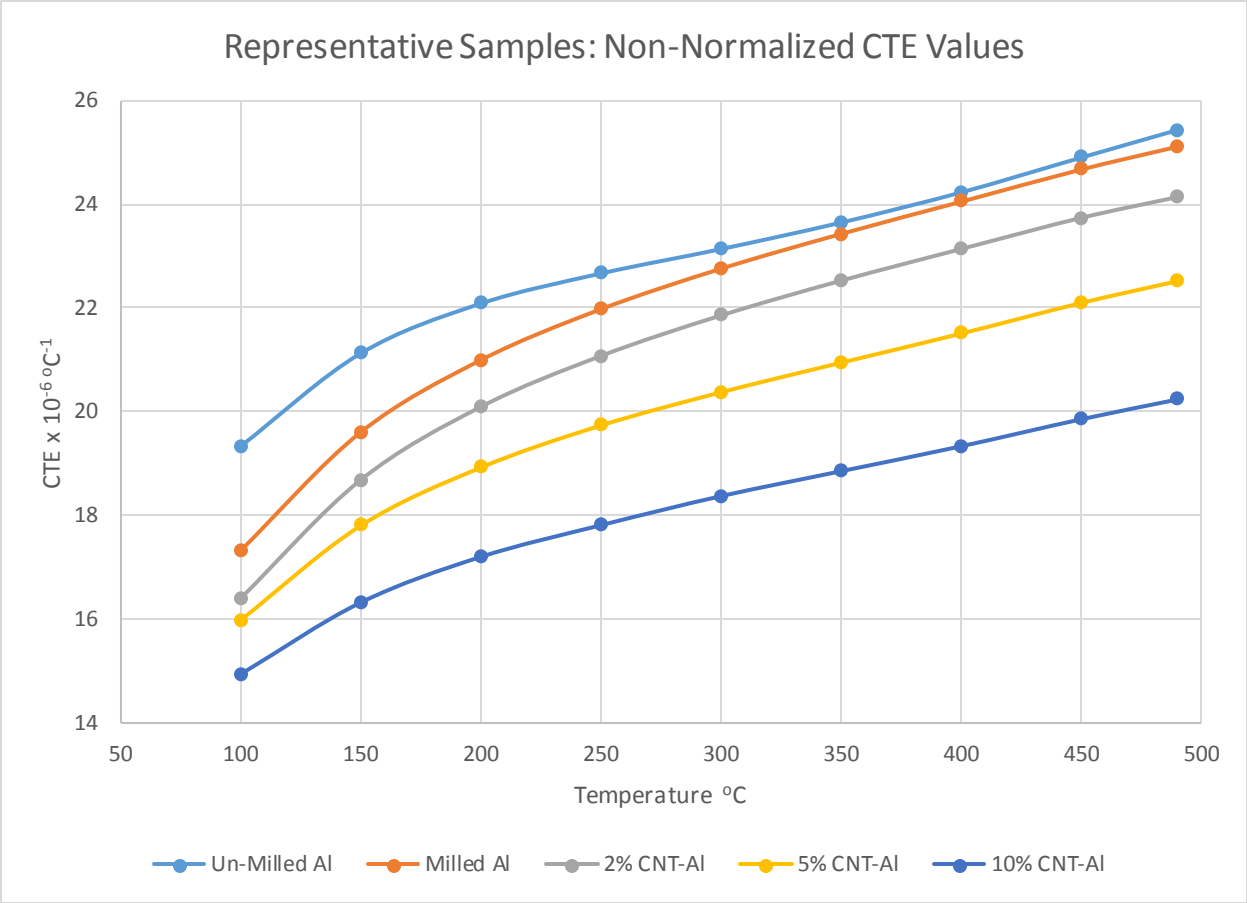

Figure 53 Non-Normalized CTE values of the Representative Cylindrical Samples

Figure 53 shows the CTE readings which were influenced by 2 variables:

i. The effect of the milling process
ii. The effect of the CNT addition

The CTE readings were then normalized to omit the milling effect, (the milled Al readings were taken to be the "Control") hence enabling direct comparison between the remaining samples to investigate the effect of adding CNT on CTE reduction alone, see Figure 54.

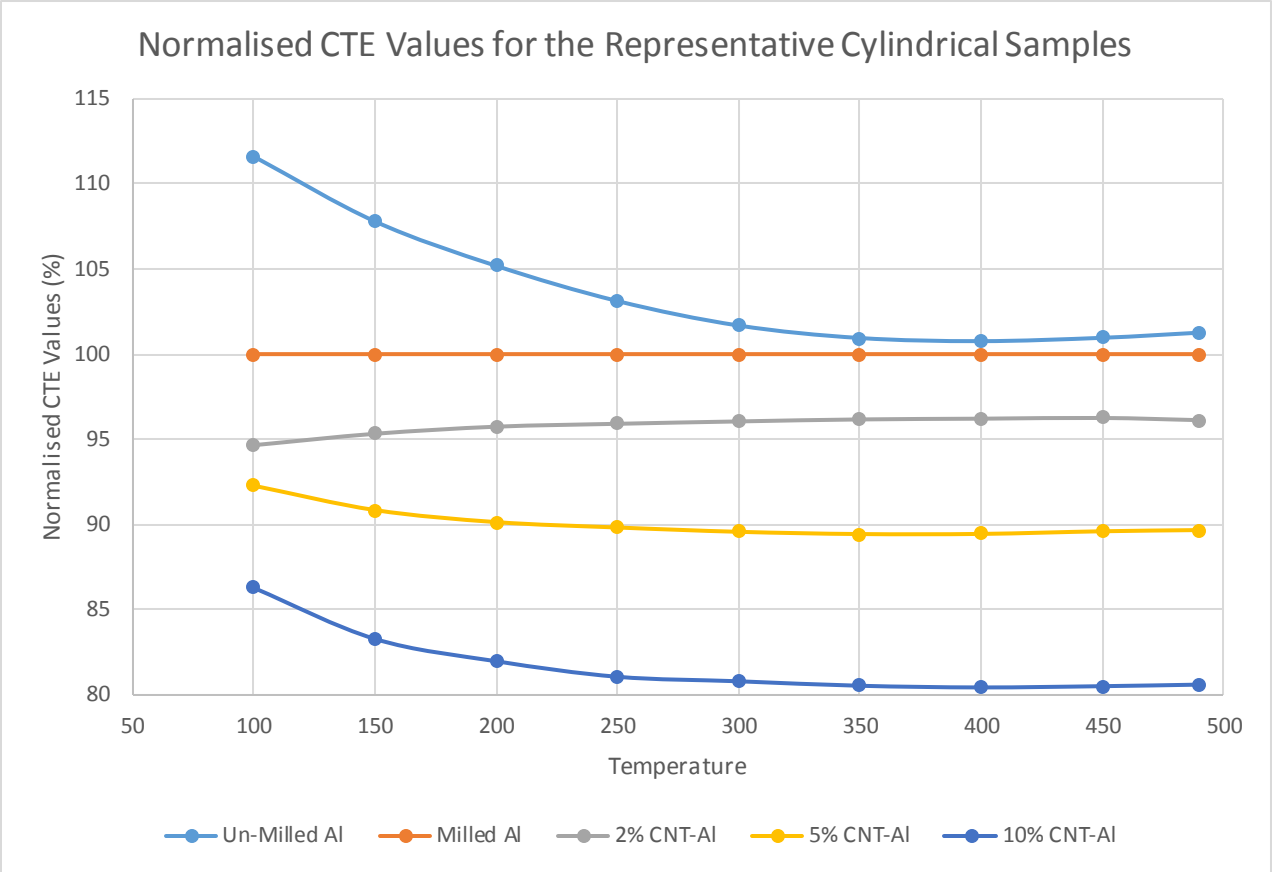

Figure 54 . Normalized CTE Values for the Representative Cylindrical Samples

Observations: Normalized CTE Values

According to Figure 54, 2 main points can be deducted:

1. Comparing the Un-Milled Al and the Milled Al curves, it seems that the milling process did have some effect on the CTE readings; causing a general reduction in the CTE readings. This effect varied however with temperatures as follows: at low temperatures (100°C) the effect was high decreasing the samples' CTE values by around 12%, however as the temperature of the samples increased the milling effect became less pronounced, reaching a low of around 1% at around 350-490°C
2. Comparing the Milled Al curve to the curves of the 2%, 5% and 10% CNT-Al, it was clearly shown that due to the addition of the CNT alone, in most cases the CTE has decreased for the given temperature range from 100°C and above. Having 10% of the total

powder weight as CNT has resulted in a max decrease in the samples' CTE by almost 20% compared to the CTE of the Milled Al sample readings.

3. The slope of the 10% CNT-curve was much higher than that of any of the other curves, so this supports another fact that the CNT addition increases the CTE change /^{o}C factor for the composite developed.

These observations agree with the main theory which states that since CNT has a lower CTE than that of Al, hence the former will not expand as much per a unit degree of temperature rise as will the Al. As mentioned earlier, according to the literature the CTE of the Al is $23x10^{-6}$ $^{o}C^{-1}$ (Soon-gil et Al, 2010), and in a study conducted by Tang et al (2004), it was found that the CTE of the coarse-grained and also the nano-sized Al to be ranging from $20\text{-}26x10^{-6}$ $^{o}C^{-1}$ for a temperature range of 100-250^{o}C, while in Figure 53 the CTE readings due to CNT addition was found to be in the range of $15\text{-}18x10^{-6}$ $^{o}C^{-1}$ for the same temperature range, i.e. around 20-30% CTE reduction was recorded compared to the Al CTE values recorded by Tang et al (2004). Thus, in essence the CNT did act as a hindering agent of Al expansion. A final note: it seems that the full hindering effect of the CNT was not achieved right away, but rather at a later temperature, in Figure 54 above, it was around 350-400^{o}C. However, this should not pose a problem as the specific problem addressed here; the co-firing process of the Si wafers to produce solar cells, reaches temperatures much higher than this – even if for a brief period of time.

VII. Mathematical Modeling

Table 6 shows the average values for the CTE readings obtained by the Dilatometer for the 26 cylindrical samples, further information about the table was provided in the next page.

Table 6 Experimental Results: Average CTE Readings recorded by the Dilatometer

	Average Values: CTE x 10^{-6} $^{o}C^{-1}$				
Temp/^{o}C	**Un-Milled Al**	**Milled Al**	**2% CNT-Al**	**5% CNT Al**	**10% CNT Al**
50	13.497	13.080	12.694	12.123	11.346
100	18.444	17.775	17.226	15.929	14.580
150	20.568	19.795	19.231	17.658	16.084
200	21.723	21.091	20.488	18.757	17.018
250	22.547	22.039	21.361	19.541	17.724
300	23.194	22.785	22.075	20.218	18.327
350	23.799	23.410	22.713	20.819	18.837
400	24.410	24.033	23.317	21.395	19.316
450	25.047	24.633	23.923	22.001	19.850
490	25.574	25.072	24.373	22.437	20.222

Table 6 shall be used as the main source of information for both mathematical models to be employed in this research:

i. Rule of Mixtures (ROM)
ii. Schapery's Model

Note

Since the CTE value of the Al changes with temperature, as shown in Table 6, one cannot use a single value for the CTE of the matrix in the mathematical model. Thus, the CTE values of the Milled Al in the second column were used, and the mathematical model equations were applied to each temperature step, i.e. at 50^{o}C, the value entered for the CTE of the matrix was 13.080 x 10^{-6} $^{o}C^{-1}$, at 100^{o}C 17.775 x 10^{-6} $^{o}C^{-1}$, and so forth generating every time a predicted set of CTE values for the 2%, 5% and 10% CNT-Al.

Rule of Mixtures

$$\propto_{Composite} = \propto_{CNT} V_{CNT} + \propto_{Matrix} (1 - V_{CNT})$$

Variables - ROM

$\propto_{Composite}$ CTE of the resulting composite (Desired Output)

$\propto_{CNT}$ CTE of the CNT

$\propto_{Matrix}$ CTE of the matrix, which was the Al in this case

V_{CNT} Volume fraction of the CNT with respect to the total sample Volume.

Input - ROM

$\propto_{CNT}$ assumed to be equal to "0"

$\propto_{Matrix}$ See Table 6, used second column of Milled Al CTE values

V_{CNT} the weight fractions of the CNT used throughout this report were converted to volume fractions to be used in the ROM equations, see table 3

Table 7 Weight fractions of CNT converted to Volume fractions of total sample Volume

Weight %	Volume %
2	2.97
5	7.32
10	14.29

Note

In the following pages, the table headings of the CNT samples were still stated according to their weight fractions. This was done only to maintain consistency throughout the report.

Schapery's Model

$$\propto_{Composite} = \frac{E_{CNT} \propto_{CNT} V_{CNT} + E_{Matrix} \propto_{Matrix} (1 - V_{CNT})}{E_{CNT} V_{CNT} + E_{Matrix}(1 - V_{CNT})}$$

"E" refers to Young's Modulus

"$\propto$" refers to CTE

"V" refers to volume fraction

Input - Schapery

E_{CNT} 300 GPa

E_{Matrix} E_{Al} = 69 GPa

$\propto_{CNT}$ "0"

$\propto_{Matrix}$ same as that used in ROM model, see table 1: "Milled Al" column

V_{CNT} same as that used in ROM model, see table 3

Note: E_{CNT} was valued at 300 GPa as based on the study conducted by Coleman et al (2006) it was found that there was a lot of variation in the reported magnitudes of Young's Modulus of MWNT produced by Chemical Vapor Deposition method; one study reported a range of 12-50 GPa, another reported a value of 450 GPa (the variation was attributed to the fact that the amount of defects in MWNT played a role in the determination of the magnitude of Young's modulus). Hence based on these numbers, and taking into account the variations between the two ranges, the Young's modulus of the MWNT used was estimated to be around 300 GPa.

Output – ROM

Table 8 and Table 9 have the CTE values generated by ROM and Schapery's models respectively

Table 8 ROM-generated CTE Values

	ROM Model: CTE-generated values (x 10^{-6} $^{o}C^{-1}$)		
Temp /^{o}C	**2% CNT Al**	**5% CNT Al**	**10% CNT Al**
50	13.096	12.509	11.569
100	17.896	17.094	15.809
150	19.957	19.063	17.630
200	21.078	20.134	18.620
250	21.877	20.897	19.326
300	22.505	21.497	19.881
350	23.092	22.058	20.399
400	23.685	22.624	20.923
450	24.303	23.214	21.469
490	24.814	23.703	21.921

Output – Schapery

Table 9 CTE- generated values by Schapery's Model

	Schapery's Model: CTE-generated values (x 10^{-6} $^{o}C^{-1}$)		
Temp /^{o}C	**2% CNT Al**	**5% CNT Al**	**10% CNT Al**
50	11.544	9.738	7.584
100	15.687	13.233	10.307
150	17.470	14.737	11.478
200	18.614	15.702	12.229
250	19.450	16.407	12.779
300	20.109	16.963	13.211
350	20.661	17.428	13.574
400	21.210	17.892	13.935
450	21.739	18.338	14.283
490	22.127	18.665	14.537

Figure 55, Figure 56, and Figure 57 represent the experimental CTE values in Table 6 compared against the predicted CTE values by the ROM and Schapery models (in Table 8 and Table 9 respectively) for the following samples 2%,5% and 10% CNT-Al respectively:

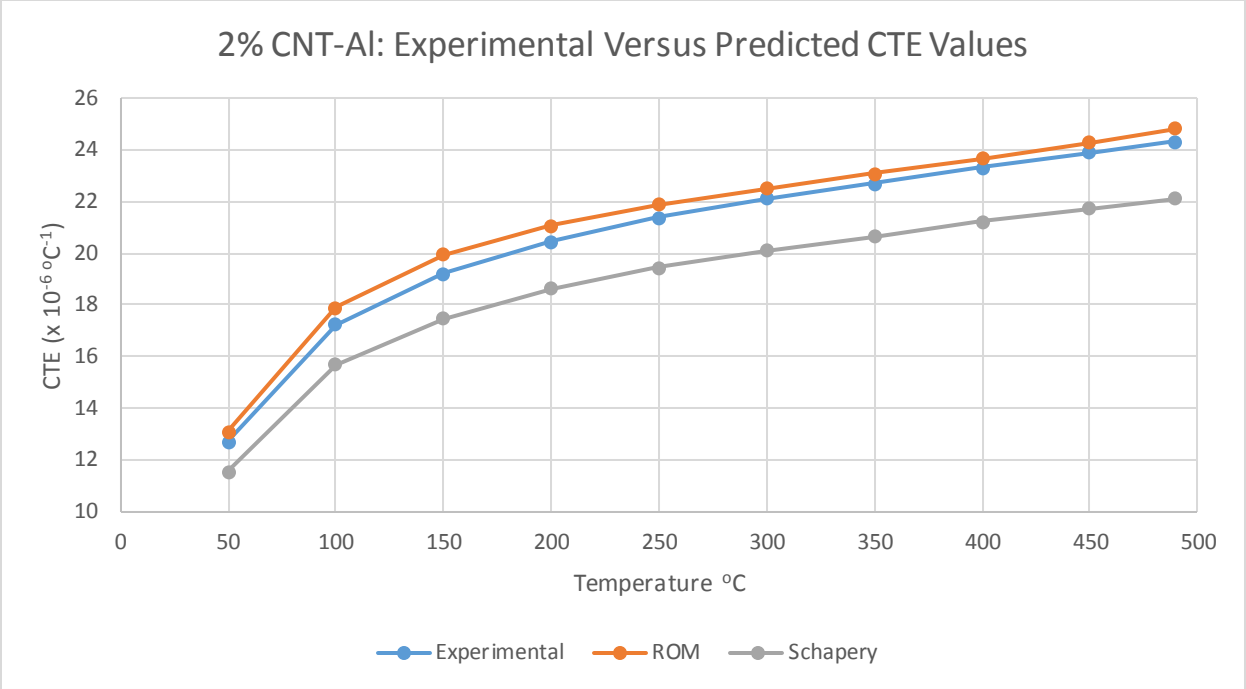

Figure 55 2% CNT-Al CTE Values: Experimental & Predicted (ROM, Schapery)

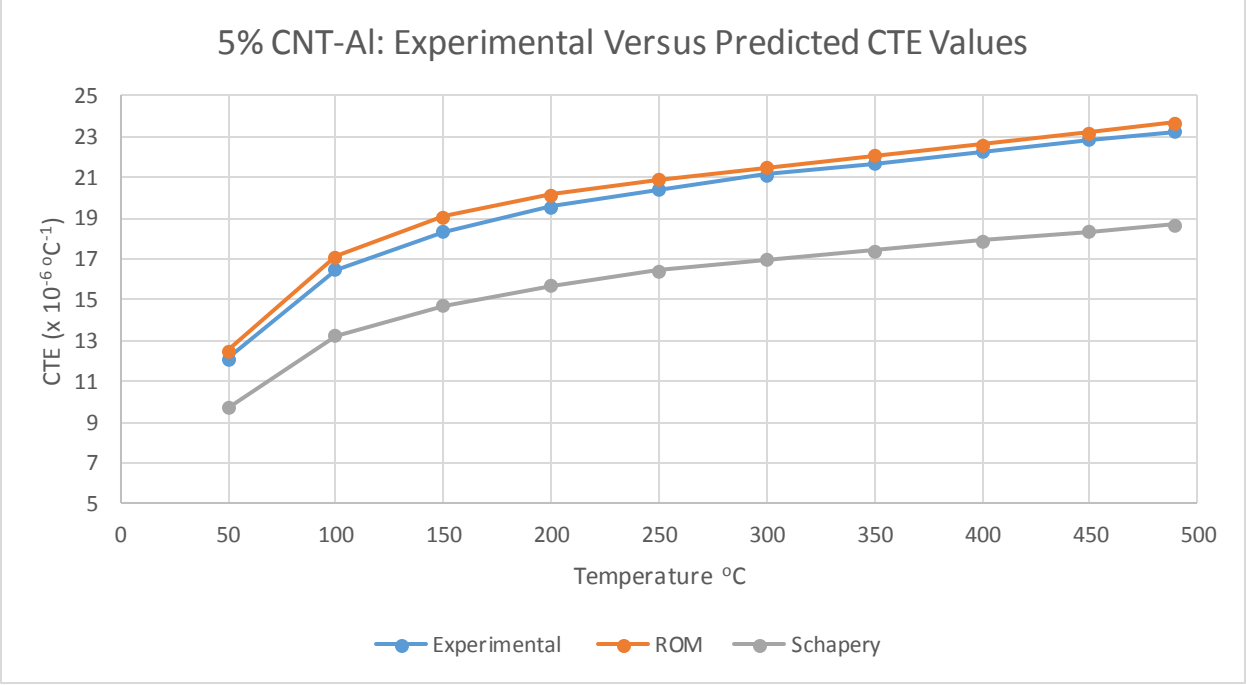

Figure 56 5% CNT-Al CTE Values: Experimental & Predicted (ROM, Schapery)

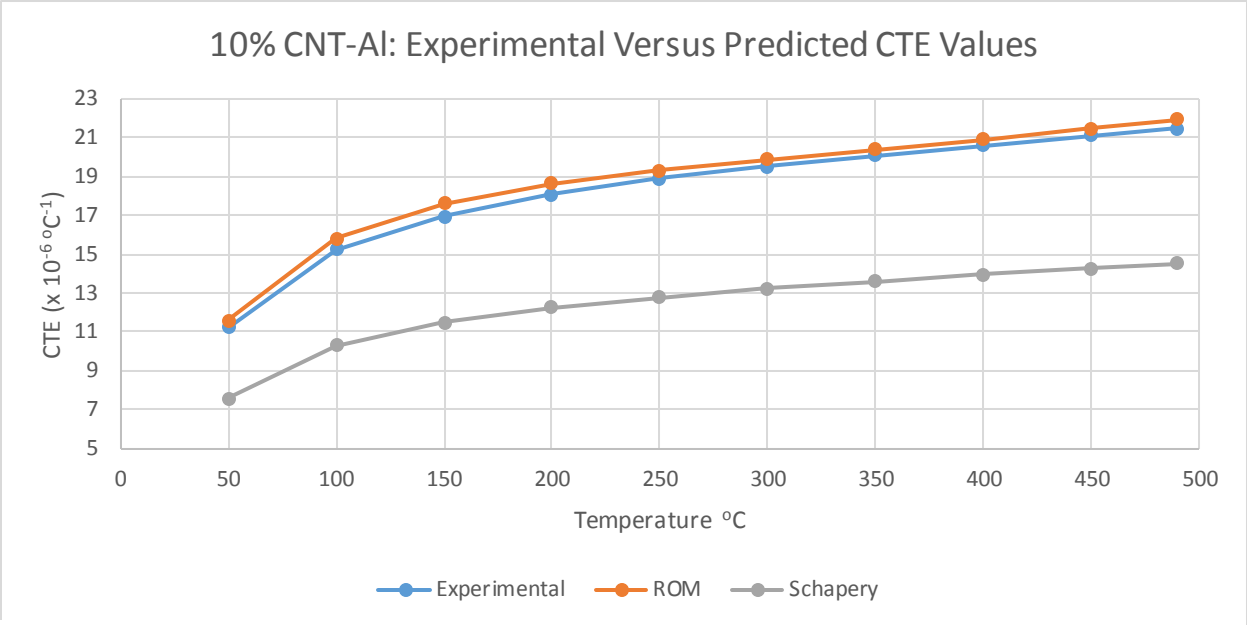

Figure 57 10% CNT-Al CTE Values: Experimental & Predicted (ROM, Schapery)

Observations

1. The ROM-generated values seem to highly agree with the CTE readings obtained from the dilatometer. The deviations noted were very small, averaging around 0.467 x 10^{-6} $^{o}C^{-1}$, and not exceeding 0.750 x 10^{-6} $^{o}C^{-1}$
2. The experimental CTE readings seem to lie between an upper limit (ROM) and a lower limit (Schapery's values).
3. The hypothesis that the CTE was reduced due to CNT addition was theoretically proved, as shown in Figure 55, Figure 56, and Figure 57, the CTE values calculated decreased as the CNT content of the samples increased.
4. Schapery's values were relatively much lower than those of the experimental. In fact, the more the CNT content in the samples, the more the deviation was noted. This could be attributed to the milling process which breaks down the CNT from long tubes to much shorter ones, hence reducing the interface area and thus the restraining effect was reduced accordingly. Also, Schapery's values were calculated using E_{CNT} = 300 GPa, which may not be the exact value of the Young's Modulus of the MWNT. When the value was changed to 100 GPa, Schapery's values were almost an exact fit to the experimental ones. Thus more investigation into the true value of E_{CNT} is required. As mentioned before, according to Coleman et al (2006), the magnitude of the modulus was reported to be either 12-50 or 450 GPa depending on the level of the defects present in the CNT.

5.2.2 Electrical Resistance

Considerations

The readings obtained for the resistance of each and every sample as shown in the next pages do not only represent the resistance of the samples, but they also represent the resistance involved in the crocodile wires connecting the sample to the device. Thus, the readings obtained here were not meant to present the exact resistance of the samples, but rather were for comparison purposes only, i.e. comparing the resistance value obtained for each and every sample category, i.e. while 1.47 Ohms is in fact a large value for the resistance of an Al sample, it is worth noting that these readings were not taken for their face value but rather to be compared to one another; comparing the resistance value for Milled Al to that of 2% CNT-Al, 5% CNT-Al sample and so forth.

So, in a nutshell the method could be described as such: The voltage was varied and the current was measured. The resistance was hence calculated and compared for each category. The resistance values were used directly as an indicator for the resistivity (since all 26 cylindrical samples had identical dimensions), which in turn was taken to be a measure for the electrical performance of the wafer samples.

The reason why this method was applied was that the resources available were very limited and the devices were not designed to handle the cylindrical samples. Having said that, it is worth noting once more that all the electrical measurements were randomly taken to avoid any possible unexpected factors playing a role in the results.

See full Electric readings in Appendix B

Note

The sample designation in the CTE test is different than that in the electrical resistivity test, i.e. Milled Al Sample A in CTE readings is not necessarily the Milled Al Sample A in the electrical resistivity test.

I. Un-Milled Al Samples

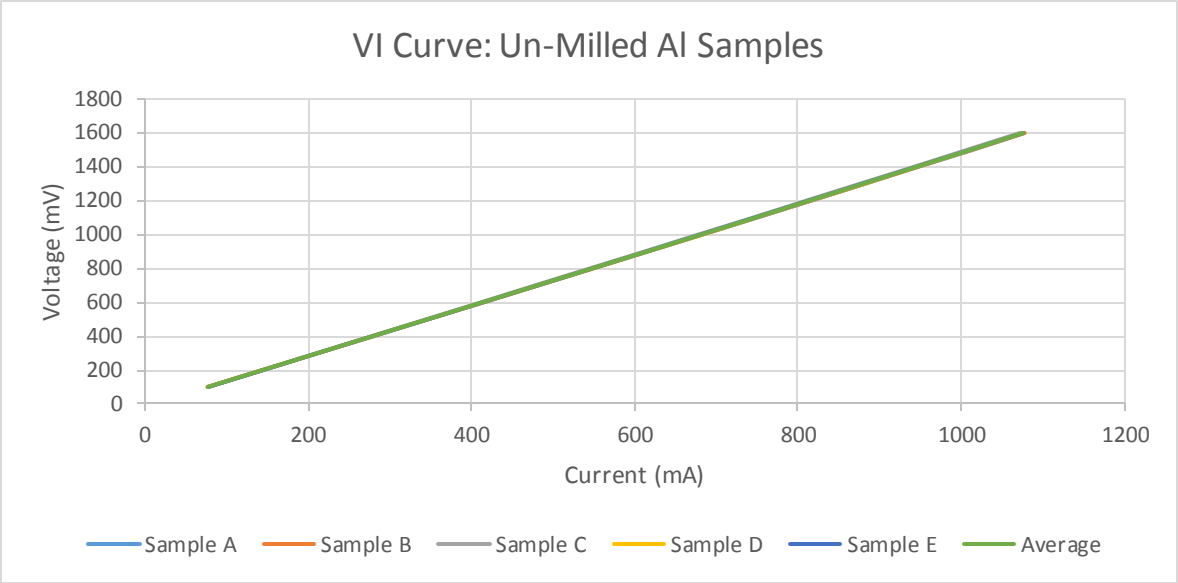

Figure 58 Voltage-Current readings for Un-Milled Al cylindrical samples

II. Milled Al Samples

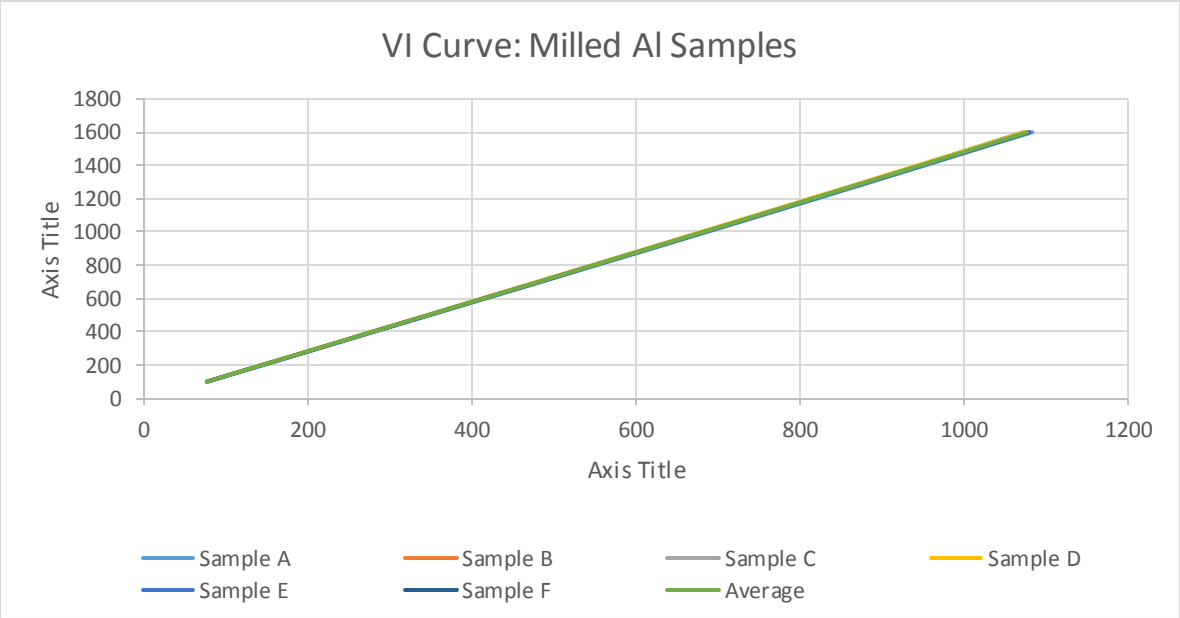

Figure 59 Voltage-Current curve for Milled Al cylindrical samples

III. 2% CNT-Al Samples

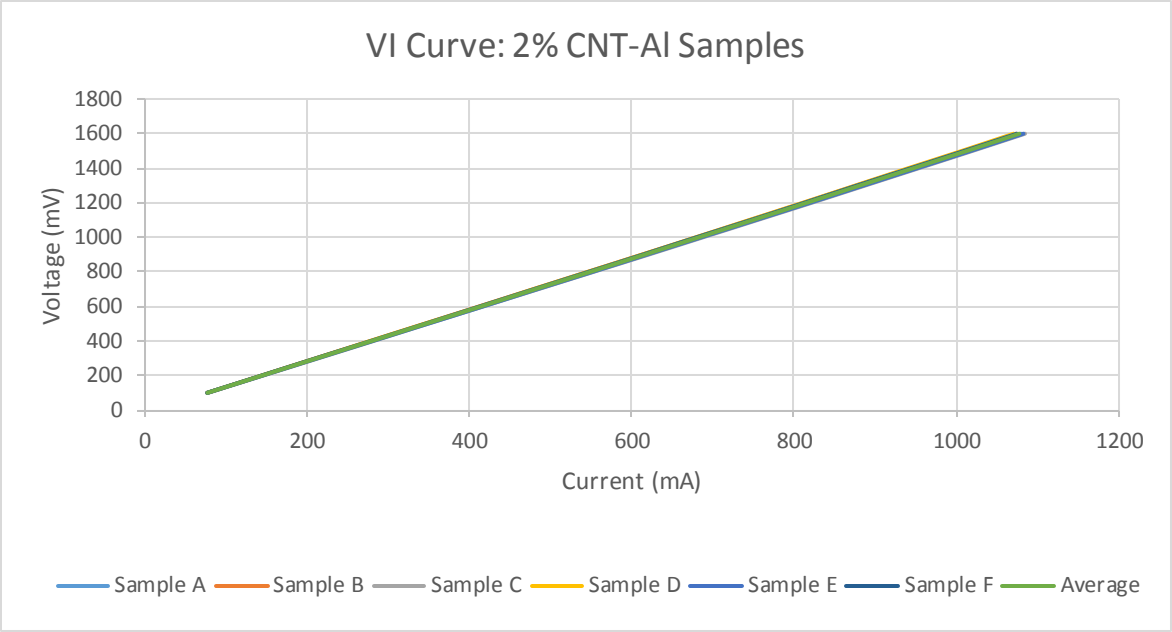

Figure 60 Voltage-Current curve for 2% CNT-Al cylindrical samples

IV. 5% CNT-Al Samples

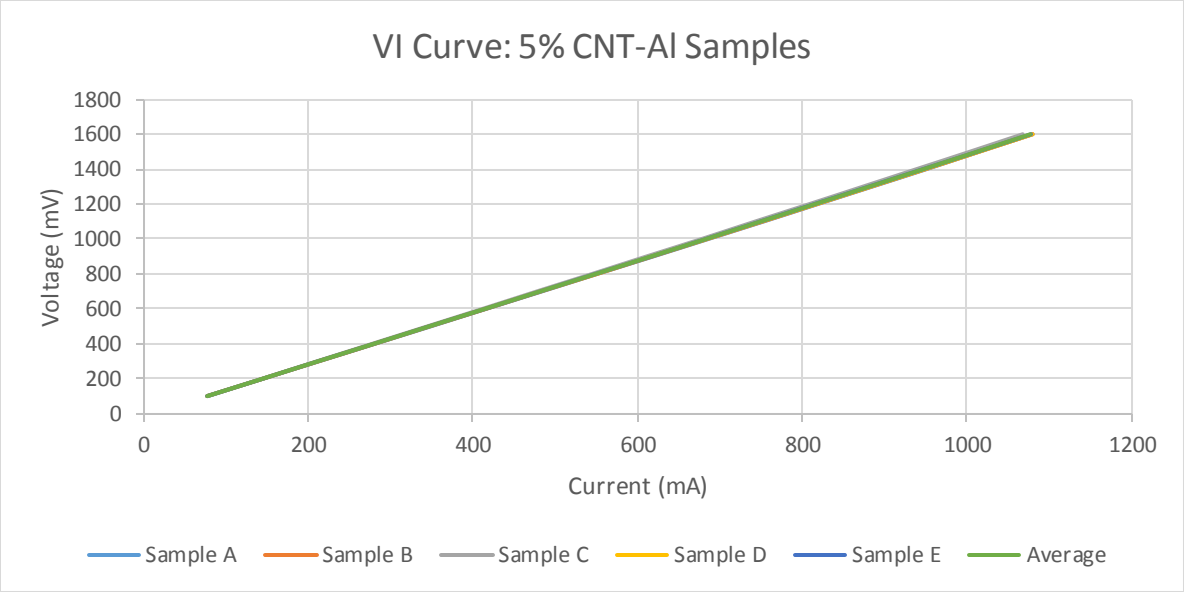

Figure 61 Voltage-Current curve for the 5% CNT-Al cylindrical samples

V. 10% CNT-Al Samples

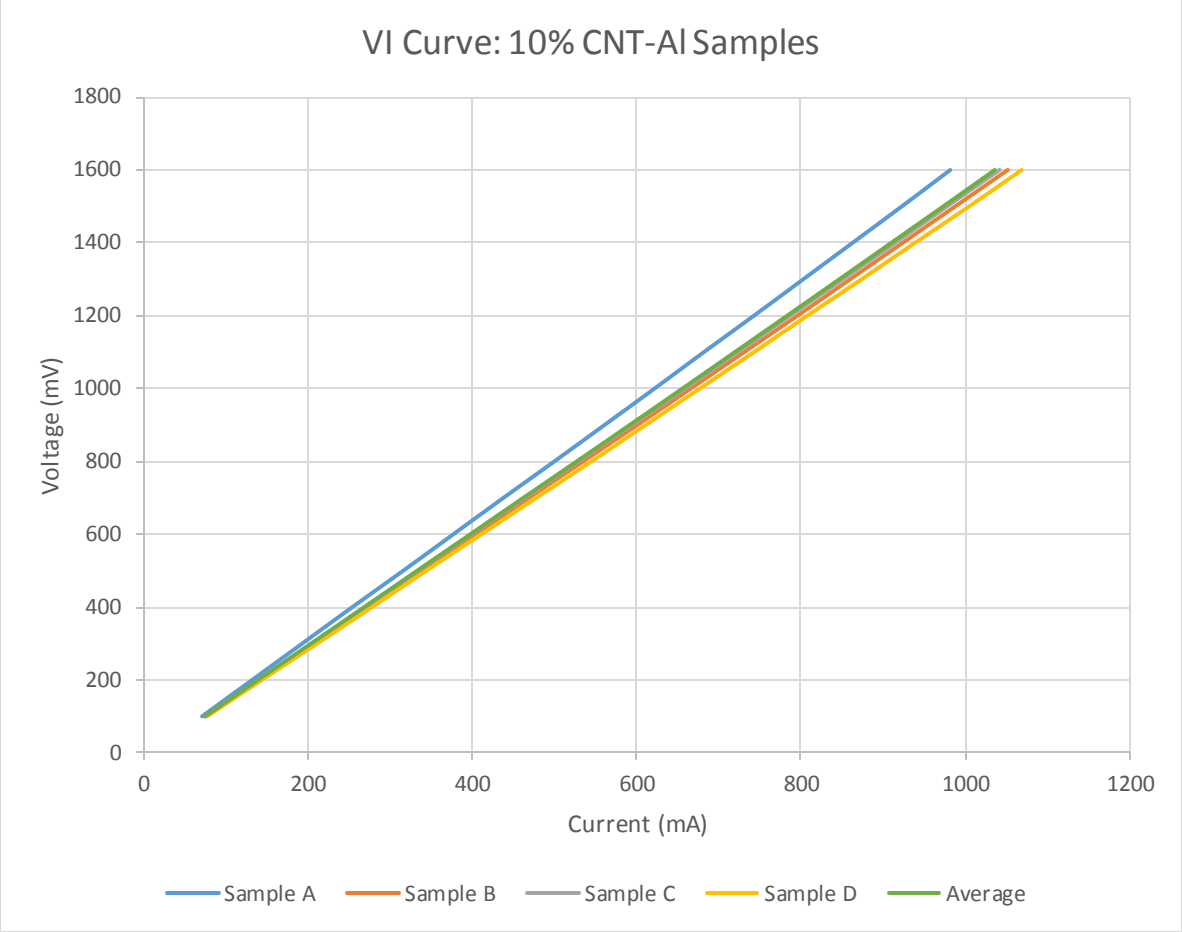

Figure 62 Voltage-Current curve for the 10% CNT-Al cylindrical samples

Observations

As in the CTE results, it is worth noting that the Figure 58 to and including Figure 62 show that all the samples Current readings under the same category were tightly clustered into a single line, e.g. in Figure 58 the Un-Milled Al sample readings were grouped together in a tight band to the extent that one could only see a single straight line instead of several, and so forth. Only perhaps in the case of the 10% CNT-Al samples, Figure 62, where it can be observed that one of the samples represented an outlier, while the remaining 3 samples were less clustered than their counterparts in other sample categories, but nonetheless they were still grouped in a relatively tight band. This reflects positively on the precision of the results.

VI. Normalized Data

The voltage - current (I) data of selected representative samples were plotted and from the trendline of each curve the resistance was determined, as shown in Table 10. These values were then normalized by taking the Milled Al reading as the control (base) reading, hence neutralizing the effect of the milling on the resistance of the resulting composite, and focusing only on the effect of CNT addition on the resistance values, see Figure 63

Table 10 Resistance Readings of non-Normalized Resistance Values

	Selected Representative Samples				
	Un-Milled Al	Milled Al	2% CNT-Al	5% CNT-Al	10% CNT-Al
Sample	E	F	A	E	C
Resistance (Ohm)	1.475	1.469	1.469	1.471	1.524

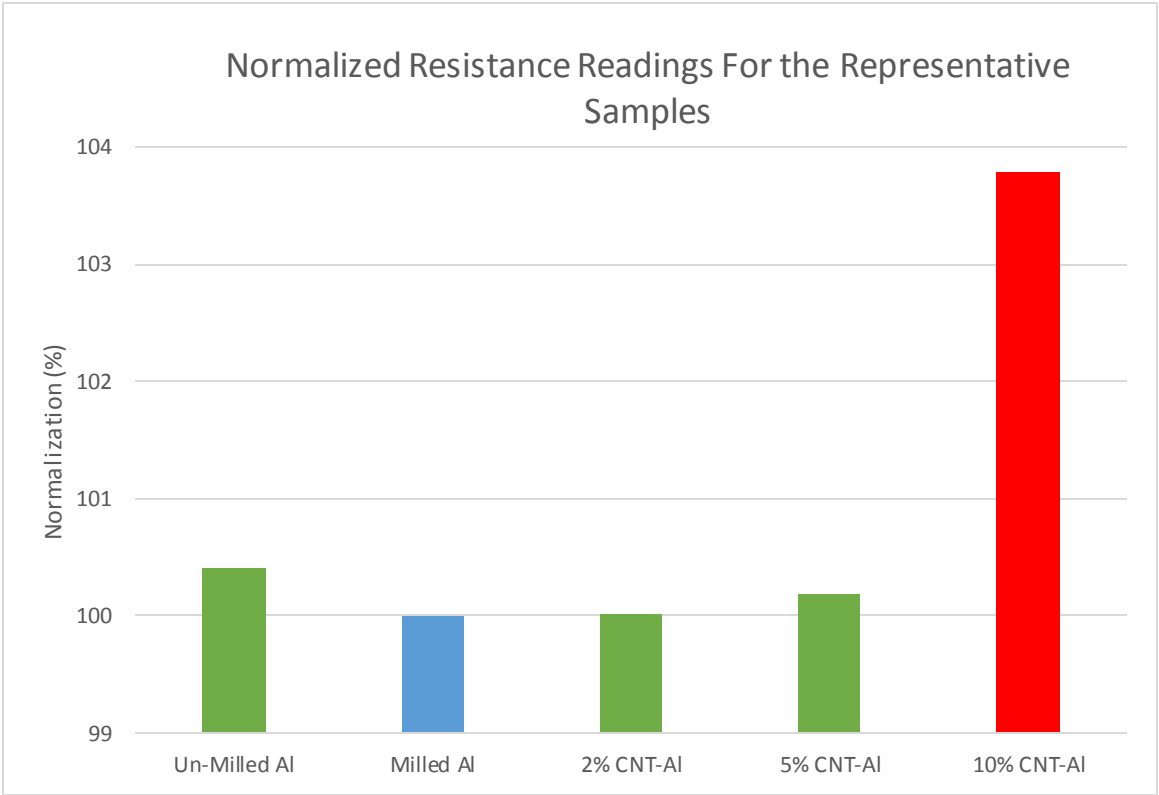

Figure 63 Graphical Representation of Data in Table 13. Normalized Electrical Resistance Readings for the Cylindrical Representative Samples

Observations: Normalized Results

Looking at Table 10 and Figure 63, one could observe the following:

i. **Milling Effect**

Comparing the Un-Milled Al and Milled Al bars, it was clear that the milling process did have a very slight effect on the resistance of the sample, reducing it by around 0.4%. This effect may be attributed to the fact that when the Al powders were milled, the small particles were fused together into larger ones creating larger grains with less boundaries, hence reflecting positively on lowering the resistance. Regardless, the effect was rather small here but is worth investigating and definitely taking into consideration if longer milling hours were applied in the future.

ii. **CNT Effect**

Comparing the bars of the Milled Al and the other CNT-containing samples (i.e. the 2%, 5% and 10% CNT-Al bars), it was clear that the addition of CNT had a negative effect on the resistance of the samples: While in the case of the 2% and 5% CNT-Al samples the effect was rather subtle; in both cases a noted increase in resistance was 0.014% and 0.191% respectively, while in the case of the 10% CNT Al sample the effect was much more pronounced; the noted increase in resistance was 3.793%. As mentioned earlier, these results should not be taken for their actual values but rather as a comparative indicator to relate the effect of adding CNT on the overall resistivity of the Al mixture. In this case, the indicated increase in resistance naturally means that resistivity would follow suit, since all the 26 samples have identical dimensions. At first, this seems counterintuitive as one would expect that the addition of Carbon, which was an excellent conductor, to a composite would reflect positively on the overall conductivity. However, upon further inspection, it becomes easier to understand why this has occurred:

When the CNT were milled, their relatively long lengths were shortened. The relatively larger Al particles were fused with the small short CNT particles, hence adding to the boundaries in between the grains. The increase in boundaries led to an increase in resistance, i.e. increasing interface resistance. This was most noticeable however in the

10% CNT-Al sample because there might have been some agglomeration of the CNT despite the milling process which may have required more time to fully disperse all of the CNT in the mixture.

Furthermore, it is worth noting that during the fabrication of the cylindrical samples, the powders were sintered at 500^{o}C. According to Esawi et al (2010) and Ci et al (2006), Nano-scaled Aluminum Carbide may have formed at the interface layer between the CNT and Al, which may have of course reflected on the electrical conductivity of the composite.

5.3 Part 2: Wafer Samples

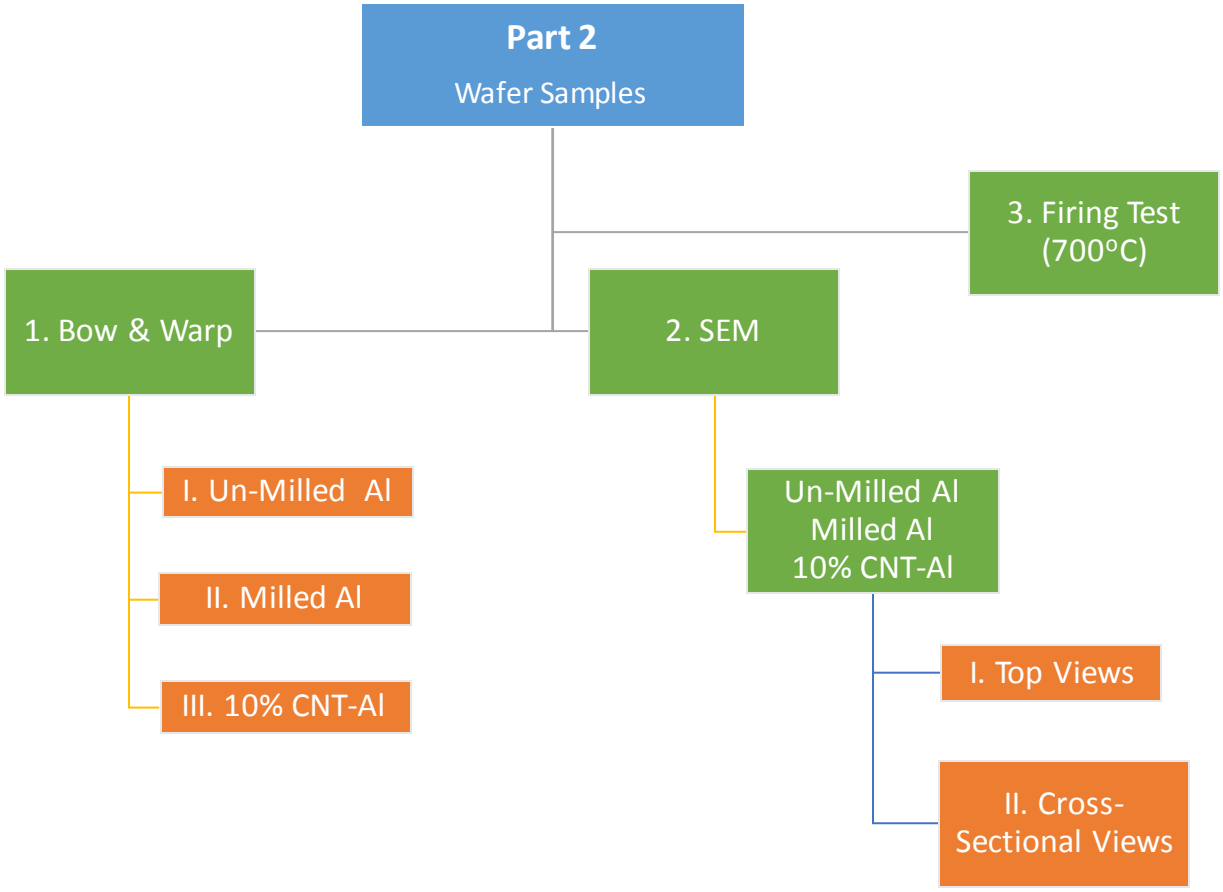

Figure 64 Outline of Part 2 of the Results & Discussion Chapter: Wafer Samples Part

Figure 64 shows an outline of the second part of the Results and Discussion chapter, which has the readings obtained from tests performed (in chapter 4) on the wafer samples this time.

5.3.1 Bow & Warp: Readings

Before Al Paste coating and firing (160°C)

Table 11 Thickness, Bow and Warp readings for the wafers before Al Paste application

Al Paste used	Wafer #	Average Thickness (µm)	Standard Deviation (µm)	Bow X-Axis (µm)	Bow Y-Axis (µm)	Total Warp (µm)
Un-Milled Al	**1**	596.65	0.58	-0.59	-1.29	4.16
	2	598.14	0.69	1.47	-2.4	6.73
	3	603.75	0.65	1.65	0.25	5.7
Milled Al	**4**	601.2	0.66	1.6	-1.66	5.9
	5	600.64	0.5	-1.25	-2.21	4.03
	6	603.64	0.6	-0.01	0.16	4.61
10% CNT-Al	**7**	602.06	0.55	0.78	-3.56	9.03
	8	601.97	0.59	0.44	-0.99	4.47
	9	601.85	0.64	-0.17	-0.56	4.76

Table 11 contains the thickness, bow and warp readings for all 9 Silicon wafers before the printing of Al paste step, i.e. dry wafers stage. Thus this means that a value of the average thickness indicates that of the thickness Silicon wafer itself, without any paste layer on it. It is worth noticing that the bow and warp readings were relatively low almost even close to zero. This was natural since there has been no Al printed and no firing hence no bow has developed yet. Kindly note that a positive value for the bow indicates a concave bow, as shown in Figure 65 ("concave bow": the wafer has bowed "inwards"; the direction of deflection went from the flat surface and inwards towards the center of the wafer)

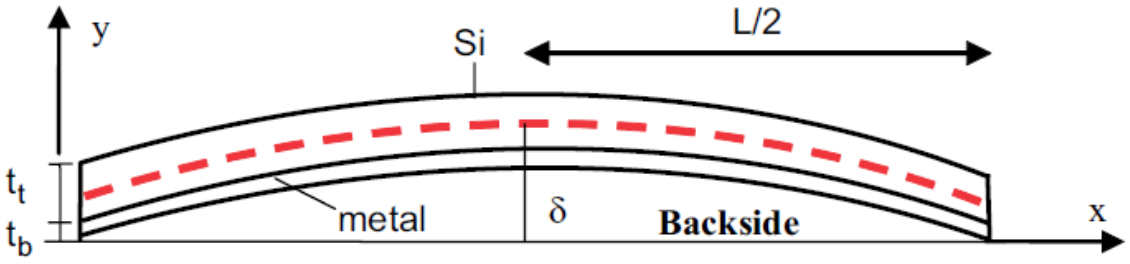

Figure 65 A concave bow, figure adopted from Hilali et Al., 2007, "Bow in screen-printed back-contact industrial silicon solar cells"

After Al Paste coating and Firing (160°C)

Table 12 Thickness, Bow and Warp readings for the wafers after Al Paste application and firing (160°C)

Al Paste used	Wafer #	Average Thickness (µm)	Standard Deviation (µm)	Bow X-Axis (µm)	Bow Y-Axis (µm)	Total Warp (µm)
Un-Milled Al	1	715.1	25.81	50.44	23.77	64.31
	2	670.86	10.16	32.18	22.5	46.52
	3	721.45	15.19	68.04	55.61	88.87
Milled Al	4	735.34	21.92	19.14	-3.36	57.68
	5	737.6	21.89	-4.71	8.29	51.5
	6	732.1	20.55	20.07	14.19	44
10% CNT-Al	7	725.37	15.95	21.29	9.54	40.63
	8	718.15	14.68	-0.75	-6.03	29.18
	9	722.99	14.52	19.05	15.36	44.21

Table 12 shows the same readings as in Table 11, but this time the wafers had Al paste coated/printed on them and the wafers were fired at 160°C for more than 3 hours.

Correction – Bow and Warp

Table 13 Thickness, Bow and Warp readings for the wafer changes due to Al Paste application and firing (160°C)

Al Paste	Wafer #	Average Thickness (µm)	Standard Deviation (µm)	Bow X-Axis (µm)	Bow Y-Axis (µm)	Total Warp (µm)
Un-Milled Al	1	118.45	25.23	51.03	25.06	60.15
	2	72.72	9.47	30.71	24.9	39.79
	3	117.7	14.54	66.39	55.36	83.17
Milled Al	4	134.14	21.26	17.54	-1.7	51.78
	5	136.96	21.39	-3.46	10.5	47.47
	6	128.46	19.95	20.08	14.03	39.39
10% CNT-Al	7	123.31	15.4	20.51	13.1	31.6
	8	116.18	14.09	-1.19	-5.04	24.71
	9	121.14	13.88	19.22	15.92	39.45

Table 13 shows the difference between before and after the coating and firing processes, i.e. the readings in Table 12 minus those in Table 11. So, an average thickness value in Table 13 would reflect that of the newly printed Al paste layer alone. Similarly, the bow and warp values in Table 13 were due only to the printing of the Al paste layer, as the effect of previous bows/warps that have pre-existed in the wafer before the printing and firing processes have now been excluded.

Averages: Thickness, Bow and Warp

Table 14 Thickness, Bow and Warp Averages of the processed wafers

	Average Values (µm)					
Al Paste used	**Wafers #**	**Average Thickness**	**Standard Deviation**	**Bow X-Axis**	**Bow Y-Axis**	**Total Warp**
Un-Milled Al	**1, 2 and 3**	102.96	16.41	49.38	35.11	61.04
Milled Al	**4,5 and 6**	133.19	20.87	11.39	7.61	46.21
10% CNT-Al	**7,8 and 9**	120.21	14.46	12.85	7.99	31.92

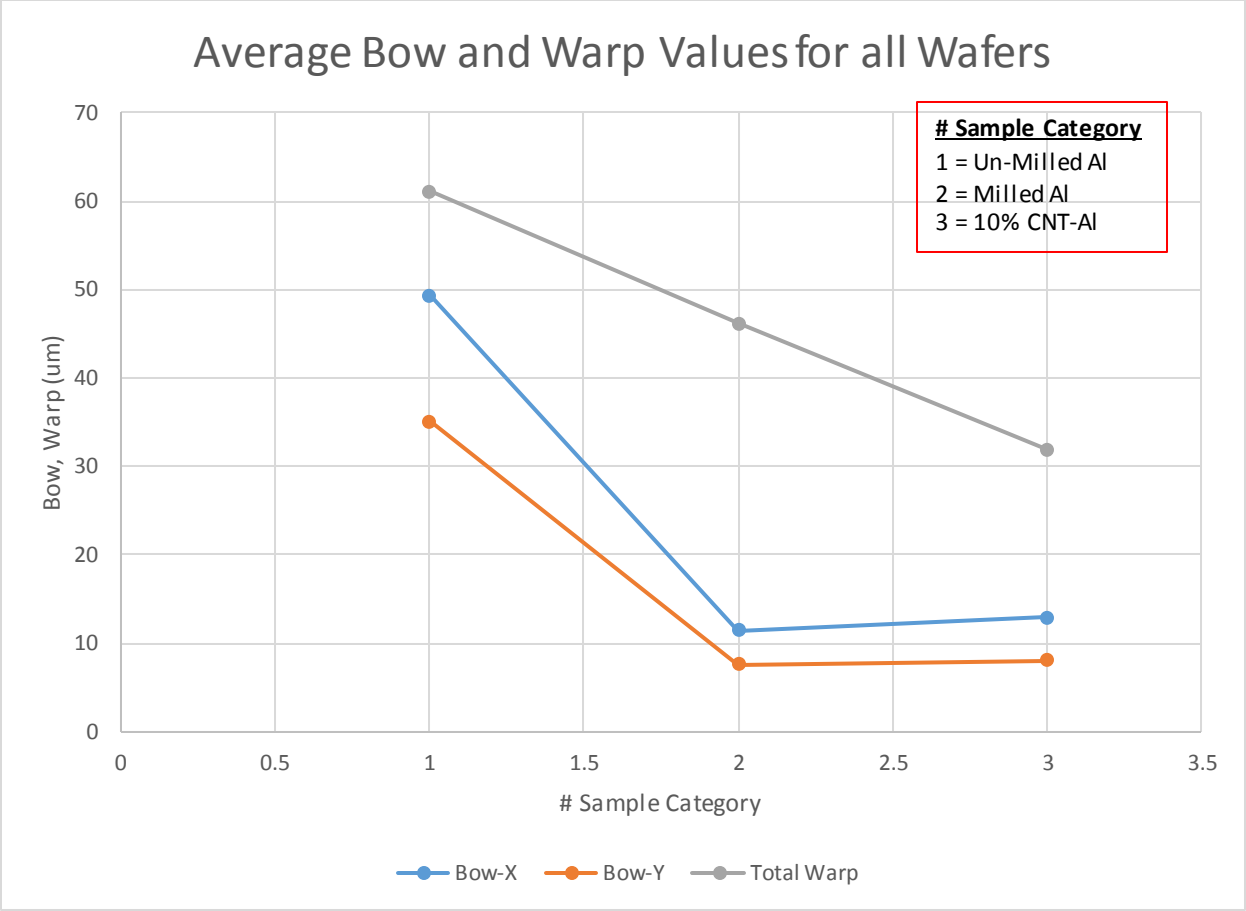

Figure 66 Graphical Representation of average values of the Bow and Warp represented in Table 14

Figure 66 is a graphical representation of the average values of bow X, Y and warp shown in Table 14. Data generated in Table 14 Thickness, Bow and Warp Averages of the processed wafers were based on data obtained from Table 13. On the X-axis, the values 1, 2 and 3 represent the Un-Milled Al, Milled Al and 10% CNT-Al samples, respectively.

Observations

I. The Bowing

Table 15 Bow and Warp Readings obtained from tables 16 and 17, all Bow and Warp readings summarized for convenience

Al Paste used	Wafer #	Average Thickness (µm)	Bow X-Axis (µm)	Bow Y-Axis (µm)	Total Warp (µm)	Average Bow-X (µm)	Average Bow-Y (µm)	Average Warp (µm)	WTT Ratio
Un-Milled Al	1	118.45	51.03	25.06	60.15	49.38	35.11	61.04	0.59
	2	72.72	30.71	24.9	39.79				
	3	117.7	66.39	55.36	83.17				
Milled Al	4	134.14	17.54	-1.7	51.78	11.39	7.61	46.21	0.35
	5	136.96	-3.46	10.5	47.47				
	6	128.46	20.08	14.03	39.39				
10% CNT-Al	7	123.31	20.51	13.1	31.6	12.85	7.99	31.92	0.24
	8	116.18	-1.19	-5.04	24.71				
	9	121.14	19.22	15.92	39.45				

Having printed the Al paste and fired the wafers, it was expected that the bow would be:

1. Having a concave shape, i.e. a positive reading from the device
2. Relatively much smaller in magnitude in the case of the 10% CNT-Al paste than in the case of the 2 other pastes: Un-Milled and Milled Al pastes

Observing the bow readings in Table 15 above, the overall values of the bow were positive, indicating that indeed the bow shape is concave. However, one could notice that there were few negative readings, indicating a convex bow in a given axis (note: if a reading is negative in the Bow-Y column, then this means that the bow along the Y-axis of the wafer has a convex shape, same goes for the Bow-X readings).

Furthermore, when the bow values for the Milled Al and the 10% CNT-Al paste wafers were compared, one could see that the magnitudes of these readings were relatively close, without the expected reduction in the bow due to CNT addition as mentioned before. The bow averages of the 10% CNT-Al wafers were in fact reported to be almost slightly higher than those of the Milled Al ones.

Finally, the bows developed by the Un-Milled Al paste were -in general- higher in magnitude than in the case of the other 2 paste samples, and they were all positive, which agrees with the 2 expectations mentioned above.

II. The Warping

In the case of the warp readings, which is another way of looking at the bow developed, they were a bit more conforming to the expectations. The warp results for the Un-Milled Al paste were higher than that of the Milled Al paste and that in turn were higher than those of the 10% CNT-Al paste, see Table 15. Naturally, the averages for the warp readings calculated followed suit

In Table 15, the final column was headed by "WTT" ratio or "Warp to Thickness" ratio, which is basically the readings in the "Total Warp" column divided by those in the "Average Thickness" column, i.e. calculating the warp developed per unit thickness of the paste layer printed on the wafer. These ratios were 0.59, 0.35 and 0.24 for the Un-Milled Al, Milled Al and the 10% CNT-Al pastes, respectively. This shows that despite the fact that there were differences in the thicknesses of the paste layer coating the wafers, on average warp developed due to a unit thickness of the 10% CNT-Al powder-based paste was lower than that for a unit thickness of the Un-Milled Al and Milled Al pastes. In fact, from the "WTT" column, it can be shown that the warp developed due to the 10% CNT-Al paste was around 30% less than that due to the Milled Al paste; a significant amount.

Interpretation

So what would explain the differences between the bow and the warp readings? Why would the bow readings show that the 10% CNT-Al paste were not much better than the Milled Al readings, while the warp readings indicate something else? Looking back at the definition of Bow-X and Bow-Y, see Figure 69 and Figure 70, in the case of the Bow-X it is basically the difference the difference between three length measurements: Bow(X) = $C - \frac{A+B}{2}$

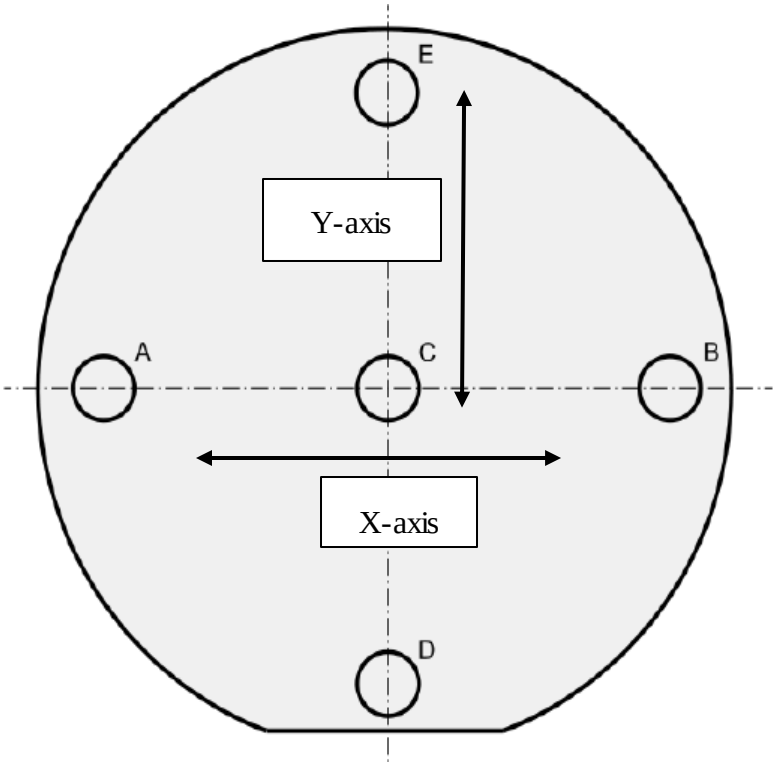

Figure 67 Top View: Main points on the wafer for Bow-X and Bow-Y measurements. Figure adopted from Contactless Wafer Geometry Gauge Manual, Eichhorn Hausmann, 2004

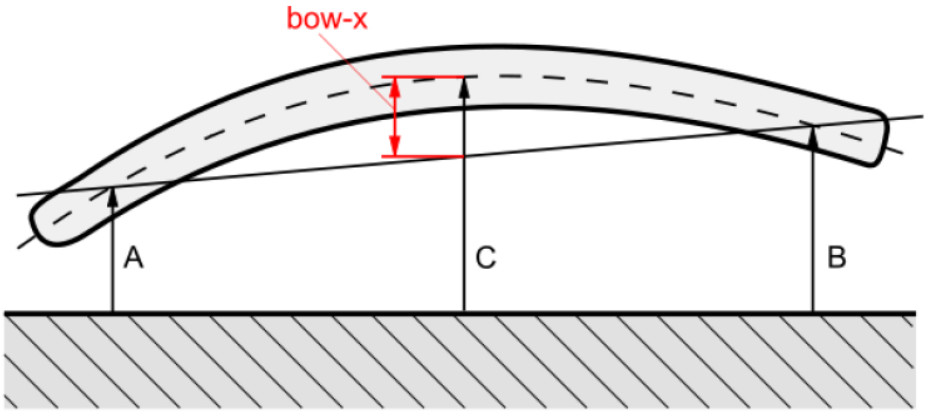

Figure 68 Cross-sectional View: How Bow-X is measured, Contactless Wafer Geometry Gauge device. Figure adopted from Contactless Wafer Geometry Gauge Manual, Eichhorn Hausmann, 2004

If the spin coating method did not evenly distribute the paste all over the wafer, this might lead to some parts having more or less paste than the other. This would reflect on the bow in such regions and hence this might have led to lengths A and B being longer than C, giving a false result of a convex bow or a negative reading instead of a positive one. Indeed, just after spin coating and before removing the wafer from the stage, sometimes it was noticed that near the periphery of the wafer along its perimeter a thick layer of the paste would be accumulated there. Furthermore, the "Contactless Wafer Geometry Gauge" individual sensor local thickness readings per wafer proved this point, see Figure 69, Figure 70 and Figure 71, where the thickness value at the center was different from other points across the wafer itself, hence affirming the earlier hypothesis that the spin coating method did not homogeneously distribute the paste over the wafer. Note that there was a significant increase in the paste layer thickness at the periphery of the wafer, along its circumference.

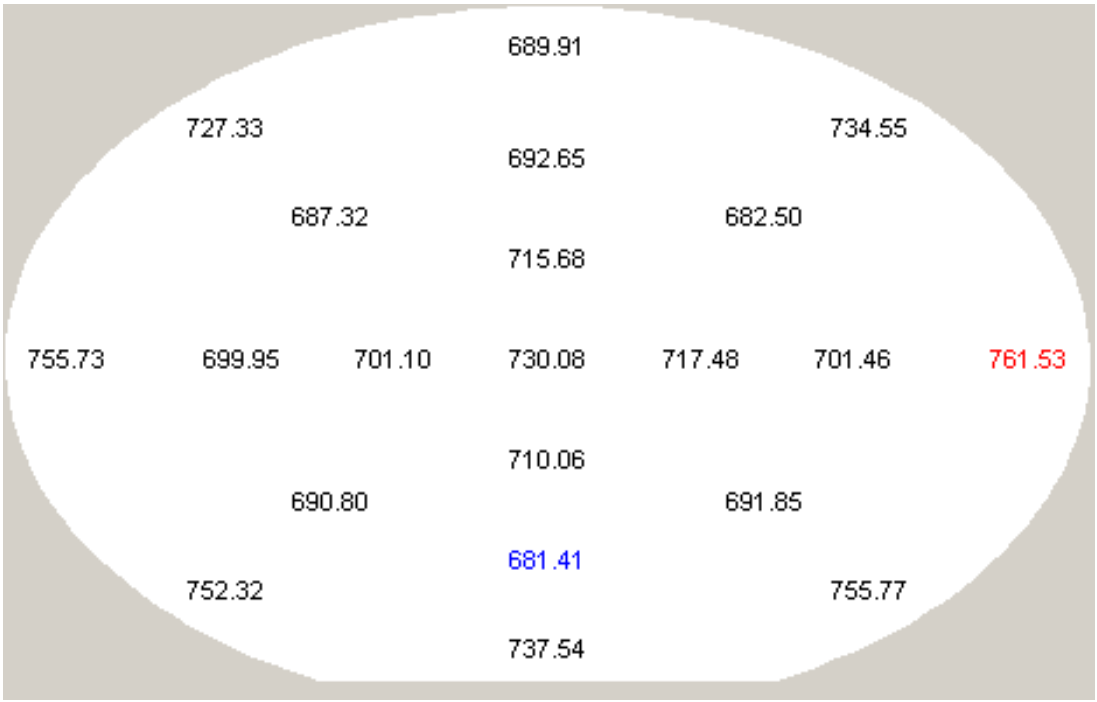

Figure 69 Wafer 1: Local thickness readings. Image adopted from Device Software

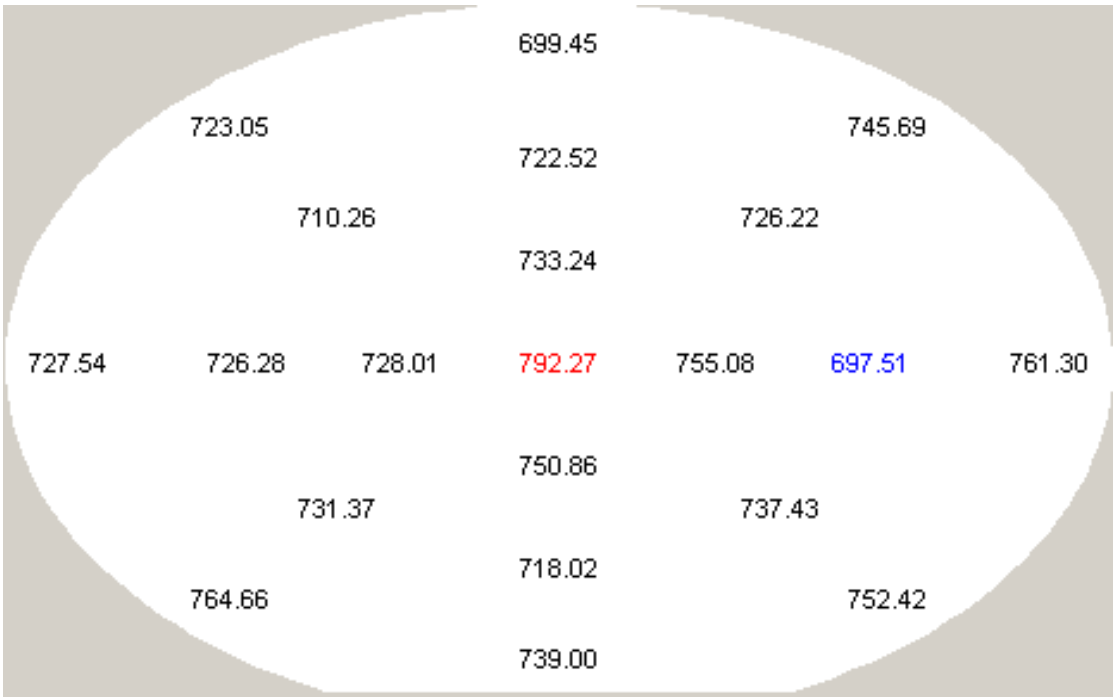

Figure 70 Wafer 4: Local thickness readings. Image adopted from Device Software

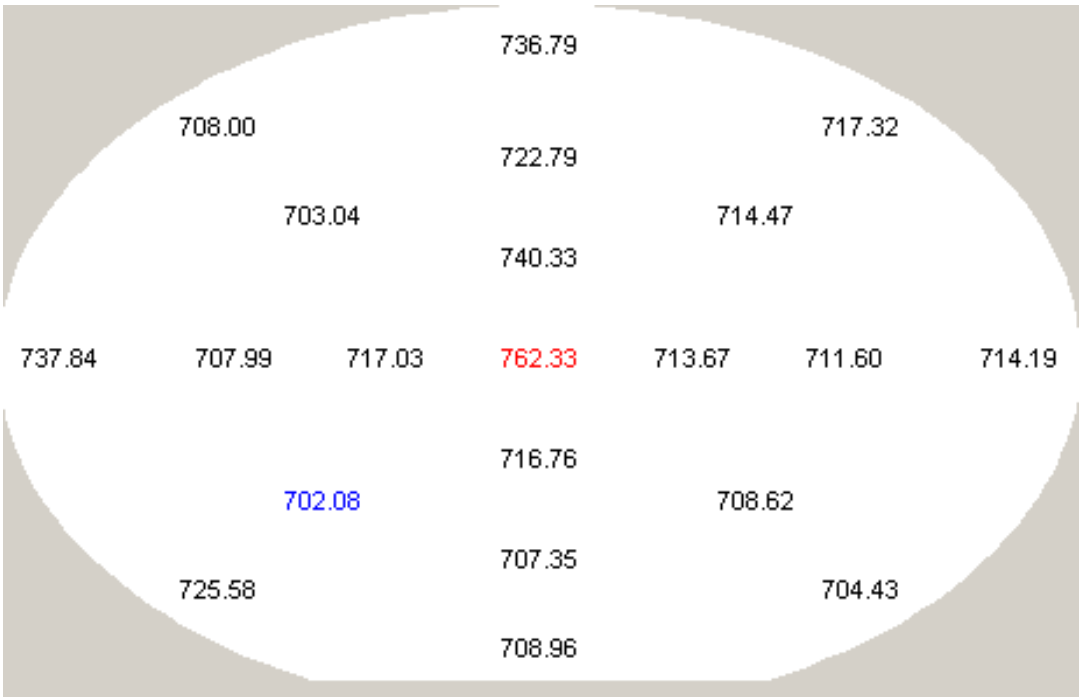

Figure 71 Wafer 8: Local thickness readings. Image adopted from Device Software

Possible explanations for the differences in the thicknesses readings are:

1. The spin coater rotating stage was not perfectly horizontal, which means that the rotating wafer was inclined.
2. Wafer was not placed exactly on the center of the rotating stage.
3. The Milled-Al and the 10% CNT-Al pastes contain particles of different sizes (see SEM images), so the pull of the centrifugal force on these particles was different, basically because the distance a particle moves depends on its size. This was most evident in the case of the Milled Al and the 10% CNT-Al wafers, as both of them had the exact same spinning program, and yet both set of samples yielded wafers with different paste layer thicknesses (check next section for SEM images of the Top and Cross-sectional views of the wafers)
4. It could be that the sensor in a particular spot hit a large particle, an outlier that does not reflect the true thickness of the wafer at this region, as shall be shown in the SEM images later on, the surface of the wafer was not exactly uniform, there were many large and small particles clumped together thus causing the thickness to vary accordingly from one point to the next
5. While transporting the wafer from the spinner to the furnace, any slight movement could easily shift the paste. This, however, may be cancelled out as the wafer was left to rest at a horizontal plane for more than 3 hours in the furnace, so the level of the paste would even out in the first couple of minutes. Of course, there might be a slight inclination in the platform upon which the wafer rests inside the furnace, which again would cause the thickness to be higher in some areas relative to other areas.

Also, it is worth noting that while the wafers were transferred into the furnace, some slight smudges of the paste contaminated the other face of the wafer, the one that should not have any paste on it (this was discovered after the firing process was finished). Despite the fact that such contamination was very little, however, having paste on the upper and lower sides of the wafer might have led to disrupting the usual bowing profile, which could explain why sometimes there has been negative values or just low bowing readings; with expansion occurring on both sides, the bow developed would be cancelled out at this particular spot or just reduced in magnitude.

Needless to say that any mishandling of the wafers at any point in time may have led to the development or reduction of some bow readings, thus it was crucial to subject the wafers to as little human contact as possible. So the irregular coating could have led to an irregular bowing profile, and hence counter-intuitive readings. The warp on the other hand offers a better picture. Recalling the earlier explanation of how the warp was measured, see Figure 72:

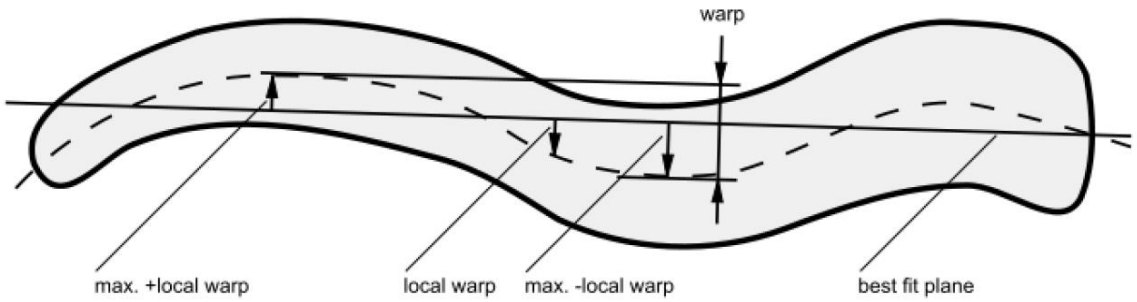

Figure 72 How the local and total warps of a wafer were measured: Contactless Wafer Geometry Gauge device. Figure adopted from Contactless Wafer Geometry Gauge Manual, Eichhorn Hausmann, 2004

A best fit plane was calculated and the wafer's deviations were determined with respect to this plane, these deviations whether above or below the plane were determined and were called Local Warps. The max deviations above and below were summed up to present the Total Warp. The key point was that this process does not happen along only 3 points like in the case of Bow-X or Bow-Y, but rather local warps were calculated many times all over the wafer's plane, hence the warp readings were relatively more reliable than the Bow readings, as the former covers a wider range of the wafer's surface.

Two Variables: Thickness & Powders

In the case of the wafer experiments, 2 variables changed:

i. Thickness of the Al layer deposited on the wafer.
ii. Powder content of the paste printed on the wafer.

Both variables affected the response being measured; the Warp readings. It is generally thought that the more the thickness of the Al paste layer, the more the bow and Warp developed. However, according to Schneider et al (2002), the composition of the paste has a higher effect on the bow than the thickness of the deposited paste layer.

Table 16 Comparing Average Thickness with Total Warp Readings

Al Paste	Wafer #	Average Thickness (μm)	Total Warp (μm)
Un-Milled Al	2	72.72	39.79
	3	117.7	83.17
	1	118.45	60.15
Milled Al	6	128.46	39.39
	4	134.14	51.78
	5	136.96	47.47
10% CNT-Al	8	116.18	24.71
	9	121.14	39.45
	7	123.31	31.6

Table 16 was generated from Table 15 which contains all readings of the bow and warp discussed earlier. The data in this table were re-arranged a little bit differently this time: In each of the 3 categories of the paste, the samples were arranged ascendingly according to their average thickness recorded. The total warp developed does not seem directly related to the average thickness measured. By checking the average thickness readings, it was found that it was not necessary that the layer with the most thickness resulted in the highest warp.

For instance, comparing wafers 4 & 5 or 9 & 7, the wafers had different thicknesses, but the resulting warp did not depend on the wafer with the thickest printed paste layer. Of course, there might be some underlying relation, however, it seems that indeed it is the composition that affects the warp more in the end.

These points were based on average thickness results, which may not be the best data to analyze since it has just been proven that the printed layer thickness was not uniform across the wafer, however, it was the best available option given that the only other data provided by the device were not any better as they considered single points while the average thickness readings provided a more general picture. These interpretations combined with the calculations made in Table 15 concerning the "WTT" data discussed earlier in the observations (Warp section) both strengthen the hypothesis that the layer thickness variable did not have the highest impact on the bow/warp generated.

5.3.2 SEM Images – Wafer Samples

5.3.3.1 Top Views

Low magnification: Un-Milled Al powder based paste: 49 X

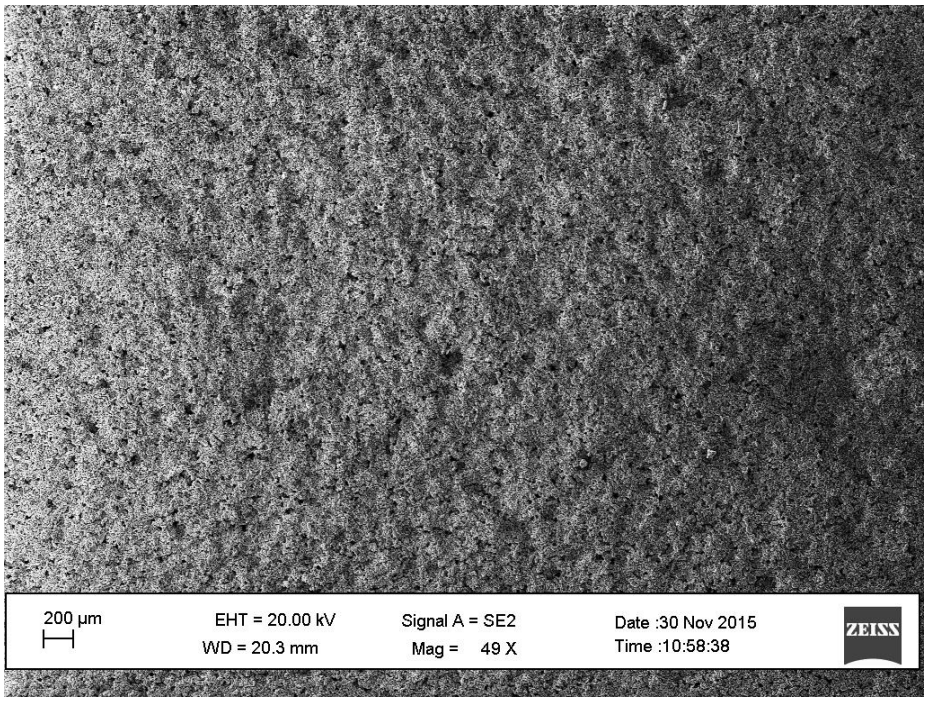

Figure 73 SEM Image: Low Magnification Top View of Silicon Wafer – Un-Milled Al Powder-Based Paste

High magnification: Un-Milled Al powder based: 456 X

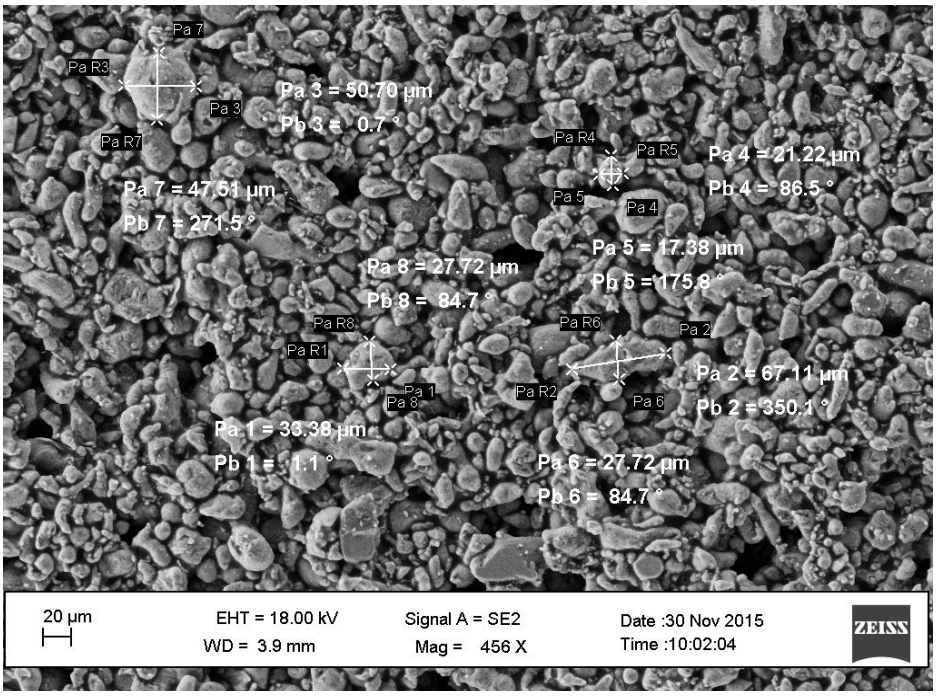

Figure 74 SEM Image: High Magnification Top View of Silicon Wafer – Un-Milled Al Powder-Based Paste

Low magnification: Milled Al powder based paste – 49 X

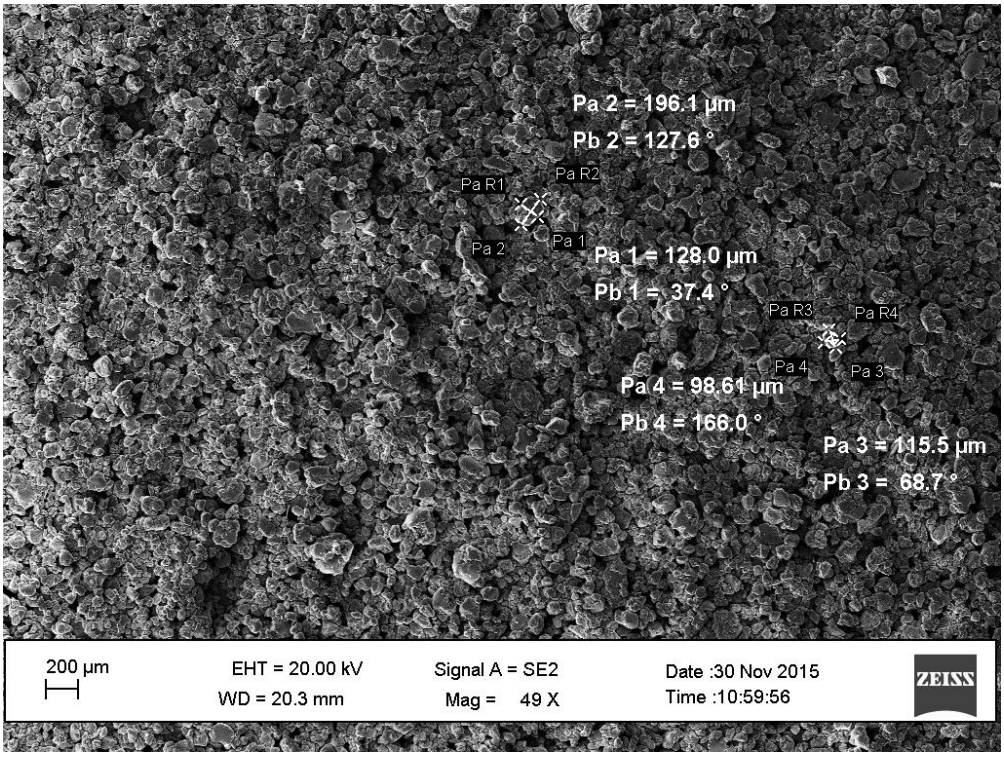

Figure 75 SEM Image: Low Magnification Top View of Silicon Wafer – Milled Al Powder-Based Paste

High magnification: Milled Al powder based paste – 456 X

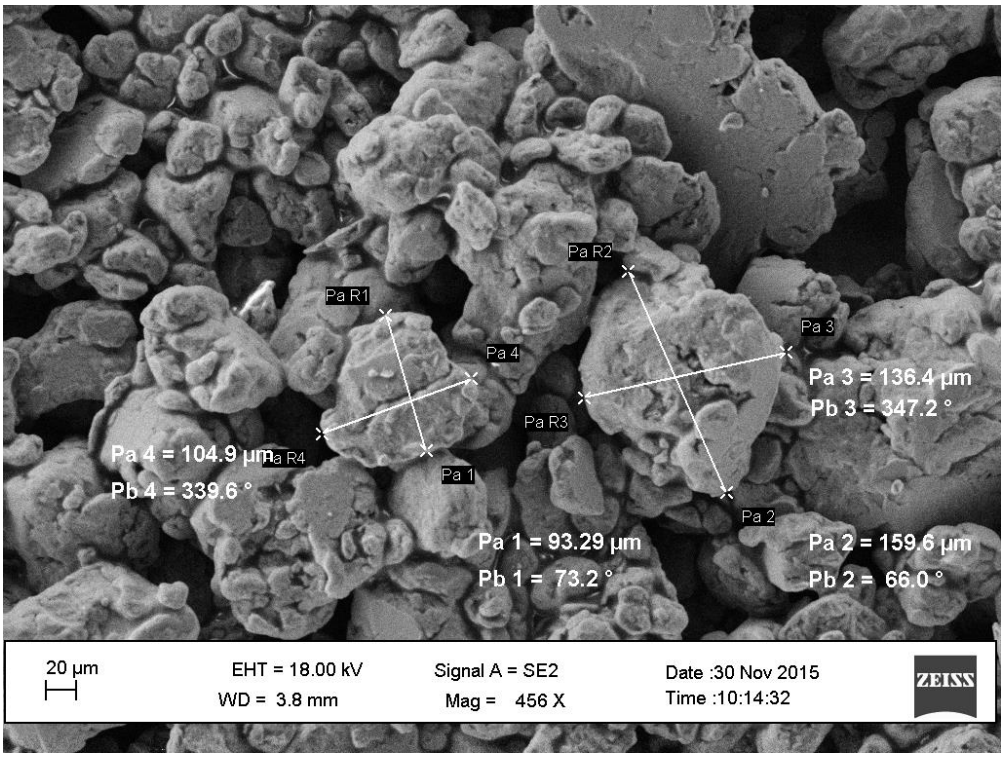

Figure 76 SEM Image: High Magnification Top View of Silicon Wafer – Milled Al Powder-Based Paste

Low magnification: 10% CNT-Al powder based paste – 49 X

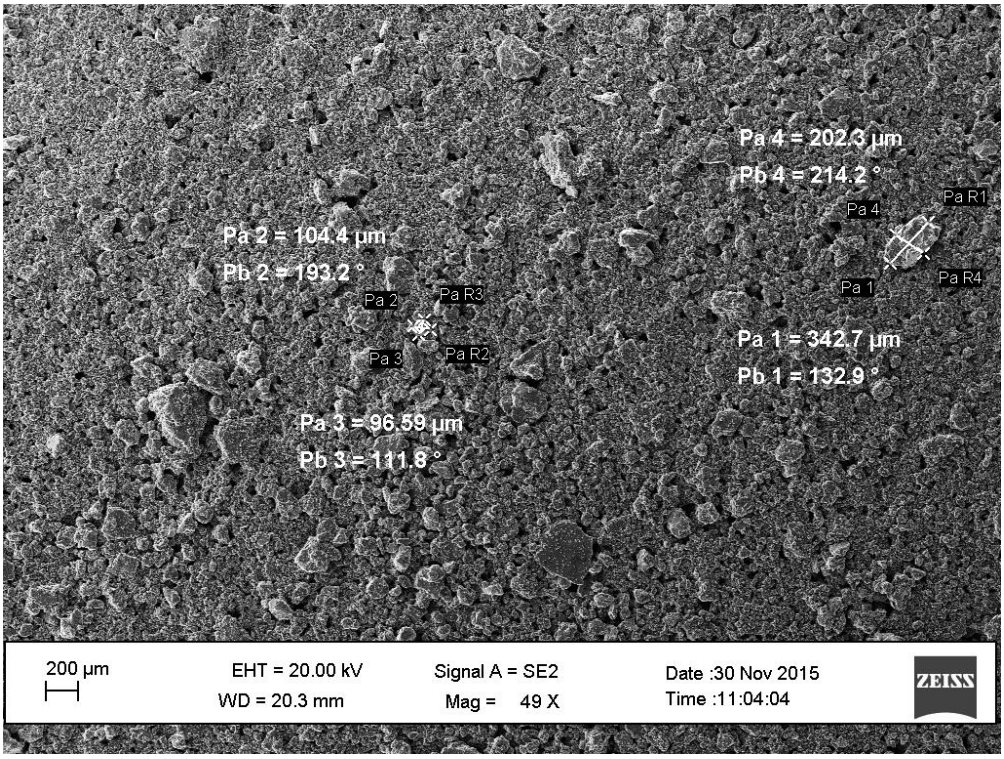

Figure 77 : Low Magnification Top View of Silicon Wafer – 10% CNT-Al Powder-Based Paste

High magnification: 10% CNT-Al powder based paste – 456 X

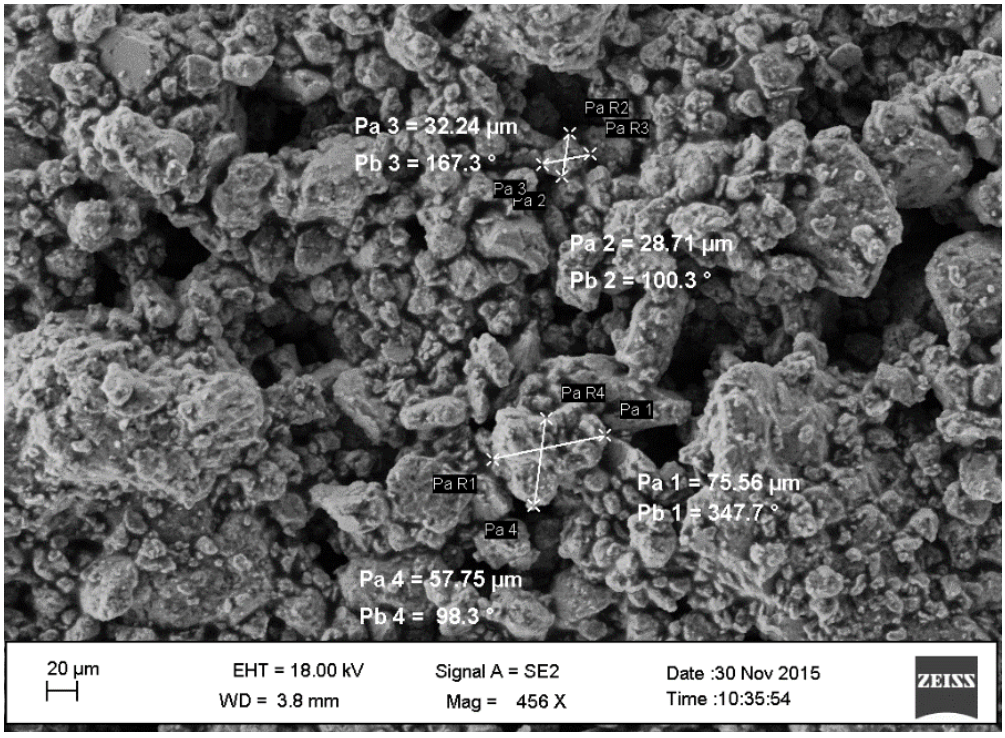

Figure 78 : High Magnification Top View of Silicon Wafer – 10% CNT-Al Powder-Based Paste

Observations

i. Un-Milled Al Wafer Sample – Figure 73 and Figure 74

It has the smallest particles, with the casual appearance of some larger particles roughly double the size of the small particles mentioned before, particle sizes ranging from 20-50μm. The particles have not fused together forming a metallic strip: many "free particles" were observed.

ii. Milled Al Wafer Sample – Figure 75 and Figure 76

The particle size here was definitely larger than that of the Un-Milled Al sample, roughly 2 to 3 times larger, 100-130μm with some larger particles of around 200μm. There seemed to be many particles of such size with some smaller ones attached to them. Again, the presence of free particles was noticed. The reason why the Milled Al particle size here was larger could be attributed to the milling process that clumps particles together.

iii. 10% CNT-Al Wafer Sample – Figure 77 **and** Figure 78

The low magnification image, Figure 77, shows a plane dominated by very small particles (Un-Milled Al particle scale), a few small-sized ones (30μm) and even fewer larger ones, much larger than the Milled Al particle size, around 200-300 μm in size. Upon closer examination, Figure 78, it can be deducted that these smaller particles appear to be a large agglomeration of much smaller particles. Once more, the presence of free particles was noticed.

Interpretation

The explanation here is that during a regular milling process, the particles were constantly hit and hence strain-hardened, till a point was reached where the particle became so hard and brittle that it broke into smaller parts. The explanation of why these smaller parts were not completely dominating the scene in the SEM images of the Milled Al and the 10% CNT-Al samples is that there was a partial disintegration of the powders during the milling process, hence the presence of both large and small particles as described before. Thus it was recommended that in the future milling variables such as total milling duration or the amount of PCA used may be increased to

further break these large particles present and thus obtain a more uniform layer when printed over the wafer.

As for the presence of the free particles, this can be attributed to the fact that the powders were not sintered at a high temperature, as in the case of the cylindrical samples, but rather the wafers were heated at a very low temperature, 160°C, which was much lower than the melting point of Al, while the industry operates at a temperature range that may go up to 900°C. Hence this did not lead to the melting of the powders and their fusing together to constitute a relatively compact single metallic strip.

5.3.3.2 Cross-Sectional Views

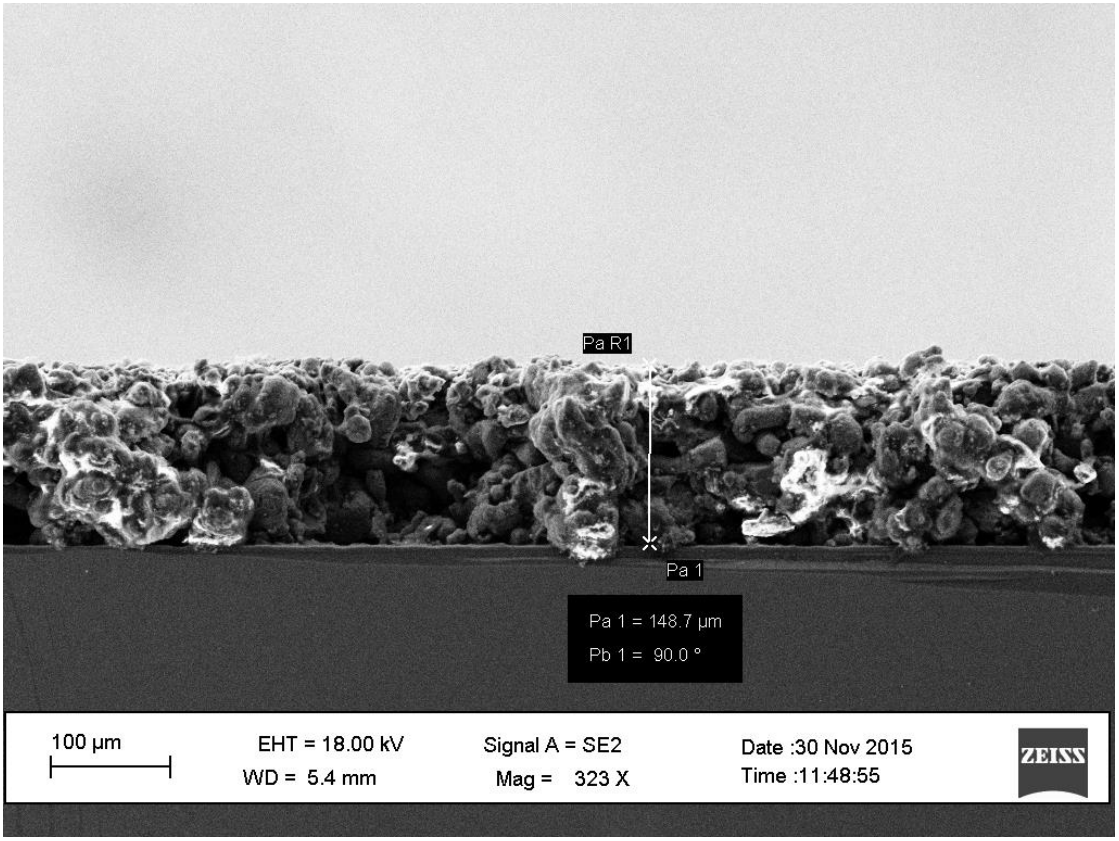

Figure 79 SEM Image: Cross-Sectional View of the Silicon Wafer: Un-Milled Al Powder-Based Paste

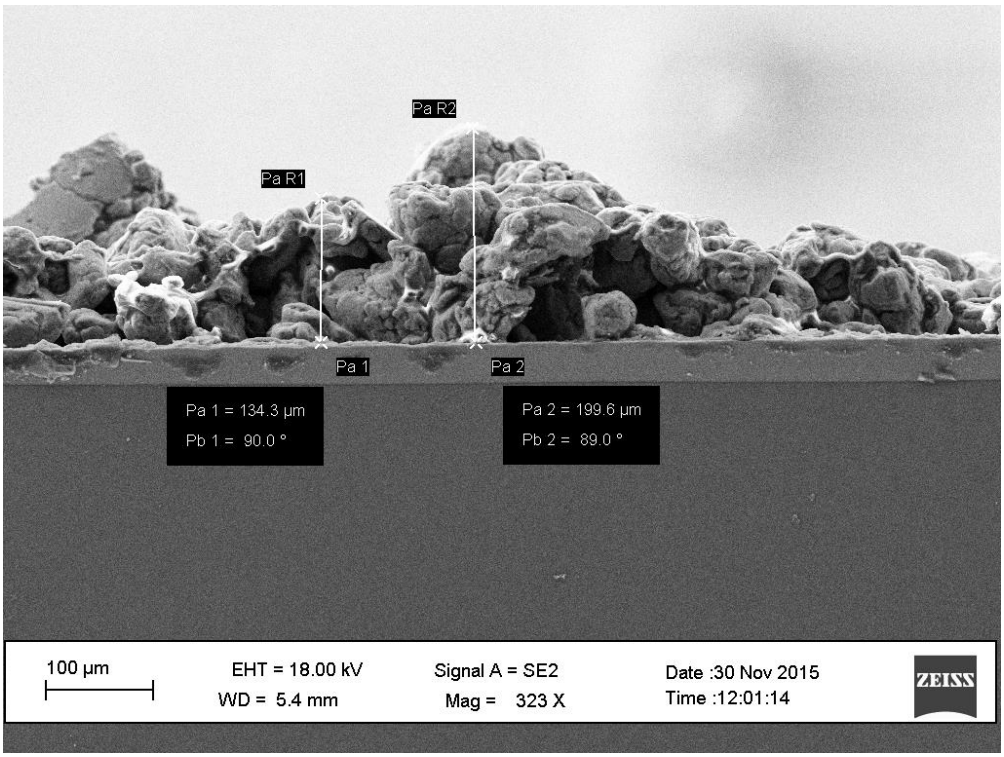

Figure 80 SEM Image: Cross-Sectional View of the Silicon Wafer: Milled Al Powder-Based Paste

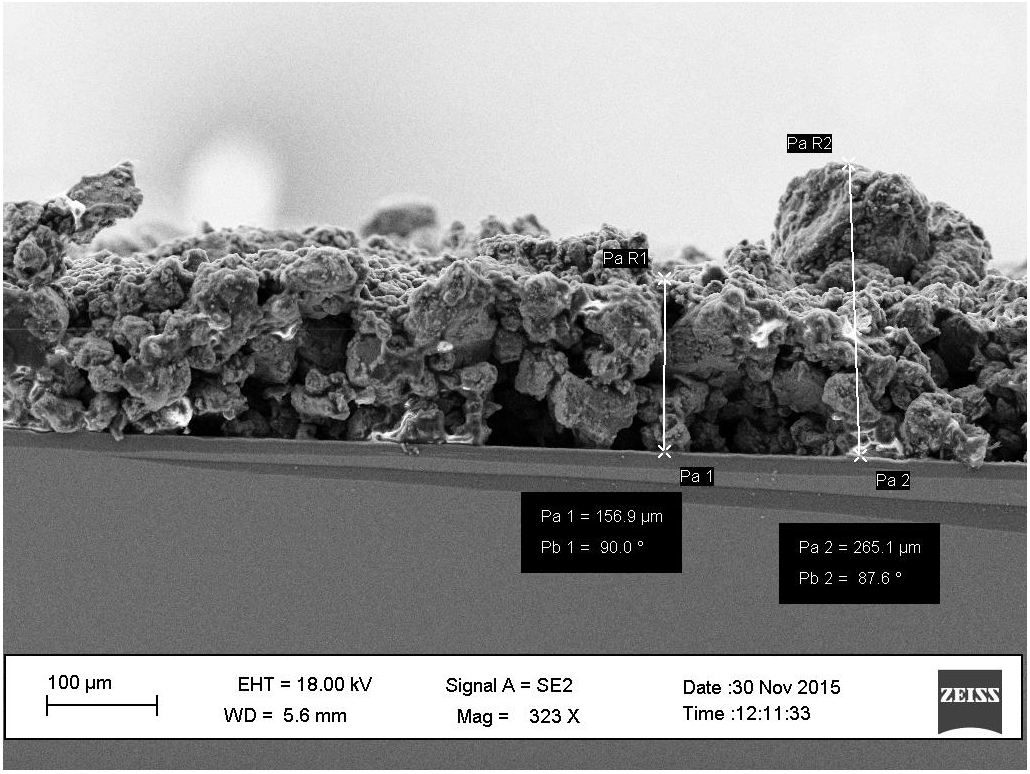

Figure 81 SEM Image: Cross-Sectional View of the Silicon Wafer: 10% CNT- Al Powder-Based Paste

Observations

For the Un-Milled Al paste layer, Figure 79, it seems fairly uniform, with small deviations across the layer. For the Milled Al layer, Figure 80, things were the exact opposite in this case: there were huge deviations with the wafer surface resembling that of a mountainous terrain, with the appearance of some smaller particles partially fused with larger ones. In the case of the final wafer, the 10% CNT-Al layer –Figure 81- the layer has an overall appearance of a uniform layer, however, this cannot be compared to the uniformity depicted in the case of the Un-Milled Al layer, the latter showing much less deviations. There were definitely some ups and downs in the 10% CNT-Al layer, yet these as well were not as much as those of the Milled-Al layer. Again the appearance of some smaller particles attached to larger ones can be seen here

5.3.3 Firing Test: 700°C

Based on SEM images obtained from section 5.3.2, the Al layer in some cases was found to be irregular with the particles of the powders separated from one another. Thus the next step was to try to combine the Al particles together to form one metallic strip rather than acting as free agents on the surface. To do so, the wafers must be subjected to a temperature higher than that of the melting temperature of Al, i.e. 660°C.

However, as mentioned before it was found that from previous tests that heating above 200°C will result in a powdering effect, i.e. the powders separate from the wafer due to the complete evaporation of the binder; the OV. This was probably due to the fact that the boiling point of some of the constituents of the OV was less than 250°C, and the recipe used to make the paste was a modified one, so combining these with a much prolonged firing curve (3 hours, 15 min), compared to the industry's curve of max few minutes with the wafer ushered from one heating zone to the next; not staying for a long time at any zone.

Thus, it was decided to test the theory out first on some samples taken from the wafers, and not heat all the 9 wafers at 700°C right away. So, from the 3 selected wafers from which the SEM rectangular samples were cut, the remaining parts of these specific wafers were taken to be further cut once again - using the diamond pen - to produce more than 20 rectangular strips of roughly the same surface area.

Table 17 Rectangular Strips for the Firing Test

Set	**Rectangular Strips**			**Heating time at ≈ 700 C**
A	Un-Milled Al	Milled Al	10% CNT-Al	1 min
B	Un-Milled Al	Milled Al	10% CNT-Al	5 min
C	Un-Milled Al	Milled Al	10% CNT-Al	10 min
D	Un-Milled Al	Milled Al	10% CNT-Al	20 min

Four sets of 3 rectangular strips were prepared as shown in Table 17 Rectangular Strips for the Firing Test. An oven was heated till around 710°C, then the oven was opened and a set was put inside for its corresponding duration, i.e. the 3 strips of set A were added together and left in the oven for 1 min, and then set A was removed from the oven, which was left for a couple of minutes

to reach the desired temperature of 710°C. Afterwards, the oven was opened once again and set B was left inside for 5 min. This process was repeated for the remaining sets; C and D. The oven was heated to 710°C instead of 700°C to account for the opening and closing of the oven.

I. Observations

The heating of all sets A, B, C and D at 700°C has resulted, as was expected, in the powdering effect where the Al powders became very loose and simply broke free from the wafer, see Figure 82 and Figure 83 . This effect was most pronounced in the case of the 10% CNT-Al strips.

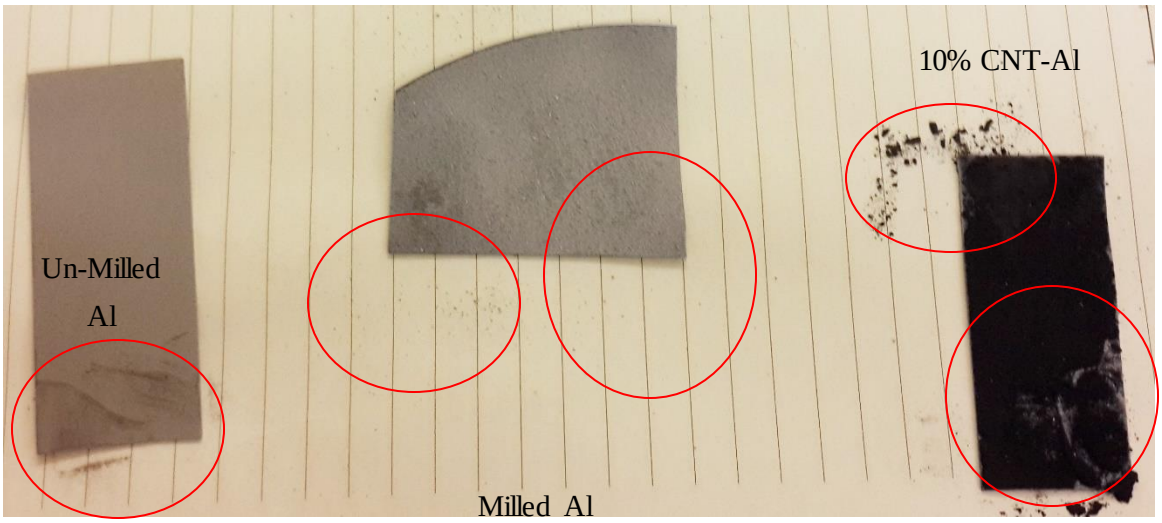

Figure 82 Firing Test: Set A- 1 min

Figure 83 Firing Test: Set B- 5 min

Note: The red circles indicate the areas where the powdering effect was most evident.

Rectangular strips where the powdering effect was most pronounced:

10% CNT-Al powder-based paste sample (Figure 84 to Figure 87):

Figure 84 10% CNT-Al Set A - 1 min

Figure 85 10% CNT-Al Set B - 5 min

Figure 86 10% CNT-Al Set C - 10 min

Figure 87 10% CNT-Al Set D - 20 min

II. Interpretation

Since the powdering effect was too overwhelming that the powders simply fell off the wafer, it was determined that further heating beyond the 200-250^{o}C threshold with the current developed paste would be risking losing the samples.

The question now would be why did the paste exhibit such a behavior at a relatively low temperature despite the fact that in the industry it is sometimes being heated to 900^{o}C. A possible explanation could be that this was not the ideal paste composition. Given that the only available method to print the paste was the Spinner device – not the ideal device for coating as shown in section 5.3.1- one could not directly use the same patented paste recipe, and hence the modification could have led to the powdering effect due to the presence of so much OV, more than the usual fraction, which required hence a lot more time for evaporation, and this led to an increase in the duration of the firing process step. Furthermore, the paste composition was limited to a few components, ignoring the glass frits and the dispersants. All of these procedures resulted in mutant paste that was similar but not identical to the one recommended and actually implemented by the patent authors.

As for the firing process, there was no way to duplicate it with the given resources, for it required movement from one temperature-controlled zone to the next at a relatively high belt speed, while the available resources included only 2 side-by-side furnaces that could not heat at a fast-enough rate to mimic the co-firing industrial process. Thus, the Al paste would not melt and then solidify to be fully attached to the rear-side of the wafer.

5.4 General Discussion

In light of all the results obtained above, it is worth noting that while the bow values were not conclusive, the warp readings gave a promising indication towards confirming the hypothesis that CNT did reduce the CTE of the Al paste and hence CNT could be used as a bow-reducing agent in Al pastes.

In the case of the cylindrical samples the powders were correctly sintered at a high temperature and the samples were fabricated using more reliable techniques than spin coating, the CTE results of these samples present a solid evidence that if processed correctly, the CNT-Al paste shall indeed succeed in reducing the bow.

Unfortunately, in the current research this was not possible as the available resources in terms of devices was very limited. Also, in order to have the processing, printing, firing and measuring of the paste and its bow/warp at a technical facility, this would have cost much more than the dedicated funds for this study, hence the only alternative was to make the best with what was available at hand.

Chapter 6

Conclusion & Future Work

6.1 Conclusion

There is a global need towards reducing the thickness of solar wafers and hence making solar energy more economical. With reducing the thickness, an already-existing problem becomes worse: the bowing problem which results due to a thermal mismatch between the Al layer on the rear side of the cell and the Silicon of the wafer. This study focused on replacing the Al paste used to make the rear-side electrode with an improved paste that would result in a reduced/eliminated bow in the cell; to improve the paste thermal characteristics, CNT were introduced. The following tests were performed:

Cylindrical Samples test

Powders were mixed by High Energy Ball Milling, sintered and then compacted to produce cylindrical samples of 4.5mm diameter, and a length of 15mm. 26 Samples were prepared of the following powder consistencies: Un-Milled Al, Milled Al, 2%, 5% and 10% CNT-Al (CNT percentages were by weight). The CTE of these samples was measured using a dilatometer, and it was found that the 10% CNT-Al samples caused the most reduction in CTE, by around 20%. This reduction was attributed to the hindering effect of the CNT on the Al metal expansion

Next, the electrical performance of the same 26 samples was measured in terms of the electrical resistivity. The voltage was varied and the current was measured. Data for the 26 samples was recorded, and based on a set of representative samples the resistance was calculated for each of the 5 sample categories. Resistance was taken to be a direct indicator of the Resistivity of the samples, since the cylindrical samples had identical dimensions. The results showed that adding CNT increased the resistance of the composite. At low levels, 2% and 5% CNT-Al, the effect was very minimal not exceeding 0.2% increase in composite resistance, but when 10% CNT was added, the effect increased to around 3.8%. The milling had a minimal effect, reducing the resistance by around 0.4%. It is believed that the more the CNT, the more the higher the interface resistance and hence the more the resistance to current (I) propagation.

Wafer Samples

Al paste was prepared using a recipe found in a patent. The recipe had Animony oxide as the active agent that played the main role in CTE reduction. It was replaced by CNT as the recipe was modified for the purposes of the current research to be limited to the Organic Vehicle and the Al powders, the latter were: Un-Milled Al, Milled Al and 10% CNT Al.

Three wafer samples for each category were prepared by spin coating the paste on them and firing them in a furnace at 160°C. The bow and warp of the wafers were measured before and after the coating and firing stages, and the difference in the values was reported accordingly. It was found that the bow readings were not conclusive, showing the Milled Al and the 10% CNT-Al bows fairly close in magnitude.

However, when the warp readings were compared, it was found that the CNT addition did have a much reduced effect on the warp development than the Milled Al or the Un-Milled Al pastes, this was evident when comparing the Warp to Thickness ratio, which was found to be 0.59, 0.35 and 0.24 for the Un-Milled Al, Milled Al and the 10% CNT Al pastes respectively, meaning that per unit thickness of paste layer printed, the 10% CNT-Al paste resulted in a reduced warp than the other pure Al pastes. More emphasis was put on the warp values as the device considers more points when determining the total warp than when determining the bow, the latter requires only 3 points of measurements.

SEM images of the top and cross-sectional views of 3 of the wafers were taken in order to study the paste printing. In the case of the Un-Milled Al, the particles had almost a regular size, which was evident in the paste layer thickness being uniform, while in the case of the Milled Al, the layer thickness was not totally uniform with a lot of changes in the layer thickness being noted, and finally in the 10% CNT-Al, things were better than the Milled Al, but not like the case of the Un-Milled Al, i.e. the layer thickness was to an extent uniform with few large particles that disrupted the layer uniformity. The reasons behind the irregularity in the layer thickness could be attributed to the spin coating device platform not being totally horizontal or that since the Milled Al and the 10% CNT-Al did not disintegrate fully due to milling, then there had been particles of varying size

and hence the centrifugal force pulled the particles differently, resulting in a non-homogeneous distribution of the paste.

Finally, a firing test was performed on a sample of the wafers. They were fired at 700^{o}C for 1,5,10 and 20 min. it was found that any firing above 700^{o}C resulted in the separation of the powders from the wafer, which was attributed to the fact that the paste recipe was modified for the current research purposes, hence it was not fit for firing above 200^{o}C, and that the appropriate firing profile could not be applied with the minimal resources available as this required special belt furnaces that were not available at AUC.

This study is an exploratory one in the field of solar energy, hence it is safe to say that a lot more research needs to be done, as shall be later detailed. However, the main objective was to see if the CNT addition would work for the paste, and the tests detailed above confirmed this thermally and electrically. More work is required to solidify the bowing/warping results, but the available results are promising and worth investigating more in the future work.

6.2 Future Improvements

The following improvements were suggested to be applied in the future. They have not been applied for the current research as either they were beyond the limited scope of the study or there were no resources available, and the alternative to go to professional facilities was expensive. In fact, one research facility in Germany offered to do the experimental work for around 5000 Euros, which was much beyond the available financial resources allocated for this work.

1. Control Particle Size

   Like in the case of the Un-Milled powders, the particle sizes were constant, which when used in the paste to coat the wafer resulted in a uniform layer. It is advised in the future that Design of experiments techniques to be applied to control the resulting particle size of the Milled-Al and CNT-Al powders. This could be done by further varying the Milling speed, time and amount of PCA added.

2. Screen Printing

   In the current research, the spin coating technique was resorted to as the resources available at AUC did not allow for any other alternative for printing. For future work, it is advised that the process should be repeated in an advanced facility with the proper resources to carry out the tests in a way similar to that performed in the industry

3. Co-Firing

   Like in the case of the screen printing, the unavailability of resources of AUC did not allow the proper firing of the wafers, where only one heating zone was used with prolonged heating time, unlike in the industry where the wafer moves from one zone to the next at a high speed.

4. Paste development

   Having fixed the screen printing issue, this would reflect on the paste used, as if one recalls, the main reason for modifying the paste recipe was to account for the spin coating step that would not have worked with viscous paste like that produced by the original recipe. Design

of experiments techniques could be applied to develop a paste with better printing and adherence properties, as well as to determine the least amount of CNT to be added to reduce the bow to an acceptable value.

5. Check Wafer Efficiency

   A further step is suggested which is to actually use the solar cells with the modified pastes and to measure their new electrical efficiencies.

6. Check Thermal conductivity

   Another aspect worth checking is the effect of adding CNT on the overall Thermal conductivity of the cell. It is a known issue that the efficiency of the solar cells decrease in hot environments, and that CNT have high thermal conductivity, thus the latter could improve the thermal conductivity of the former and hence accordingly increase its efficiency. This factor is worth investigating in the future work proposed for this research project.

References

ASM International. "Chapter 2: Thermal Expansion." *ASM Ready Reference: Thermal Properties of Metals.*, 2002. Print.

Bähr, M., et al. "Comparison of Bow-Avoiding Al-Pastes for Thin, Large-Area Crystalline Silicon Solar Cells ." *Proc. 20th EU PVSEC, Barcelona, Spain* (2005): 926-9. Print.

Bowden, S., et al. "Rear Passivation of Thin Multicrystalline Silicon Solar Cells." *Opto-Electronics review* 8 (2000): 307-10. Print.

Brenner, P., A. G. Prince, and R. J. S. Young. *Aluminum Pastes and use Thereof in the Production of Silicon Solar Cells*. Google Patents, 2013. Web. US8398896 B2.

Bunkenburg, B., et al. "Enabling Thin Wafers for today's High Efficiency Silicon Solar Cells." Print.

Carroll, Alan F., et al. "Advances in Pv Metallisation Technology". *20th European Photovoltaic Solar Energy Conference*. 2005, Barcelona, Spain. 2005. Print.

Ci, Lijie, et al. "Investigation of the Interfacial Reaction between Multi-Walled Carbon Nanotubes and Aluminum." *Acta Materialia* 54.20 (2006): 5367-75. Web.

Coleman, Jonathan N., et al. "Small but Strong: A Review of the Mechanical Properties of Carbon nanotube–polymer Composites." Carbon 44.9 (2006): 1624-52. Web.

Deng, C. F., et al. "Thermal Expansion Behaviors of Aluminum Composite Reinforced with Carbon Nanotubes." *Materials Letters* 62.15 (2008): 2301-3. Web.

Eichhorn Hausmann, E+H Metrology GMBH, “MX 203-8-37 Contactless Wafer Geometry Gauge”, Version 1.1

Eichhorn Hausmann, E+H Metrology GMBH, “Wafer Geometry Characteristics”, 2004

Esawi, Amal. *MENG 530: "Nano-Structured Materials"*. The American University in Cairo, Fall 2014. “Carbon Nanotubes”.

Esawi, A. M. K., et al. "Effect of Carbon Nanotube (CNT) Content on the Mechanical Properties of CNT-Reinforced Aluminium Composites." *Composites Science and Technology* 70.16 (2010): 2237-41. Web.

Hilali, Mohamed M., James M. Gee, and Peter Hacke. "Bow in Screen-Printed Back-Contact Industrial Silicon Solar Cells." *Solar Energy Materials and Solar Cells* 91.13 (2007): 1228-33. Web.

Kaushik, Brajesh Kumar, and Manoj Kumar Majumder. "Carbon Nanotube: Properties and Applications." *Carbon Nanotube Based VLSI Interconnects*.Springer India, 2015. 17-37. Print.

Kim Dong Suk, Jae Ho Kim, Hyun Don Kim, et al. “Aluminum Paste and Solar Cell”. Patent US20120037855. 2012.

Kim, S., et al. "Aluminum Pastes (Lead-free/low-Bow) for Thin Wafers". *Photovoltaic Specialists Conference, 2005. Conference Record of the Thirty-first IEEE*. Web.

Koval, T., J. Wohlgemuth, and B. Kinsey. "Dependence of Cell Performance on Wafer Thickness for BSF and Non-BSF Cells". *Photovoltaic Specialists Conference, 1996., Conference Record of the Twenty Fifth IEEE*. Web.

Liu, Z. Y., et al. "Elevated Temperature Tensile Properties and Thermal Expansion of CNT/2009Al Composites." *Composites Science and Technology* 72.15 (2012): 1826-33. Web.

Microphase Co. Ltd. Web. <http://www.microphase.jp/e/e_product0201.html>.

Mimovrste. 2015.Web. <https://www.mimovrste.com/blenderji/braun-blender-jb-3010-tribute?v=667089>.

Nova. Web. <http://www.pbs.org/wgbh/nova/solar/insi-nf.html>.

Popovich, V. A., et al. "Microstructure and Mechanical Properties of Aluminum Back Contact Layers." *Solar Energy Materials and Solar Cells* 95.1 (2011): 93-6. Web.

Rohatgi, P. K., N. Gupta, and Simon Alaraj. "Thermal Expansion of Aluminum–Fly Ash Cenosphere Composites Synthesized by Pressure Infiltration Technique." *Journal of Composite Materials* 40.13 (2006): 1163-74. Web.

Rose, M., and R. Young. Aluminum Thick Film Compositions(s), Electrode(s), Semiconductor Device(s) and Methods of Making Thereof. Patent US20070079868. 04/12. <http://www.google.com/patents/US20070079868>.

Schneider, A., et al. "Al Bsf for Thin Screenprinted Multicrystalline Si Solar Cells." (JANUARY 2001) Print.

Schneider, A., et al. "Bow Reducing Factors for Thin Screenprinted MC-Si Solar Cells with Al BSF". *Photovoltaic Specialists Conference, 2002. Conference Record of the Twenty-Ninth IEEE*. Web.

Schwenke, Thomas. "**Solar energy / Solar photovoltaics / Photovoltaic effect (3D animation)**." 2011.Web. <https://www.youtube.com/watch?v=1gta2ICarDw&feature=related>.

Soon-gil Kim, et al. "Enhancing the Solar Cell Efficiency with Optimized Metal Paste". *Nanotechnology (IEEE-NANO), 2010 10th IEEE Conference on*. Web.

TA Instruments, "Dilatometry" manual, 2013

Tang, Yongbing, et al. "Thermal Expansion of a Composite of Single-Walled Carbon Nanotubes and Nanocrystalline Aluminum." *Carbon* 42.15 (2004): 3260-2. Web.

van Amstel, T., V. Popovich, and I. J. and Bennett. "A Multiscale Model of the Aluminium Layer at the Rear Side of a Solar Cell". *24th European Photovoltaic Solar Energy Conference and Exhibition*. September 2009, Hamburg, Germany. 2009. Print.

Yosida, Y. "High-Temperature Shrinkage of Single-Walled Carbon Nanotube Bundles Up to 1600 K." *Journal of Applied Physics* 87.7 (2000): 3338-41. Web.

Zhang, L., et al. "Strain in the Process of Eliminating Wafer Bow of Finished Solar Cell". *Physical and Failure Analysis of Integrated Circuits, 2009. IPFA 2009. 16th IEEE International Symposium on the.* Web.

Appendix A

CTE Readings

I. Un-Milled Al Samples

Table 18 CTE readings for Un-Milled Al cylindrical samples

	Un-Milled Al Samples: CTE (X 10^{-6} °C^{-1})						
Temp/C	**Sample A**	**Sample B**	**Sample C**	**Sample D**	**Sample E**	**Average**	**STD Dev**
30	10.55	12.60	12.52	3.69	4.51	8.77	4.35
40	12.77	13.79	13.07	8.92	9.64	11.64	2.20
50	14.44	15.44	14.59	11.21	11.81	13.50	1.87
60	15.95	16.53	15.94	13.21	13.63	15.05	1.52
70	16.83	17.46	16.87	14.66	14.96	16.16	1.26
80	17.68	18.23	17.70	15.82	15.95	17.07	1.11
90	18.40	18.82	18.41	16.74	16.71	17.82	1.01
100	18.90	19.33	19.02	17.54	17.43	18.44	0.89
110	19.41	19.72	19.54	18.24	18.03	18.99	0.79
120	19.79	20.08	20.00	18.82	18.53	19.45	0.72
130	20.13	20.55	20.40	19.32	18.95	19.87	0.70
140	20.41	20.82	20.77	19.78	19.37	20.23	0.64
150	20.71	21.12	21.09	20.17	19.74	20.57	0.60
160	20.95	21.35	21.02	20.54	20.00	20.77	0.52
170	21.16	21.56	21.32	20.86	20.30	21.04	0.49
180	21.32	21.73	21.56	21.15	20.56	21.26	0.45
190	21.51	21.91	21.83	21.45	20.79	21.50	0.44
200	21.71	22.08	22.09	21.71	21.03	21.72	0.43
210	21.86	22.22	22.33	21.97	21.24	21.92	0.43
220	21.99	22.35	22.52	22.20	21.43	22.10	0.42
230	22.10	22.45	22.71	22.41	21.60	22.25	0.43
240	22.19	22.56	22.89	22.61	21.74	22.40	0.44
250	22.32	22.66	23.05	22.79	21.91	22.55	0.44
260	22.45	22.77	23.22	22.97	22.05	22.69	0.46
270	22.55	22.86	23.37	23.14	22.20	22.82	0.47
280	22.63	22.95	23.53	23.31	22.33	22.95	0.49
290	22.73	23.04	23.67	23.46	22.47	23.08	0.50
300	22.84	23.13	23.80	23.61	22.60	23.19	0.51
310	22.93	23.23	23.95	23.75	22.72	23.32	0.52
320	23.02	23.32	24.06	23.90	22.86	23.43	0.53
330	23.14	23.42	24.20	24.03	23.00	23.56	0.54
340	23.26	23.53	24.33	24.16	23.13	23.68	0.54

350	23.37	23.64	24.45	24.28	23.25	23.80	0.54
360	23.48	23.75	24.56	24.42	23.38	23.92	0.54
370	23.60	23.86	24.68	24.55	23.51	24.04	0.54
380	23.73	23.98	24.81	24.67	23.64	24.17	0.54
390	23.85	24.11	24.92	24.81	23.77	24.29	0.54
400	23.97	24.22	25.04	24.93	23.89	24.41	0.54
410	24.11	24.35	25.15	25.05	24.02	24.54	0.53
420	24.26	24.48	25.26	25.19	24.14	24.67	0.52
430	24.38	24.61	25.37	25.30	24.28	24.79	0.52
440	24.51	24.74	25.50	25.43	24.39	24.91	0.52
450	24.65	24.89	25.60	25.56	24.53	25.05	0.51
460	24.79	25.03	25.73	25.68	24.67	25.18	0.50
470	24.92	25.15	25.85	25.81	24.80	25.31	0.49
480	25.06	25.29	25.97	25.94	24.94	25.44	0.48
490	25.22	25.42	26.09	26.06	25.09	25.57	0.47

II. Milled Al Samples

	Milled Al Samples: CTE (X 10^{-6} $^{o}C^{-1}$)							
Temp/C	**Sample A**	**Sample B**	**Sample C**	**Sample D**	**Sample E**	**Sample F**	**Average**	**STD Dev**
30	12.09	12.62	12.19	4.89	3.94	5.99	8.62	4.08
40	13.38	13.38	12.76	9.67	9.21	10.40	11.47	1.92
50	14.77	14.52	14.32	11.49	11.27	12.12	13.08	1.62
60	15.94	15.62	15.28	13.26	13.17	13.84	14.52	1.24
70	16.73	16.49	16.22	14.47	14.38	14.93	15.54	1.06
80	17.53	17.29	16.99	15.56	15.42	15.89	16.45	0.93
90	18.11	17.90	17.59	16.40	16.30	16.67	17.16	0.80
100	18.62	18.48	18.21	17.05	16.97	17.32	17.78	0.75
110	19.10	18.97	18.65	17.66	17.59	17.89	18.31	0.68
120	19.45	19.39	19.09	18.19	18.12	18.37	18.77	0.61
130	19.81	19.74	19.46	18.65	18.51	18.82	19.16	0.57
140	20.10	20.07	19.77	19.04	18.80	19.22	19.50	0.56
150	20.39	20.38	20.10	19.39	18.92	19.60	19.80	0.59
160	20.67	20.64	20.40	19.73	19.14	19.91	20.08	0.60
170	20.89	20.88	20.70	20.02	19.45	20.22	20.36	0.57
180	21.08	21.09	20.97	20.29	19.73	20.48	20.61	0.54
190	21.29	21.30	21.23	20.56	19.99	20.74	20.85	0.53
200	21.51	21.51	21.50	20.80	20.24	20.99	21.09	0.52
210	21.70	21.71	21.71	21.03	20.49	21.22	21.31	0.50
220	21.88	21.88	21.90	21.24	20.73	21.43	21.51	0.47
230	22.03	22.05	22.08	21.42	20.95	21.63	21.69	0.45
240	22.20	22.20	22.25	21.61	21.17	21.80	21.87	0.43
250	22.35	22.35	22.40	21.78	21.37	21.97	22.04	0.41
260	22.50	22.47	22.55	21.96	21.55	22.15	22.20	0.39
270	22.64	22.62	22.70	22.12	21.73	22.30	22.35	0.38
280	22.80	22.77	22.82	22.28	21.89	22.45	22.50	0.37
290	22.92	22.90	22.97	22.43	22.04	22.61	22.64	0.36
300	23.08	23.02	23.10	22.59	22.18	22.75	22.78	0.36
310	23.21	23.16	23.22	22.57	22.33	22.88	22.90	0.38
320	23.35	23.30	23.34	22.72	22.45	23.02	23.03	0.37
330	23.47	23.42	23.48	22.86	22.57	23.15	23.16	0.37
340	23.60	23.54	23.54	22.99	22.71	23.29	23.28	0.36
350	23.73	23.68	23.68	23.13	22.83	23.42	23.41	0.36
360	23.86	23.80	23.85	23.26	22.96	23.54	23.54	0.37
370	23.98	23.92	23.99	23.38	23.08	23.67	23.67	0.37
380	24.11	24.04	24.12	23.50	23.19	23.79	23.79	0.38
390	24.24	24.17	24.24	23.63	23.31	23.92	23.92	0.38
400	24.36	24.29	24.34	23.75	23.42	24.04	24.03	0.38

410	24.49	24.40	24.45	23.88	23.52	24.16	24.15	0.39
420	24.61	24.52	24.57	24.01	23.63	24.29	24.27	0.39
430	24.74	24.64	24.72	24.13	23.74	24.42	24.40	0.40
440	24.87	24.76	24.83	24.25	23.84	24.54	24.52	0.40
450	25.00	24.88	24.93	24.39	23.94	24.66	24.63	0.41
460	25.11	25.02	25.05	24.51	24.03	24.79	24.75	0.42
470	25.22	25.15	25.15	24.62	24.13	24.89	24.86	0.42
480	25.34	25.27	25.25	24.73	24.21	25.01	24.97	0.44
490	25.45	25.40	25.37	24.84	24.27	25.10	25.07	0.45

III. 2% CNT-Al Samples

	2% CNT-Al Samples: CTE (X 10^{-6} $^{o}C^{-1}$)							
Temp/C	**Sample A**	**Sample B**	**Sample C**	**Sample D**	**Sample E**	**Sample F**	**Average**	**STD Dev**
30	10.99	11.50	11.74	4.86	4.41	5.36	8.14	3.60
40	12.63	12.73	12.71	9.47	9.09	8.88	10.92	1.95
50	14.13	14.31	14.25	11.38	10.97	11.13	12.69	1.69
60	15.03	15.38	15.22	13.13	12.76	13.03	14.09	1.24
70	15.64	16.24	16.07	14.34	14.01	14.29	15.10	0.99
80	16.41	16.99	16.74	15.33	14.94	15.24	15.94	0.87
90	17.07	17.57	17.34	16.15	15.74	16.04	16.65	0.77
100	17.66	18.06	17.80	16.77	16.40	16.66	17.23	0.70
110	18.14	18.52	18.22	17.33	16.99	17.20	17.73	0.63
120	18.57	18.92	18.59	17.81	17.49	17.59	18.16	0.60
130	18.94	19.25	18.91	18.20	17.94	18.01	18.54	0.56
140	19.27	19.59	19.26	18.58	18.32	18.40	18.90	0.53
150	19.56	19.92	19.55	18.94	18.68	18.73	19.23	0.51
160	19.83	20.18	19.80	19.27	19.03	19.04	19.53	0.48
170	20.08	20.42	20.05	19.52	19.32	19.31	19.78	0.46
180	20.32	20.61	20.28	19.78	19.59	19.57	20.02	0.44
190	20.53	20.79	20.49	20.03	19.84	19.80	20.25	0.41
200	20.79	21.03	20.72	20.26	20.09	20.04	20.49	0.41
210	20.99	21.19	20.91	20.49	20.33	20.25	20.69	0.39
220	21.17	21.35	21.09	20.69	20.54	20.44	20.88	0.37
230	21.33	21.51	21.27	20.85	20.73	20.61	21.05	0.37
240	21.49	21.63	21.44	21.02	20.90	20.78	21.21	0.35
250	21.65	21.77	21.60	21.14	21.07	20.93	21.36	0.35
260	21.80	21.92	21.75	21.26	21.26	21.09	21.51	0.35
270	21.96	22.06	21.91	21.44	21.41	21.22	21.67	0.35
280	22.11	22.19	22.06	21.58	21.56	21.37	21.81	0.35
290	22.26	22.31	22.20	21.65	21.71	21.51	21.94	0.36
300	22.40	22.46	22.34	21.77	21.85	21.63	22.08	0.36
310	22.54	22.59	22.49	21.91	21.98	21.77	22.21	0.36
320	22.68	22.71	22.64	22.01	22.12	21.89	22.34	0.37
330	22.81	22.84	22.76	22.12	22.25	22.01	22.47	0.38
340	22.94	22.96	22.90	22.23	22.38	22.11	22.59	0.39
350	23.07	23.08	23.04	22.33	22.52	22.24	22.71	0.40
360	23.20	23.20	23.18	22.44	22.64	22.34	22.84	0.40
370	23.32	23.32	23.31	22.55	22.77	22.47	22.96	0.41
380	23.46	23.44	23.45	22.66	22.89	22.58	23.08	0.42
390	23.60	23.54	23.58	22.77	23.01	22.69	23.20	0.42
400	23.73	23.67	23.70	22.87	23.13	22.81	23.32	0.43

410	23.85	23.77	23.83	22.98	23.26	22.92	23.43	0.43
420	23.99	23.89	23.96	23.11	23.38	23.04	23.56	0.44
430	24.11	24.00	24.11	23.22	23.49	23.16	23.68	0.45
440	24.25	24.11	24.23	23.33	23.61	23.28	23.80	0.45
450	24.39	24.23	24.35	23.45	23.73	23.39	23.92	0.45
460	24.53	24.35	24.47	23.56	23.83	23.50	24.04	0.47
470	24.67	24.45	24.59	23.68	23.95	23.61	24.16	0.47
480	24.80	24.56	24.72	23.78	24.05	23.71	24.27	0.48
490	24.93	24.66	24.84	23.87	24.13	23.81	24.37	0.50

IV. 5% CNT-Al Samples

	5% CNT-Al Samples: CTE (X 10^{-6} $^{o}C^{-1}$)						
Temp/C	**Sample A**	**Sample B**	**Sample C**	**Sample D**	**Sample E**	**Average**	**STD Dev**
30	10.25	10.59	9.07	7.46	6.80	8.83	1.67
40	11.52	11.46	10.55	10.27	10.00	10.76	0.70
50	12.94	12.75	11.91	11.56	11.45	12.12	0.68
60	13.94	13.70	13.19	12.91	12.76	13.30	0.50
70	14.69	14.43	14.04	13.81	13.68	14.13	0.42
80	15.35	15.11	14.84	14.44	14.50	14.85	0.39
90	15.88	15.60	15.45	15.03	15.14	15.42	0.34
100	16.35	16.06	15.98	15.57	15.68	15.93	0.31
110	16.78	16.50	16.45	16.01	16.06	16.36	0.32
120	17.15	16.84	16.86	16.41	16.44	16.74	0.32
130	17.47	17.14	17.19	16.78	16.77	17.07	0.29
140	17.75	17.43	17.52	17.09	17.10	17.38	0.28
150	18.01	17.69	17.80	17.38	17.40	17.66	0.27
160	18.24	17.94	18.06	17.64	17.65	17.91	0.26
170	18.45	18.16	18.30	17.87	17.89	18.13	0.25
180	18.66	18.39	18.52	18.08	18.11	18.35	0.25
190	18.84	18.58	18.71	18.31	18.31	18.55	0.24
200	19.02	18.80	18.92	18.53	18.52	18.76	0.23
210	19.18	18.99	19.12	18.72	18.71	18.95	0.22
220	19.34	19.17	19.28	18.90	18.87	19.11	0.22
230	19.46	19.34	19.44	19.04	19.02	19.26	0.21
240	19.54	19.50	19.59	19.19	19.18	19.40	0.20
250	19.66	19.64	19.73	19.33	19.33	19.54	0.19
260	19.76	19.80	19.86	19.48	19.47	19.67	0.19
270	19.94	19.95	20.00	19.63	19.59	19.82	0.19
280	20.05	20.09	20.12	19.76	19.73	19.95	0.19
290	20.19	20.23	20.23	19.90	19.88	20.09	0.18
300	20.33	20.36	20.37	20.01	20.02	20.22	0.19
310	20.43	20.50	20.49	20.13	20.14	20.34	0.19
320	20.57	20.63	20.61	20.24	20.26	20.46	0.19
330	20.71	20.75	20.72	20.35	20.38	20.58	0.20
340	20.84	20.88	20.84	20.46	20.50	20.70	0.20
350	20.94	21.01	20.94	20.58	20.63	20.82	0.20
360	21.08	21.13	21.05	20.69	20.75	20.94	0.21
370	21.21	21.24	21.17	20.79	20.86	21.05	0.21
380	21.33	21.36	21.28	20.90	20.97	21.17	0.22
390	21.43	21.49	21.39	21.00	21.09	21.28	0.22
400	21.54	21.60	21.50	21.11	21.22	21.40	0.22

410	21.66	21.74	21.62	21.21	21.34	21.51	0.23
420	21.78	21.86	21.74	21.33	21.47	21.63	0.22
430	21.88	21.99	21.86	21.44	21.63	21.76	0.22
440	22.00	22.10	21.98	21.55	21.78	21.88	0.22
450	22.10	22.24	22.09	21.65	21.92	22.00	0.22
460	22.21	22.36	22.19	21.76	22.04	22.11	0.23
470	22.32	22.49	22.30	21.85	22.17	22.23	0.24
480	22.40	22.61	22.41	21.96	22.30	22.34	0.24
490	22.48	22.73	22.51	22.03	22.44	22.44	0.25

V. 10% CNT-Al Samples

	10% CNT-Al Samples: CTE (X 10^{-6} $^{o}C^{-1}$)					
Temp/C	**Sample A**	**Sample B**	**Sample C**	**Sample D**	**Average**	**STD Dev**
30	8.30	10.02	8.92	8.71	8.99	0.73
40	9.49	10.80	9.95	10.11	10.09	0.55
50	10.82	11.99	11.05	11.51	11.35	0.52
60	11.84	12.86	12.05	12.54	12.32	0.46
70	12.60	13.50	12.76	13.22	13.02	0.41
80	13.25	14.05	13.39	13.88	13.64	0.39
90	13.78	14.50	13.85	14.42	14.14	0.37
100	14.25	14.94	14.29	14.84	14.58	0.36
110	14.66	15.26	14.66	15.20	14.94	0.33
120	15.00	15.57	14.97	15.53	15.27	0.32
130	15.47	15.81	15.24	15.81	15.58	0.28
140	15.78	16.07	15.42	16.11	15.84	0.32
150	16.03	16.32	15.64	16.35	16.08	0.33
160	16.24	16.54	15.84	16.60	16.31	0.35
170	16.41	16.73	16.03	16.82	16.50	0.36
180	16.56	16.88	16.21	16.96	16.65	0.34
190	16.74	17.04	16.40	17.17	16.84	0.34
200	16.92	17.20	16.57	17.38	17.02	0.35
210	17.08	17.32	16.75	17.55	17.18	0.34
220	17.23	17.42	16.90	17.70	17.31	0.34
230	17.36	17.54	17.04	17.85	17.45	0.34
240	17.53	17.67	17.18	17.99	17.59	0.34
250	17.66	17.81	17.32	18.11	17.72	0.33
260	17.78	17.93	17.46	18.24	17.85	0.32
270	17.90	18.05	17.59	18.37	17.98	0.32
280	18.02	18.15	17.71	18.50	18.10	0.33
290	18.14	18.26	17.84	18.63	18.22	0.32
300	18.24	18.37	17.95	18.74	18.33	0.33
310	18.34	18.48	18.06	18.85	18.43	0.33
320	18.45	18.58	18.17	18.96	18.54	0.33
330	18.55	18.66	18.26	19.07	18.64	0.33
340	18.65	18.77	18.37	19.18	18.74	0.34
350	18.75	18.85	18.47	19.27	18.84	0.33
360	18.83	18.96	18.55	19.38	18.93	0.34
370	18.91	19.05	18.65	19.48	19.02	0.35
380	18.99	19.14	18.74	19.59	19.11	0.35
390	19.08	19.24	18.85	19.70	19.22	0.36
400	19.17	19.33	18.94	19.82	19.32	0.37

410	19.27	19.43	19.07	19.92	19.42	0.37
420	19.36	19.54	19.18	20.03	19.53	0.37
430	19.45	19.65	19.30	20.14	19.63	0.37
440	19.54	19.75	19.42	20.27	19.75	0.37
450	19.63	19.85	19.54	20.38	19.85	0.37
460	19.71	19.94	19.66	20.50	19.95	0.38
470	19.78	20.06	19.79	20.60	20.06	0.38
480	19.84	20.15	19.90	20.70	20.15	0.39
490	19.87	20.23	19.99	20.80	20.22	0.41

VI. Representative Samples: Non-Normalized CTE Data

Table 19 CTE Values for the Representative Cylindrical Samples

	CTE x 10^{-6} $^{o}C^{-1}$				
	Un-Milled Al	**Milled Al**	**2% CNT-Al**	**5% CNT-Al**	**10% CNT-Al**
Temp/^{o}C	**Sample B**	**Sample F**	**Sample E**	**Sample C**	**Sample B**
100	19.33	17.32	16.40	15.98	14.94
150	21.12	19.60	18.68	17.80	16.32
200	22.08	20.99	20.09	18.92	17.20
250	22.66	21.97	21.07	19.73	17.81
300	23.13	22.75	21.85	20.37	18.37
350	23.64	23.42	22.52	20.94	18.85
400	24.22	24.04	23.13	21.50	19.33
450	24.89	24.66	23.73	22.09	19.85
490	25.42	25.10	24.13	22.51	20.23

VII. Representative Samples: Normalized CTE Data

Table 20 Normalized CTE Readings for the Representative Cylindrical Samples

	Normalized CTE Readings as a % – Representative Samples				
	Un-Milled Al	Milled Al	2% CNT-Al	5% CNT-Al	10% CNT-Al
Temp/°C	Sample B	Sample F	Sample E	Sample C	Sample B
100	111.61	100.00	94.65	92.27	86.26
150	107.80	100.00	95.32	90.84	83.26
200	105.19	100.00	95.74	90.13	81.95
250	103.12	100.00	95.91	89.81	81.04
300	101.68	100.00	96.05	89.56	80.77
350	100.95	100.00	96.16	89.43	80.51
400	100.76	100.00	96.21	89.44	80.41
450	100.96	100.00	96.25	89.59	80.49
490	101.26	100.00	96.12	89.66	80.58

Appendix B

Electrical Resistance Readings

I. Un-Milled Al Samples

Table 21 Voltage-Current readings and Resistance Values for the Un-Milled Al cylindrical samples

	Un-Milled Al Samples: Current (I: mA)						
Voltage (mV)	**A**	**B**	**C**	**D**	**E**	**Average**	**Std Dev**
100	77	77	77	77	78	77.20	0.45
200	145	145	144	144	145	144.60	0.55
300	212	212	211	212	212	211.80	0.45
400	280	280	278	279	279	279.20	0.84
500	347	347	345	347	347	346.60	0.89
600	415	415	412	414	414	414.00	1.22
700	482	482	478	481	481	480.80	1.64
800	549	549	545	549	548	548.00	1.73
900	616	616	612	616	615	615.00	1.73
1000	683	683	678	683	681	681.60	2.19
1100	750	749	745	748	747	747.80	1.92
1200	816	816	810	814	813	813.80	2.49
1300	882	882	876	881	879	880.00	2.55
1400	947	947	942	946	945	945.40	2.07
1500	1014	1013	1007	1012	1011	1011.40	2.70
1600	1077	1078	1072	1076	1076	1075.80	2.28
Resistance (Ohm)	**1.4709**	**1.4711**	**1.4803**	**1.4729**	**1.4745**	**1.4739**	0.00

II. Milled Al Samples

Table 22 Voltage-Current readings and Resistance values for the Milled Al cylindrical samples

	Milled Al Samples: Current (I: mA)							
Voltage (mV)	**A**	**B**	**C**	**D**	**E**	**F**	**Average**	**Std Dev**
100	78	77	77	77	77	77	77.17	0.41
200	145	144	144	144	145	145	144.50	0.55
300	213	212	212	211	213	213	212.33	0.82
400	281	278	279	279	280	280	279.50	1.05
500	349	346	346	346	348	348	347.17	1.33
600	417	413	413	413	415	415	414.33	1.63
700	485	481	480	480	483	483	482.00	2.00
800	552	548	547	547	550	550	549.00	2.00
900	620	615	614	614	617	617	616.17	2.32
1000	687	681	681	680	684	684	682.83	2.64
1100	754	748	747	747	751	751	749.67	2.80
1200	821	814	813	813	817	817	815.83	3.13
1300	887	880	880	879	884	883	882.17	3.06
1400	953	946	945	944	949	949	947.67	3.33
1500	1018	1012	1009	1010	1015	1015	1013.17	3.43
1600	1084	1077	1073	1075	1080	1080	1078.17	3.97
Resistance (Ohm)	**1.4626**	**1.4736**	**1.476**	**1.4759**	**1.4683**	**1.4685**	**1.4708**	0.01

III. 2% CNT-Al Samples

Table 23 Voltage-Current readings and Resistance values for the 2% CNT- Al cylindrical samples

	2% CNT-Al Samples: Current (I: mA)							
Voltage (mV)	**A**	**B**	**C**	**D**	**E**	**F**	**Average**	**Std Dev**
100	77	77	78	77	77	77	77.17	0.41
200	145	144	146	144	145	144	144.67	0.82
300	212	211	214	211	213	211	212.00	1.26
400	280	278	282	278	281	279	279.67	1.63
500	347	345	349	345	349	346	346.83	1.83
600	415	412	417	413	417	413	414.50	2.17
700	482	479	485	479	484	480	481.50	2.59
800	550	546	553	546	552	547	549.00	3.10
900	617	613	621	613	619	614	616.17	3.37
1000	684	680	688	679	686	680	682.83	3.71
1100	751	746	755	745	753	747	749.50	4.09
1200	817	812	822	811	820	813	815.83	4.54
1300	883	877	888	876	886	878	881.33	5.05
1400	949	943	954	941	952	944	947.17	5.27
1500	1015	1009	1020	1007	1018	1010	1013.17	5.27
1600	1080	1074	1085	1071	1083	1075	1078.00	5.51
Resistance(Ohm)	**1.4687**	**1.4779**	**1.4607**	**1.48**	**1.464**	**1.4761**	**1.47**	0.01

IV. 5% CNT-Al Samples

Table 24 Voltage-Current readings and Resistance values for the 5% CNT-Al cylindrical samples

	5% CNT-Al Samples: Current (I: mA)						
Voltage (mV)	**A**	**B**	**C**	**D**	**E**	**Average**	**Std Dev**
100	78	77	77	77	77	77.20	0.45
200	145	145	144	145	145	144.80	0.45
300	213	213	211	212	212	212.20	0.84
400	281	281	278	280	280	280.00	1.22
500	349	348	345	347	347	347.20	1.48
600	416	416	412	415	415	414.80	1.64
700	484	483	478	482	482	481.80	2.28
800	551	551	545	550	549	549.20	2.49
900	619	618	611	617	617	616.40	3.13
1000	686	685	678	684	683	683.20	3.11
1100	753	752	743	750	749	749.40	3.91
1200	819	818	809	817	815	815.60	3.97
1300	885	884	874	883	881	881.40	4.39
1400	951	950	939	949	947	947.20	4.82
1500	1015	1015	1004	1015	1013	1012.40	4.77
1600	1080	1080	1068	1080	1078	1077.20	5.22
Resistance (Ohm)	**1.466**	**1.4672**	**1.4835**	**1.4689**	**1.4713**	**1.47**	0.01

V. 10% CNT-Al Samples

Table 25 Voltage-Current readings and Resistance values for the 10% CNT-Al cylindrical samples

	10% CNT-Al Samples: Current (I: mA)					
Voltage (mV)	**A**	**B**	**C**	**D**	**Average**	
100	71	75	75	77	74.50	2.52
200	132	140	140	144	139.00	5.03
300	193	206	205	211	203.75	7.63
400	254	272	270	278	268.50	10.25
500	316	338	334	344	333.00	12.06
600	377	404	399	411	397.75	14.68
700	438	469	464	478	462.25	17.17
800	500	535	529	545	527.25	19.33
900	561	601	594	611	591.75	21.65
1000	622	666	659	677	656.00	23.85
1100	682	731	723	743	719.75	26.47
1200	743	796	787	808	783.50	28.34
1300	803	860	851	874	847.00	30.82
1400	863	924	915	939	910.25	33.02
1500	923	988	978	1005	973.50	35.46
1600	982	1052	1042	1069	1036.25	37.85
Resistance/Ohm	**1.6154**	**1.5084**	**1.5242**	**1.4836**	**1.5329**	0.057482